PUSHKOV INSTITUTE OF TERRESTRIAL MAGNETISM,
IONOSPHERE AND RADIO WAVE PROPAGATION
RUSSIAN ACADEMY OF SCIENCES (IZMIRAN)

Gennady Chernov
Valery Fomichev

RECENT RESULTS ON THE FINE STRUCTURE OF SOLAR RADIO BURSTS

MOSCOW • NAUKA • 2025

Reviewers:
Dr. Sc. in Physics and Mathematics *V. D. Kuznetsov*
Corresponding member RAS *A. V. Stepanov*

Chernov G. P., Fomichev V. V.

Recent results on the fine structure of solar radio bursts. – Moscow: Nauka, 2025. – 109 p. – ISBN 978-5-02-041191-3

The study of the fine structure of the solar radio emission is a key to understanding of plasma processes in the solar corona. Understanding the nature of the fine structure of radio emission is one of the most important criteria for testing the mechanisms of radio emission. Discussion on the origin of the zebra structure (ZS) has been going on for more than 50 years. Here, we continue a comparative analysis of competing generation mechanisms of the ZS (under conditions of the Double Plasma Resonance (DPR)) and in the model with whistlers based on new data. In most papers it is usually postulated that the DPR mechanism always works if there are fast particles in the magnetic trap. However, it encounters difficulties in explaining the dynamics of the ZS bands. So, works on its improvement began to appear. The whole game goes on the variability of the ratio of magnetic field and density height scales and the tolerance of some plasma turbulence in the source. Here we show that all the main details of the sporadic zebra-structure in many phenomena can be explained within the framework of a unified model of zebra-structure and radio fibers in the interaction of plasma waves with whistlers. The main changes in the zebra-structure bands are caused by the scattering of fast particles on whistlers, leading to a switch of the whistler instability from the normal Doppler effect to the anomalous one. We also tried to clarify the generation mechanism for type II bursts.

The book covers wide field of the Solar Radio Physics and it will be suitable for researchers and graduate students.

ISBN 978-5-02-041191-3

CONTENTS

PREFACE

Solar radio astronomy has been developing for over 70 years. The first steps of research of Solar Radio Bursts are described in the famous monographs by Zheleznyakov (1964) and Kundu (1965). The rapid progress of the Solar radio astronomy was regarded in the excellent textbook by Krüger (1979). The theoretical description of radio emission mechanisms was published by Zheleznyakov (1998) in «*Radiation in Astrophysical Plasmas*». The fine structure of the solar radio emission was regarded in the monograph by Chernov (2011) «*Fine structure of Solar Radio Bursts*».

Recent advances in the study of the solar radio emission fine structure were presented in several reviews (Chernov, 2012, 2016) and monograph (Chernov, 2019, see References in the Introduction).

Here, we continue a comparative analysis of competing gene-ration mechanisms of the zebra pattern (ZP) (under conditions of double plasma resonance and in the model with whistlers) based on new data. The zebra structure has long been recorded in Jupiter's magnetosphere, and here we note major differences from solar observations.

We also tried to clarify the generation mechanism of type II bursts, since a difficult situation has now emerged, when many papers appeared with a detailed investigation of the relationship between shock waves (sources of type II bursts) and coronal mass ejections (CMEs) but without analyzing the mechanisms of radio emission. It is recalled here that the main generation mechanism of type II bursts is related to the Bunemann instability.

This textbook covers wide field of the solar radio physics and it will be suitable for graduate students and researchers.

The authors are grateful to Chinese colleagues for kindly providing spectra from Huairou Station of the National Astronomical Observatory of China (NAOC).

Our gratitude to all co-authors for help in collecting of information and to colleagues for the agreement to demonstrate their published data.

November, 2023

G. P. Chernov
Moscow, Troitsk (IZMIRAN)

Chapter 1
INTRODUCTION

Studies of the fine structure of solar radio bursts are of great importance for both the refinement of the burst generation mechanisms and the diagnostics of the corona plasma. The most intriguing fine structure is undoubtedly the zebra pattern (ZP) in continuous type IV radio bursts. The nature of the ZP has been a subject of wide discussion for more than 30 years. The ZP in the solar radio emission is the simultaneous excitation of waves at many (up to a few tens) of closely spaced, nearly equidistant frequencies. The basic parameters of ZP in the meter wave band are represented in the atlas of Slottje (1981). The historical development of observations and theoretical models is assembled in the review and monograph of Chernov (2006, 2011).

Many recent results were presented in the monograph Chernov (2019) with an emphasis on a comparative analysis of competing generation mechanisms: under conditions of double plasma resonance and in the model with whistlers.

Each new phenomenon provides uncommon parameters of fine structure, and the entire variety of the parameters does not succeed in the statistical systematizing. Just such a situation stimulates many authors to elaborate on new mechanisms. Previously, up to a dozen new mechanisms for the ZP were proposed; their brief analysis was carried out in previous reviews (Chernov, 2012, 2016).

Chapter 2 is devoted to the main features of the ZP model with whistlers, as there are sometimes erroneous references in the literature, mainly when explaining many ZP stripes. A number of properties of the emission and absorption bands seen against the background of the type IV radio continuum (zebra structure) are explained by resonance switching in whistler instabilities for an anisotropic-beam-type distribution function (similar to the fan instability). The whistler instability can switch from a normal to an anomalous Doppler resonance in accordance with the shift of the distribution function maximum during a hollowing of the beam. This effect manifests itself as smooth or abrupt (depending on the whistler energy density) oscillations of the zebra-structure bands

on the dynamical spectrum. Simultaneously, absorption appears at the low-frequency edge of the bands (Chernov, 1996).
Chapter 3 deals with slow drifting radio fibers. So far, no attention has been paid to the isolated fibers that occasionally appear in the meter and decimeter ranges. Here we give and discuss examples of the dynamic spectra of such bursts obtained many years ago. As a generation mechanism for such fibers, the process of interaction of whistlers with Langmuir plasmons was suggested. An analysis of conditions for the realization of this process in solar magnetic arch structures and its efficiency was carried out (Chernov, Fomichev, 2023).

Chapter 4 is devoted to analysis of fine structure differences in the dynamic spectra of moving and stationary type IV radio bursts. For the case of a moving source, the generation mechanism largely depends on the magnetic structure of the source (expanding magnetic arcade or isolated plasma cloud). In this case, the connection with coronal mass ejections and shock waves is also important. Second pulsations are explained by MHD oscillations of the source in the form of a magnetic loop or a cloud. The absence of other fine structures in the continuum of moving type IV bursts may be due to the critical angle of the loss cone for the excitation of whistlers (Fomichev, Chernov, 2023).

Chapter 5 is devoted to the main generation mechanism of type II radio bursts. In studies of solar radio bursts of type II, a difficult situation has now emerged, where many papers appeared with a detailed investigation of the relationship between shock waves (sources of type II bursts) and coronal mass ejections (CMEs), but without analyzing the mechanisms of radio emission, without which it is impossible to understand the fragmented structure of the dynamic spectra and the connection between type II bursts in the meter range and type II interplanetary bursts (in dkm and km wavelengths). Here, the model of the radio source is based on the generation of radio emission within the front of the collisionless shock wave where the Buneman instability of plasma waves is developed. In the frame of this model, the Alfven magnetic Mach number must exceed the critical value, and there is a strict restriction on the perpendicularity of the front. Estimations of the critical Mach numbers for the ordinary plasma parameters in solar flares give values M_{cr} 1.1–1.3 easily realized in the flare events. The model allows us to obtain information about the parameters of the

shock waves and the medium by the parameters of type II bursts. The estimates, obtained in this paper for several events with the band-splitting of the fundamental and harmonic emission bands, confirm the necessary conditions of the model. This mechanism allows to explain all the main parameters of radio bursts including the fine structure (Chernov, Fomichev, 2021).

Chapter 6 gives the analysis of a series of works to improve the mechanism on improving the zebra model on DPR in the background of complex spectra in comparison with the whistler model.

The DPR mechanism encounters difficulties in explaining the dynamics of the ZS bands (sharp change in the frequency drift of the bands, a large number of harmonics, frequency splitting of the bands, their ultra-thin structure in the form of millisecond spikes, the transition of radio fibers into zebra stripes and back). So, works on its improvement began to appear (mostly in a dozen papers by Karlicky and Yasnov). The whole game goes on the variability of the ratio of magnetic field and density height scales and the tolerance of some plasΔma turbulence in the source. This already indicates unsuitability of the DPR model. Several phenomena are known in which it is clear that the ratio of height scales does not change in the ZS loop-source. It was noted earlier that the realization of the DPR at many harmonics of the cyclotron frequency is not realized for any models of the density and magnetic field in the corona (Chernov, 2019, p. 215–220). It was shown that all the main details of the sporadic zebra-structure in the August 1, 2010 phenomenon (and in many other phenomena) can be explained within the framework of a unified model of zebra-structure and radio fibers in the interaction of plasma waves with whistlers. The main changes in the zebra-structure bands are caused by the scattering of fast particles on whistlers, leading to a switch of the whistler instability from the normal Doppler effect to the anomalous one.

References

Chernov G. P., 1996. A Manifestation of Quasilinear Diffusion in Whistlers in the Fine Structure of Type IV Solar Radio Bursts // Astronomy Reports. Vol. 40, No. 4. P. 561–568.

Chernov G. P., 2006. Solar radio bursts with drifting stripes in emission and absorption // Space Sci. Rev. Vol. 127, No. 195.

Chernov G. P., 2011. Fine structure of solar radio bursts. Heidelberg: Springer ASSL. Vol. 375. https://doi.org/10.1007/978-3-642-20015-1. http://adsabs.harvard.edu/abs/ 2011fssr.book

Chernov G. P., 2012. Complex Radio Zebra Patterns escaping from the Solar Corona and New Generation Mechanisms // Horizons in World Physics. Vol. 278 / Eds. Albert Reiner, Nova Science Publisher. New York. Ch. 1. P. 1–75. https://www.novapublishers.com/catalog/product_info.php?products_id=30998

Chernov G. P., 2016 // Solar Flares: Investigations and Selected Research. Ed. By Sarah L. Jones. Nova Science Publishers. Ch. 5: Latest News on Zebra Patterns in the Solar Radio Emission. P. 101–150. https://lccn.loc.gov/2016041838

Gennady Chernov, 2019. Latest Data on the fine Structure in Solar radio Emission. LAMBERT Academic Publishing, Book Market Service Ltd. Beau Bassin, Mauritius. 294 p. https://www.morebooks.de/store/gb/book/latest-data-on-the-fine-structure-in-solar-radio-emission/isbn/978-620-0-00165-8

Chernov G. P., Fomichev V. V., 2021. On the issue of the origin of type II solar radio bursts // The Astrophysical Journal. Vol. 922, No. 82. 11 p. https: //doi.org/10.3847/1538–4357/ac1f32

Chernov G. P., Fomichev V. V., 2023. Slowly drifting radio fibres. MNRAS. Vol. 522. P. 1930–1938.

Fomichev V. V., Chernov G. P., 2020. Termination Shock as a Source of Unusual Solar Radio Bursts // Ap. J. 901:65.9 p. September 20. / doi.org/10.3847/1538-4357/abad9f

Fomichev V. V., Chernov G. P., 2023. Fine Structure of type IV solar radio bursts, connected with stationary and moving sources // Geomagnetism and Aeronomy. Vol. 63, No. 2. P. 153–160.

Karlický M., 2013 // Astron. Astrophys. Vol. 552, A90.

Krüger A., 1979 // Introduction to Solar radio astronomy and radio physics. D. Reidel Publ. Comp. P. 128.

Kundu M., 1965 // Solar Radio Astronomy. New York: Interscience.

Slottje C., 1981 // Atlas of fine structures of dynamic spectra of Solar type IV -dm and some type II bursts. Utrecht Observatory.

Zheleznyakov V. V., 1964 // Radio Emission of the Sun and Planets (in Russ.). Moscow: Nauka (Engl. transl. Oxford: Pergamon Press, 1970).

Zheleznyakov V. V., 1998 // Radiation in Astrophysical Plasmas. Dordrecht: Kluwer Academic Publisher (Engl. transl. of Russ. Moscow: Nauka, 1977).

Chapter 2
MANIFESTATION OF QUASI–LINEAR DIFFUSION IN WHISTLERS IN THE FINE STRUCTURE OF TYPE IV SOLAR RADIO BURSTS

Abstract. A number of properties of the emission and absorption bands seen against the background of the type IV radio continuum (zebra structure) are explained by resonance switching in whistler instabilities for an anisotropic-beam type distribution function (similar to the fan instability). There should be continuous diffusion in whistlers when there is a prolonged injection of particles. The instability can switch from a normal to an anomalous Doppler resonance in accordance with the shift of the distribution function maximum during a hollowing of the beam. This effect manifests itself as smooth or abrupt (depending on the whistler energy density) oscillations of the zebra-structure bands on the dynamical spectrum. Simultaneously, absorption appears at the low-frequency edge of the bands, since the instability of plasma waves within the whistler wave packet instantaneously decreases due to diffusion.

2.1. Introduction

The sources of type IV solar radio bursts are magnetic traps in which a loss-con distribution of energetic particles forms, exciting high-frequency (plasma) and low-frequency waves, in particular, whistlers. Emission and absorption bands against the background of the type IV continuum are conventionally divided into two types: zebra structure, observed at meter wavelengths (<300 MHz), with a predominantly positive frequency drift, and fiber bursts (intermediate drift bursts, IDB), with a negative drift (Slottje, 1981).

The radio emission (t) of IDB fibers is unambiguously associated with the merging of plasma waves (l) with whistlers (w): $l + w \rightarrow t$ (Kuijpers, 1975). The absorption accompanying every fiber at the low-frequency edge is explained by the efficient removal of plasma waves by the process $l + w \rightarrow t$ or by screening of the radio emission by density inhomogeneities (Kuijpers, 1975; Mann et al., 1987).

The most common mechanism proposed for the zebra structure is emission in bands at double-plasma-resonance (Zheleznyakov,

Zlotnik, 1975) and related schemes (Mollwo, 1988; Winglee, Dulk, 1986); in nearly all such mechanisms, the origin of the absorption between the bands of enhanced emission is not considered. The most substantial inconsistency of double-plasma-resonance mechanisms is that they require a rapid time variation of the magnetic field to explain the dynamics of the zebra structure bands, while very low magnetic field strengths are implied by the approximate equality of the frequency separation of the bands (Δf) and of the electron gyrofrequency (f_{ce}). As a rule, the implied magnetic field strengths (H) in the source vary irregularly with height in the corona (Slottje, 1981), and are considerably lower than those required for the magnetic pressure to be greater than the kinetic pressure ($\beta < 1$), which is a condition for the existence of a magnetic trap.

In most of their basic parameters, however, zebra structure bands and IDB fibers display notable similarities: they have the same frequency separation between bands (Slottje, 1981), location for the absorption at the low-frequency edge, and depth of continuum modulation. They also both have strong polarization, corresponding to the ordinary wave (Chernov, 1976a). The collected observational data suggest that the zebra structure bands and IDB fibers are related, and that their origin can be explained by a common mechanism– the interaction of plasma waves with whistlers: $l + w \rightarrow t$ (Chernov, 1976b). The fibers are likely associated with channeled propagation of whistlers from the depths of the corona along a trap, while the zebra structure is associated with non-channeled propagation oblique to the magnetic field, mainly at the top of the trap (Mal'tseva, Chernov, 1989). Long-term spectral fine structure observations reveal a number of features that cannot be easily described in the framework of proposed mechanisms for the zebra structure. For instance, in a number of events, we observed quasi-parallel bands with a wavelike frequency drift (Fig. 2.1); a continuous transition of zebra-structure bands with wave-like drifts to typical IDB fibers with constant negative drift; or strange fibers in type II bursts, similar to the zebra structure, but without absorption at the low-frequency edge. We do not yet have a satisfactory explanation for the absorption at the low-frequency edge of the enhanced emission bands.

We show in this paper that these previously unexplainable features, as well as a number of basic properties of the zebra structure and fibers, can be understood in the framework of the $l + w \rightarrow t$ mechanism, but only if we take quasi-linear effects into

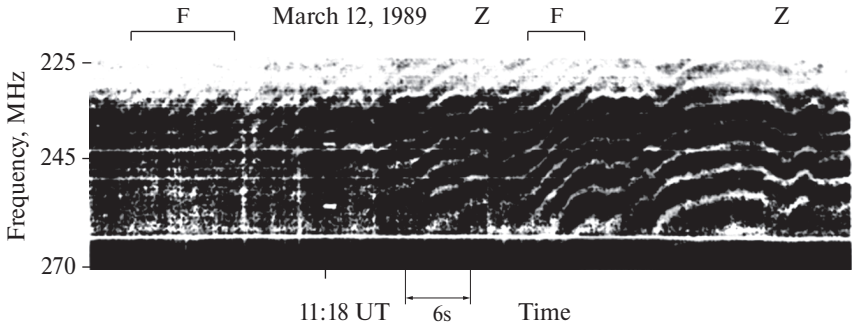

Fig. 2.1. Dynamical spectrum of zebra-structure bands with wave-like frequency drift in the type IV burst of March 12, 1989. The «F» labels above the spectrum refer to the times when zebra-structure bands (Z) with a constant drift toward low frequencies ($df/dt < 0$) become similar to fiber bursts

consideration – the scattering of fast electrons on the whistlers excited by them and on plasma waves (Breizmann, 1987; Omura, Matsumoto, 1987).

In models for the merging of plasma waves with whistlers for fibers with intermediate frequency drift (IDB fibers), quasi-linear effects have been used to explain the periodic excitation of whistlers (Kuijpers, 1975). In some models, the passage of electrons into the loss cone during interaction with whistlers and the formation of an electron distribution with a «gap» have been employed to explain pulsations of the radio emission (Yao, 1985). For the moderate and strong diffusion that is most likely to occur in solar magnetic traps, however, finer features of the dynamics of the loss-cone distribution function should also appear in the radio emission. The particles could be accelerated both by electric fields in the explosive phase of a flare and by shock waves at large heights in the corona. At the top of the trap (especially for small bottle ratios), a distribution of electrons can form in which the longitudinal velocities exceed the transverse velocities ($\upsilon_{||} > \upsilon_{\perp}$) and the loss-cone angles are moderate. Such distributions excite whistlers at arbitrary angles to the magnetic field (Kennel, 1966; Yip, 1970).

The possibility of non-longitudinal wave propagation considerably broadens the energy range of the electrons interacting with whistlers in a given frequency band; this is so because, in this case, diffusion takes place not only in the normal Doppler effect

(conventionally used for longitudinal propagation), but also in the anomalous Doppler effect and Cherenkov resonance (Bespalov, Trakhtengerts, 1986; Shapiro, Shevchenko, 1987). Real hollow-beam distributions have been directly measured at the fronts of interplanetary shock waves (Potter, 1981).

2.2. Formulation of the problem

Numerous data has been accumulated from theoretical and numerical studies of wave-particle interaction, mainly aimed at explaining satellite and ground-based observations of magnetospheric whistlers (Breizmann, 1987; Omura, Matsumoto, 1987; Kennel, 1966; Bespalov, Trakhtengerts, 1986; Shapiro, Shevchenko, 1987; Trakhtengerts, 1984; Gendrin, 1981; Ossakov et al., 1973; Ossakov et al., 1972). In fact, these results have not been applied to the interpretation of solar phenomena, although whistlers are widely used to explain the fine structure of solar radio bursts.

In this work, we explore the possibility of applying known theoretical and numerical results on wave-particle interactions to the conditions in the solar corona. The most complete numerical simulations, which included both whistlers and electrostatic (plasma) waves, were carried out by Omura and Matsumoto (1987) using a distribution function in the form of a monoenergetic and warm beam with a loss-cone. Such beams may also be typical for energetic particles captured in solar magnetic traps which are sources of type IV bursts. Under the conditions of moderate or strong diffusion occurring in whistlers (typical for the solar corona), the lifetime of fast electrons is ~10 min, which is comparable to the duration of series of the radio emission fine structure (Bespalov, Trakhtengerts, 1986). Omura and Matsumoto (1987) showed that diffusion in whistlers and plasma waves is separated in time. Initially, there is energy diffusion in plasma waves (hollowing of the beam); however, it is known that nonlinear effects can damp the plasma wave instability (Stepanov, 1985). At the second stage, there is diffusion in whistlers, primarily in angle. It is important to note here that only a small fraction of the particles fall into the loss cone (Omura, Matsumoto, 1987; Ossakov et al., 1987), and the instability may be supported by a series of particle bounces between the ends of the magnetic traps.

After discussing general aspects of the quasi-linear theory in Section 2.3, we chose a distribution function in the form of

an anisotropic beam (2.8, see after Fig. 2.2) and investigated its possible dynamics during diffusion in whistlers; this investigation is based on Gendrin (1981), the results of which are fully applicable to conditions in the solar corona. Below, this analysis, together with the numerical simulations of Omura and Matsumoto (1987), the analytical results of Breizmann (1987), and the theory of fan instability in whistlers of Shapiro and Shevchenko (1987), allows us to qualitatively show that it is possible for a whistler instability to switch from a normal Doppler resonance to an anomalous resonance during diffusion. Thus, without solving a new quasi-linear problem, we will attempt to estimate possible manifestations of these effects in the fine structure of solar radio bursts.

In Section 2.4, we apply the necessary numerical estimates to the conditions in the solar corona. It is usually assumed that the energy release in sources of type IV bursts is extended, which eases the problem of replenishment of the distribution function during diffusion by both bounces in the trap and periodic injection of new particles.

In Section 2.5, we show that only by taking into account the diffusion of fast particles in whistlers and plasma waves it is possible to explain naturally the most controversial observational fact– the formation of absorption in the continuum between bands of enhanced emission.

2.3. Some aspects of the quasi-linear theory

It is known that the spectra of naturally-excited whistler waves satisfy the validity condition of the quasi-linear approximation, in which particles wander in a multiple-wave field. Essentially, the spectrum ($\Delta\omega^w$) must be rather broad and the relative amplitude of the wave must be modest (Bespalov, Trakhtengerts, 1986; Trakhtengerts, 1984; Karpman, Shklyar, 1976):

$$\Delta\omega^w \gg [(H^w/H_0)\, k\omega_{ce} v_\perp]^{1/2}, \qquad (2.1)$$

where H^w/H_0 is the relative amplitude of the magnetic field of the wave, k is the wave number, ω_{ce} is the electron gyrofrequency, and $\upsilon_\perp$ is the electron velocity component transverse to the magnetic field. Condition (2.1) is better satisfied by solar whistlers than by magnetospheric whistlers. For example, for typical values of $H^w/H_0 \sim 10^{-4}$, $\omega^w/\omega_{ce} \sim 0.1$, and an approximate equality of the wave phase velocity ω^w/k, and $\upsilon_\perp$ we obtain from (2.1) $\Delta\omega^w/\omega^w > 3 \times$

$\times 10^{-2}$. For the inverse inequality to (2.1), the particle is completely trapped in the wave field (Trakhtengerts, 1984). Note that loss-cone instability yields whistler spectra bounded above, $\Delta\omega^w/\omega^w < < 0.1–0.2$, excluding significant group spreading of the whistlers over several seconds of propagation in the corona.

If a fast particle interacts with whistlers at the cyclotron resonance

$$\omega^w - k||v|| - s\omega_{ce} = 0 \tag{2.2}$$

($k_{||}$ and $v_{||}$ are components of the wave vector and velocity parallel to the magnetic field), it moves along the diffusion curves

$$\upsilon_\perp^2 + (v_{||} - \omega^w/k_{||})^2 = \text{const} \tag{2.3}$$

in the direction of decrease of the distribution function $F(\upsilon_\perp, v_{||})$ (Gendrin, 1981). If the resulting flux of particles in velocity space is directed toward increasing particle energy, energy in the given range of velocities will be transferred from resonant waves to particles, and the wave will weaken. This physical process finds its theoretical reflection in the identity operator [which has the meaning of a derivative along the curve (2.3)] in formulas for the whistler instability increment γ^w and the distribution function diffusion equation (Gendrin, 1981; Gul'el'mli, 1979):

$$\hat{\Lambda} = (s\omega_{ce}/\omega\upsilon_\perp)\,(\partial/\partial\upsilon_\perp) + (k_{||}/\omega)\,(\partial/\partial v_{||})\,|\,v_{||} = (\omega - s\omega_{ce})/k_{||}. \tag{2.4}$$

According to Bespalov, Trakhtengerts (1986) and Gul'el'mli (1979), the general expressions for γ^w and $\partial F/\partial t$ have the form

$$\gamma^w = 8\pi^3\left(\omega/k_\parallel\right)\left(n^h/n^c\right)\sum_{s=0,\pm1}\int d\upsilon^3 G_{ks}\,\delta\left(\omega - k_\parallel\upsilon_\parallel - s\omega\right)\hat{\Lambda}F, \tag{2.5}$$

$$\partial F/\partial t = \upsilon_\perp^{-1}\hat{\Lambda}\{\upsilon_\perp G_{ks}\hat{\Lambda}F\}, \tag{2.6}$$

where n^h/n^c is the relative number density of hot and cold particles and G_{ks} is a weighting function defining the emission contribution per particle per whistler wave. The sign of the increment depends on the sign of the operator $\hat{\Lambda}$. For example, in the normal Doppler resonance, when $s = +1$ in (2.2), the waves and particles are oppositely directed ($k_{||} < 0$ or $\omega/k_\parallel < 0$), and should be negative for positive values of the operator γ^w. Therefore, the dominant contribution to the emission comes from the part of the

distribution where $\partial F/\partial v_{||} < 0$ and $\partial F/\partial \upsilon_{\perp} > 0$. The contribution to the anomalous Doppler instability ($s = -1$ in (2.2)) comes from particles in the part of the distribution where the signs of these derivatives are opposite. Therefore, whether the predominant instabilities are in normal or anomalous resonances, will depend on whether there is an excess of particles with $\upsilon_{\perp}$ or $v_{||}$, respectively.

The operator $\hat{\Lambda}$ can be simply expressed in terms of the derivative of the distribution function with respect to the particle energy $\partial F/\partial E$ (Gendrin, 1981):

$$\hat{\Lambda} \sim 2\upsilon_{\perp}\upsilon_{p}\partial F/\partial E\,|E \sim \upsilon_{\perp}^{2} + \upsilon_{\|}^{2};\upsilon_{p} = \omega/k_{\|}. \quad (2.7)$$

This relationship implies that, for positive increments, the derivative $\partial F/\partial E$ should be positive for motion in the direction of decreasing F. This in turn means that the diffusion curve (D) should lie between the constant-density curve (F) and the constant-energy circle (E) (Gendrin, 1981). This relation and the physical meaning of the diffusion interaction are visually depicted by the graphical determination of the increment signs for different resonances presented in Fig. 2.2 for an anisotropic beam distribution function

$$F\left(\upsilon_{\perp},\upsilon_{\|}\right) = C_{n}\upsilon_{\perp}^{j}\exp\left[-\left(m_{e}\upsilon_{\perp}^{2}/2kT_{\perp}\right) - \right. \\ \left. -\left(m_{e}\left(\upsilon_{\|} - \upsilon_{\perp}\right)^{2}/\,2kT_{\perp}\right)\right], \quad (2.8)$$

where C_n is a normalization constant and j is the loss-cone index.

Quasi-linear diffusion establishes a plateau along the diffusion line, i.e., $\hat{\Lambda} = 0$ (by analogy with the plateau state in the quasi-linear theory of plasma oscillations (Galeev, Sagdeev, 1973). Interaction in the normal resonance leads to the passage of particles into the loss cone (Ossakov et al., 1973; Karpman, Shklyar, 1976). In the anomalous Doppler effect, the longitudinal velocities are hollowed out of a beam-type distribution (2.8), but the particles do not fall into the loss cone; instead, they diffuse in pitch angle toward high $\upsilon_{\perp}$ (Shapiro, Shevchenko, 1987; Lyons, Williams, 1984).

During the lifetimes of particles in a trap in the moderate and strong diffusion whistler modes (several tens of seconds for solar magnetic traps (Bespalov, Trakhtengerts, 1986; Bespalov et al., 1987)), the loss cone is emptied twice during each bounce period. Therefore, after a short period of particle injection, the instability

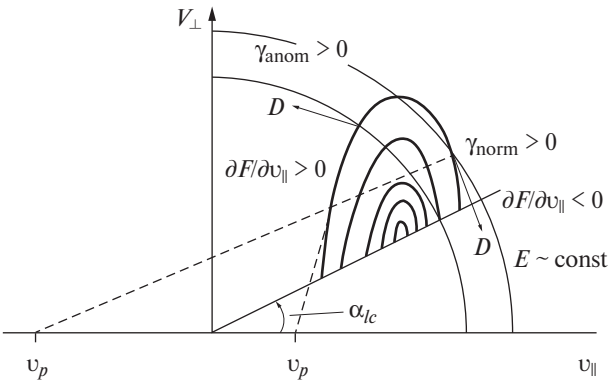

Fig. 2.2. An anisotropic-beam type (2.8) distribution function (F) in the ($\upsilon_{||}$,) plane with loss cone α_{lc}. Thin circular lines denote levels of constant particle energy E. Arrows labelled D indicate the direction of particle diffusion toward decreasing F. Thick lines are levels of equal density of F. v_p is the phase velocity, $\gamma_{anom} > 0$ is the domain of anomalous Doppler whistler instability, and $\gamma_{norm} > 0$ is the region of normal Doppler resonance instability

for both normal and anomalous resonance will be periodic, with a period (tp) of the order of a second: for a trap length $l \sim 10^{10}$ cm and velocity $v \sim 10^{10}$ cm/s, we obtain $tp \sim (1/2)(l/v) \sim 0.5$ s.

The abnormal-resonance instability favors the confinement of particles in the trap. This confinement probably explains the longer sequences of zebra structure caused by anomalous-resonance whistler instability compared to those of IDB fibers, due to normal-resonance whistlers.

The above effects allow us to estimate the importance of alternating switch-on of whistler instabilities due to the normal and anomalous Doppler effects, if the distribution function can support this dynamic transition. Two such distribution functions are an anisotropic high-energy beam (2.8), which can form in shock fronts (Wu, 1984), or a ring distribution (Vlahos, Sprangle, 1987). The loss-cone anisotropy of these distributions is determined by the acceleration mechanism – reflection from magnetic mirrors (shock fronts). Whistler instability has primarily been considered for longitudinal propagation in the normal Doppler effect (Kuijpers, 1975; Kennel, 1966; Berney, Benz, 1978). It is known, however, that the contributions from all three resonances ($s = 0, \pm 1$) to the instability are comparable for oblique propagation (Kennel, 1966).

Shapiro and Shevchenko (1987) considered a turn of the beam in transverse velocity for the anomalous resonance, termed the fan instability. An initial distribution function in the form of a beam in longitudinal velocity turns in transverse velocity as a result of the excitation of oscillations and quasi-linear diffusion; a new distribution function in the form of a beam in transverse velocity is established, if $\omega/k_{\|} < v_{\|}$. In our case, this last inequality is fulfilled even more strictly. In addition, this is one of the conditions for excitation of whistler waves in the anomalous resonance.

An initial distribution function in the form of a beam in longitudinal velocity is most probable under the conditions of multiple, repeated flare processes at large coronal heights during large-scale events. The unusual properties of the zebra structure (Fig. 2.1) can be understood in the framework of a mechanism of periodic whistler instability. The analog of fan instability considered above provides smooth (or rapid) switching of the instability from the anomalous to the normal Doppler resonance, which implies a smooth (or abrupt) change of the frequency drift of the zebra-structure bands. The frequency drift is determined by the direction of the whistler group velocity. In the anomalous resonance, the directions of the waves and particles coincide, while in the normal resonance, they move in opposite directions. The character of the fan instability will depend on the specific parameters of the plasma and beam.

2.4. Numerical estimates

The complete solution of the quasi-linear problem for the three resonances with particle sources and losses is very difficult, and has not yet been obtained either analytically or numerically. Usually, a simplified problem is posed, and quasi-linear equations are solved numerically for one resonance and one oscillation mode with a loss-cone distribution function (Ossakov, 1972; Ashour-Abdalla, 1972). In addition to the known effects of the passage of slower particles into the loss cone and the formation of a «gap» in the distribution, the calculations in (Ossakov et al., 1973; Ossakov et al., 1972) also showed a simple shift of the distribution function maximum toward the initial loss cone for large velocities.

Periodic fan instability in a self-oscillatory mode was first considered in (Parail, Pogutse, 1981) in the framework of a theory of microwave spikes with millisecond periods; this analysis was

based on instability switching from the Cherenkov to the normal resonance for tokamak plasma parameters, which are far from cosmic parameters.

The condition for switch-on of the self-oscillatory mode obtained in (Parail, Pogutse, 1981) indicates that the increments for both resonances are comparable if there is sufficient beam temperature anisotropy and if the longitudinal velocity source power is moderate, so that particles cannot instantaneously leave the emission region. In our case, these conditions are fulfilled for a hollow-beam distribution function.

It is known that whistler diffusion occurs mainly in the pitch angle. Transforming the expression for $\partial F/\partial t$ to a dependence of the distribution function F on pitch angle α, we obtain a diffusion equation in which the pitch angle diffusion coefficient D_α significantly exceeds the velocity diffusion coefficients when $v \gg \omega/k_\parallel$, which is satisfied in our case. According to Kennel (1969), the coefficient D_α is proportional to the wave energy:

$$D_\alpha \sim \left(H^w/H_0\right)\left(\omega_{ce}/\cos\alpha\right). \qquad (2.9)$$

For a reasonable wave amplitude relative to the background field $H^w/H_0 \sim 10^{-4}$ and $\omega_{ce} \sim 10^7\ \mathrm{s}^{-1}$, we obtain a simple estimate for the timescale for pitch angle diffusion by $\Delta\alpha \sim 1$: $tD = D_\alpha^{-1} \sim 1{-}2$ s.

These values are consistent with the timescales for sign alternation of the zebra-structure band frequency drift in Fig. 2.1. Thus, we indeed observe the diffusion of fast electrons in whistlers in the radio emission fine structure.

The most complete numerical simulation of whistler diffusion of a beam with conical anisotropy in the normal Doppler resonance has been carried out by Omura and Matsumoto (1987). Fig. 5 in Omura and Matsumoto (1987) shows the initial values of the volume and planar distribution functions $F(v_\perp, v_\parallel)$, the linear increment γ, and the distribution height at the beam center. This figure also shows the hollowing of F in pitch angle. It is important to note that, when F is hollowed in $v_\perp$, a beam in the longitudinal velocities is formed in time $t \sim 1300\omega_{ce}^{-1}$: $\partial F/\partial v_\parallel > 0$.

Thus, the term $\partial F/\partial v_\parallel$ in operator $\hat{\Lambda}$ in (2.4) remains positive, the operator $\hat{\Lambda}$ in (2.5) and (2.6) will be non-zero, and diffusion toward increasing $v_\perp$ will continue, but in the anomalous Doppler resonance. As can be seen from Fig. 5 in Omura and Matsumoto

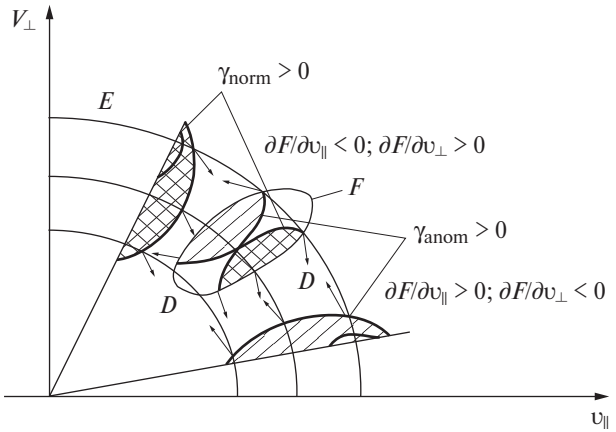

Fig. 2.3. Schematic presentation of the fan instability – switching of whistler instability from normal Doppler cyclotron resonance (cross-hatched F regions) to anomalous resonance (single-hatched regions) due to the shift of the maximum (bump) of the distribution function F during diffusion along the diffusion curves D (arrows) from large values of $v_\perp$ (where the operator $\hat{\Lambda} < 0$) to large $v_\parallel$ (where $\hat{\Lambda} > 0$)

(1987), the wave gradually weakens (decreases with spreading of the beam in pitch angle). Since only a small fraction of the slowest particles falls into the loss-cone, however, the resonance switching can repeat many times, as in the tokamak spike mode (Parail, Pogutse, 1981). Particle replenishment will occur through bounce motions in the trap; if the particles arrive in phase with the growth of the longitudinal velocity bump (i.e., at the moment of alternation of the sign of the frequency drift), the instability will be sharply enhanced. We probably observe this effect when we detect short zebra-structure spikes in the dynamical spectra in some events, seen as herring-bone structures over a broad frequency range.

The beam relaxation time-scale $t_{rel} \sim \gamma^{-1}$ in Omura and Matsumoto (1987) is of the order of 3000 ω_{ce}^{-1}. Correcting for coronal plasma and beam parameters (plasma frequency ratio $\omega_{pe}/\omega_{ce} \sim 20$, $n^h/n^c \sim 10^{-6}$), this time-scale should be about $3 \cdot 10^7$ gyro-periods (in Omura and Matsumoto (1987) $n^h/n^c \sim 10^{-2}$, $\omega_{pe}/\omega_{ce} \sim 2$). For a gyrofrequency of $\sim 5 \cdot 10^7$ Hz, we obtain $t_{rel} \sim 0.8$ s, which is close to our estimate of the diffusion timescale $t_D \sim 1$ s.

An initial distribution in the form of a beam with conical anisotropy (2.8) will be unstable to both normal and anomalous

resonances. The regions of positive increment instability determined from Fig. 2.2 are shaded in Fig. 2.3. The cross-hatched areas refer to particles that are unstable to the normal resonance ($\gamma_{norm} > 0$, where $\partial F/\partial v_{\|} < 0$, and $\partial F/\partial v_{\|} > 0$), and the single-hatched areas refer to those unstable to the anomalous Doppler resonance ($\gamma_{anom} > 0$, where $\partial F/\partial v_{\|} > 0$, and $\partial F/\partial v_{\|} < 0$). According to the calculations of Omura and Matsumoto (1987), the beam will empty in pitch angle. The gradual diffusive accumulation of particles with maximum F along $v_{\|}$ (later along $v_{\|}$) will mean a gradual switching of the instability from anomalous to normal resonance. Fig. 2.3 schematically shows the shapes of the distribution at small and large pitch angles for two such times. Pitch angles close to 90° cannot be reached when there is particle motion with conservation of the first adiabatic invariant. At a qualitative level, we can say that when there is a large particle number density in the beam, diffusion will be rapid and resonance switching (alternation of the sign of the frequency drift) will be abrupt.

2.5. Formation of absorption between emitting filaments

The origin of the absorption usually accompanying the fibers and zebra structure at the low-frequency edge is a very nontrivial question, often bypassed by many authors. For example, the double plasma resonance mechanism produces only emission bands (Kuijpers, 1975; Zheleznyakov, Zlotnik, 1975; Winglee, Dulk, 1986). In the whistler fiber model, it was assumed without proper detailed analysis that plasma waves within the whistler wave packet volume are efficiently evacuated in the process of merging with whistlers, $l + w \to t$, and only residual l-waves scattered on thermal ions result in a decreased continuum level (Kuijpers, 1975; Chernov, 1976b).

A more concrete basis for this effect can only be associated with the evacuation of resonant l-waves with small wave numbers k_l in the process $l + w \to t$, which are achieved in the course of the differential scattering of l-waves. The maximum transformation to electromagnetic radiation takes place precisely at low kl, since, according to Tsytovich (1967), the rate of growth of the radio emission is

$$\partial W^t/\partial t = \alpha^{li} W^t \left[\left(W^l/k^l + \left(\partial W^l/\partial k^l\right)\right]\right., \qquad (2.10)$$

where W^t and W^l are the energy densities of electromagnetic and plasma waves and α^{li} is a transformation coefficient. For small k^l, the dominant term in the brackets is W^l/k^l. Small k^l are also resonant in the process $l + w \to t$, however. Turning to quantitative estimates, only $\sim 10^{-2}$–10^{-3} Wl is transformed to electromagnetic waves in a source that is optically thick to the process $l + w \to t$. Detection of such weak absorption is at the resolution limit of spectrographs.

Another explanation of absorption is based on the assumption that the radio emission is screened by plasma-density enhancements created by the whistler wave packet (Mann, 1987; Bernold, Treumann 1983). However, simple estimates show that the creation of a one-percent plasma density enhancement requires the improbably high relative density of whistler energy $W^w/n_eT_e \sim \sim 10^{-3}$, while the values achieved by weak turbulence are five orders of magnitude lower (Kuijpers, 1975; Fomichev, Fainshtein, 1988).

In relation to this, we will consider the role of quasi-linear effects. First of all, it is natural to adopt a Maxwellian distribution function with loss-cone anisotropy for the electrons responsible for type IV continuum emission (Kuijpers, 1975; Winglee, Dulk, 1986). Since this distribution is unstable to whistlers, we must take into account the influence exerted by the diffusion of fast particles in whistlers to plasma wave excitation.

For large loss-cone angles ($v_\parallel > v_\parallel$), the main contribution to whistler instability is given by the normal Doppler resonance for longitudinal propagation ($k^w \parallel H_0$). In this case, plasma waves with the maximum increment are excited at the double plasma resonance frequency for quasi-transverse propagation ($k^w \parallel H_0$) (Stepanov, 1985; Fomichev, Fainshtein, 1988). This situation is characteristic for the bases of magnetic traps (for heights at decimeter emission wavelengths). Because of the diffusion of fast particles on whistlers, the distribution function maximum instantaneously shifts toward greater longitudinal velocities (Omura, Matsumoto, 1987) and smaller pitch angles. As a result, the plasma-wave instability sharply weakens, because the l-wave excitation increment at the upper hybrid frequency is several times more sensitive to changes of the loss-cone angle αlc than are whistlers. A comparison of Figs. 3 and 8 in Berney and Benz (1978) shows that the increments γw and γl are nearly equal for $\alpha_{lc} \approx 10°$, while for $\approx 2 \cdot 10^{-5}\omega_{ce}$, we have $\gamma_l \approx 5\gamma^w$. This decrease of γ^l with decreasing α_{lc} is the main cause of continuum suppression within the whistler wave packet volume.

As in the first hypothesis, the zebra-emission band will lie at a higher frequency $\omega^t = \omega^l + \omega^w$.

The calculations of (Omura, Matsumoto, 1987; Ossakov et al., 1973; Ashour-Abdalla, 1972) obviously show that a gap distribution with positive derivative $\partial F/\partial v_\parallel$ is formed in the course of diffusion in the normal Doppler resonance. Melrose (1975) was the first to stress the importance of this effect in astrophysical plasma. The minimum velocity at which the beam forms is determined by the minimum frequency in the whistler spectrum, in accordance with the resonance condition (2.2). For typical values $k_\parallel \sim \omega_{pe}/c$ (c is the velocity of light) and $\omega/\omega_{ce} \sim 0.1$, we obtain $v_\parallel \approx 43 v_A$ (v_A is the Alfvenic velocity). A beam with such velocities efficiently excites plasma waves along the field ($k_\parallel^l H_0$) in the Cherenkov resonance. Therefore, the emission of plasma waves (and, consequently, of radio continuum) will be enhanced in regions adjacent to the whistler wave packet, amplifying the contrast of the continuum depression along the low-frequency edge of the fiber. This scheme offers a natural explanation for the continuum enhancement usually observed in a series of fibers and zebra structure (Aurass, Chernov, 1983).

If the initial whistler diffusion proceeds in the anomalous Doppler resonance in «oblique» whistlers (when $v_\parallel > v_\perp$) and the plasma waves have $k^l \| H_0$, the plasma-wave level will also be reduced because of the beam turn in transverse velocity. The plasma-wave instability at the upper hybrid frequency will gradually grow, also increasing the absorption contrast.

Thus, in any case, the reduction of the plasma-wave level due to electron diffusion on whistlers can explain the absorption at the low-frequency edge of a fiber. Another important observational fact is simultaneously explained: the small delay of the beginning of the emission band relative to that of the absorption in fibers (see Fig. 2 in Bernold, Treumann, 1983).

According to the arguments above, the weakening of plasma waves should begin instantaneously, and the merging mechanism at the combined frequency $\omega^t = \omega^l + \omega^w$ requires, according to conservation laws, either oppositely directed or nearly aligned wave vectors and in order for decay at the difference frequency $\omega^t = \omega^l - \omega^w$ to take place (Chernov, Fomichev, 1989).

Therefore, in any case, some time is needed for the isotropization of the wave vectors. While the plasma waves become isotropic nearly

immediately, whistlers undergo comparatively slow scattering on thermal electrons, and especially on thermal ions (Tsytovich, 1971). According to estimates given in Chernov (1989), this time should be ~0.2–0.3 s. Radio flux fluctuations in both emission and absorption on profiles along fibers occur on nearly the same timescales; these fluctuations could also be associated with the quasi-linear diffusion of fast particles on whistlers, which proceeds at different rates at different levels in the trap during the lifetime of a fiber.

In a number of events, we have also observed fiber structure in type II bursts (see, e.g., Fig. 3 in Aurass, Chernov, 1983), associated with the propagation of shock waves through the solar corona. The main peculiarities of these fibers are the absence of any evident absorption at the low-frequency edge and their long duration (up to 40–50 s). Observations of interplanetary shock waves (Richter et al., 1985; Tokar et al., 1984) testify to the presence of plasma waves and whistlers in front of the shock. It is therefore natural to interpret the fiber structure of type II bursts as a manifestation of whistler propagation through clusters of plasma waves ahead of the shock front. Plasma waves and whistlers can be generated only by electrons reflected from the shock and therefore possessing loss-cone anisotropy. However, there cannot be trapped fast particles in front of an oblique, collisionless (in a general case) shock wave, and therefore the interaction of whistlers with fast particles cannot be extended. After each pulse injection of particles, the excited whistlers and fast electrons disperse in space. Judging from the negative frequency drift of fibers, whistlers propagate forward from the front (or remain nearly standing). Therefore, whistlers should be excited in the anomalous Doppler resonance, when the particles and waves propagate in the same direction, but at large angles. Thus, a beam of particles with conical anisotropy escapes along the magnetic force lines, while whistlers propagate at a large angle to the field and, after a certain isotropization, interact with plasma waves. The lack of strict periodicity of fibers is also a consequence of the absence of quasi-linear effects. Without the diffusion of fast particles in whistlers, there should not be any absorption at the low frequency edge of fibers, which is confirmed by observations.

Thus, we have shown that it is natural and necessary to take into account the quasi-linear effects of the diffusion of fast electrons with

loss-cone anisotropy on whistlers; this allows us to explain certain very important properties of fibers with intermediate frequency drifts (IDB or fiber bursts) and the zebra structure in type II and IV solar radio bursts. This analysis demonstrates the suitability of mechanisms for the merging of plasma waves with whistlers to explain the structures considered above.

References

Ashour-Abdalla M., 1972. Amplification of whistler waves in the magnetosphere // Planet. Space Sci. Vol. 20. P. 639–662. https://doi.org/10.1016/0032-0633(72)90151-1

Aurass H., Chernov G. P., 1983. Zebra pattern flux density observations during the type IV burst on October 12, 1981 // Sol. Phys. Vol. 84. P. 339–345. https://doi.org/10.1007/BF00157466

Berney M., Benz A. O., 1978. Plasma lnstabilities of Trapped Particles in Solar Magnetic Fields // Astron. Astrophys. Vol. 65. P. 369–384.

Bernold T. X.B., Treumann R. A., 1983. The fiber fine structure during solar type IV radio bursts: observations and theory of radiation in presence of localized whistler turbulence // Astrophys. J. Vol. 264. P. 677–688.

Bespalov P. A., Trakhtengerts V. Yu., 1986. Al'fvenovskie mazery (Alfvenic Masers), Gor'kii: Inst. of Applied Physics, USSR Acad. Sci. (in Russ.). 189 p.

Bespalov P. A., Zaitsev V. V., Stepanov V. V., 1987. On the origin of time delays in the hard X-ray and gamma-ray // Sol. Phys. Vol. 114. P. 127–140. https://doi.org/10.1007

Breizmann B. N., 1987. Voprosy teorii plazmy (Problems in Plasma Theory) / Ed. B. B. Kadomtsev. Moscow: Energoatomizdat. No. 15. 155 p.

Chernov G. P., 1976a. Microstructure in continuous emission of type IV meter bursts. Observations and model of the source // Soviet Astronomy. Vol. 20. P. 449–459.

Chernov G. P., 1976b. Microstructure in continuous emission of type IV meter bursts. Modulation of continuous emission of wave packets of whistlers // Soviet Astronomy. Vol. 20. P. 582–589.

Chernov G. P., 1989. Behavior of low frequency waves in coronal magnetic traps // Soviet Astronomy. Vol. 33(6). P. 649–655.

Chernov G. P., 1990. Whistlers in the solar corona and their relevance to fine structures of type IV radio emission // Sol. Phys. Vol. 130. P. 75–82.

Chernov G. P., Fomichev V. V., 1989. Testing of conservation laws for the interaction of plasma waves with difference-frequency whistlers in the solar corona // Sov. As. Lett. Vol. 15(5). P. 410–412.

Fomichev V. V., Fainshtein S. M., 1988. Theory of the fine structure of solar type IV radio bursts // Sov. Astron. Vol. 65(5). P. 552–557.

Galeev A. A., Sagdeev R. Z., 1973. Voprosy teorii plazmy (Problems in Plasma Theory) / Ed. M. A. Leontovich. Moscow: Atomizdat, No. 7. P. 3–33.

Gendrin R., 1981. General relationships between wave amplification and particle diffusion in a magnetoplasma // Rev. Geophys. Space Phys. Vol. 19. P. 171–184. https://doi.org/10.1029/RG019i001p00171
Gul'el'mli A.V., 1979. MGD-volny v okolozemnoi plazme (MHD Waves in the Circumterrestrial Plasma). Moscow: Nauka. 139 p.
Karpman V. I., Shklyar D. P., 1976. Particle precipitation caused by a single whistler-mode wave injected into the magnetosphere // Planet. Space Sci. Vol. 25. P. 395–403.
Kennel C. F., 1966. Low-frequency whistler mode // Phys. Fluids. Vol. 9. P. 2190–2202. https://doi.org/10.1063/1.1761588
Kennel C. F., 1969. Consequences of a magnetospheric plasma // Rev. Geophys. Vol. 7. P. 379–419.
Lyons L. R., Williams D. J., 1984. Quantitative Aspects of Magnetospheric Physics. Dordrecht: Reidel (Translated under the title Fizika magnitosfery. Kolichestvennyi podkhod. Moscow: Mir, 1987).
Mal'tseva O.A., Chernov G. P., 1989. Kinetic whistlers growing (decay) in the solar corona // Kinematika Fiz. Nebesnykh Tel. Vol. 5, No. 6. P. 44–54.
Mann G., Karlicky M., Motschmann U., 1987. On the intermediate drift burst model // Sol. Phys. Vol. 110. P. 381–389.
Mollwo L., 1988. The magneto-hydrostatic field in the region of zebra patterns in solar type IV dm-bursts // Sol. Phys. Vol. 116. P. 323–348.
Omura Y., Matsumoto M. J., 1987. Competing processes of whistler and electrostatic instabilities in the magnetosphere // Journal Geophys. Res. Vol. 92. P. 8649–8659. https://doi.org/10.1029/JA092iA08p08649
Ossakov S. L., Ott E., Haber I., 1972. Nonlinear Evolution of Whistler Instabilities // Phys. Fluids. Vol. 15. P. 2314–2326. https://doi.org/10.1063/1.1693875
Ossakov S. L., Ott E., Haber I., 1973. Theory and computer simulation of whistler turbulence and velocity space diffusion in the magnetospheric plasma // J. Geophys. Res. Vol. 78, No. 16. P. 2945–2958. https://doi.org/10.1029/JA078i016p02945
Parail V. V., Pogutse O. P., 1981. Voprosy teorii plazmy (Problems in Plasma Theory) / Ed. B. B. Kadomtsev. Moscow: Atomizdat. No. 11. P. 5–15.
Potter D. W., 1981. Acceleration of electrons by interplanetary shocks //
J. Geophys. Res. Vol. 86. P. 11111–11116. https://doi.org/10.1029/JA086iA13p11111
Richter A. K., Hsich K. C., Luttrell A. H., Marsh E., Schwenn R., 1985. Collisionless Shocks in the Heliosphere: Reviews of Current Research / Eds. B. T. Tsurutani, G. R. Stone. Washington, DC: Amer. Geophys. Union. P. 33.
Shapiro V. D., Shevchenko V. I., 1987. Plasma Turbulence in Space // Itogi Nauki Tekh. Ser. Astronomiya. Vol. 235.

Slottje C., 1981. Atlas of Fine Structures of Dynamic Spectra of Solar Type IV dm and Some Type II Radio Bursts. Dwingeloo. 234 p.

Stepanov A. V., 1985. Theory of the Radio Emission of Coronal Arches, Doctoral (Phys.-Math.): Dissertation. Irkutsk: Siberian Inst. of Terrestrial Magnetism, Aeronomy, and Radiowave Propagation, USSR Acad. Sci. 375 p.

Tokar R. L., Gurnett D. A., Feldmann W. C., 1984. Whistler Mode Turbulence Generated by Electron Beams in Earth's Bow Shock // Geophys. Res. Vol. 89. P. 105–114. DOI:10.1029/ja089ia01p00105

Trakhtengerts V. Yu., 1984. Osnovy fiziki plazmy (Fundamentals of Plasma Physics). Moscow: Energoatomizdat. Vol. 2. 498 p.

Tsytovich V. N., 1967. Nelineinye effekty v plazme (Nonlinear Effects in Plasmas). Moscow: Nauka. 286 p. (Translated: Vadim N. Tsytovich, 1970. Nonlinear Effects in Plasma. New York, NY: Springer. 332 p.)

Tsytovich V. N., 1971. Teoriya turbulentnoi plazmy (Theory of Turbulent Plasma). Moscow: Nauka. 423 p. (Translated: Tsytovich, V.N. 1977. Theory of Turbulent Plasma. Springer US. 535 p.)

Vlahos L., Sprangle P., 1987. Evolution of the axial electron cyclotron maser instability, with applications to solar microwave spikes // Astrophys. J. Vol. 322. P. 463–472. DOI:10.1086/165742

Winglee R. M., Dulk G. A., 1986. The electron-cyclotron maser instability as a source of plasma radiation // Astrophys. J. Vol. 307. P. 808–819. DOI: 10.1086/165742

Wu C. S., 1984. A fast Fermi process: Energetic electrons accelerated by a nearly perpendicular bow shock // J. Geophys. Res. Vol. 89(A10). P. 8847–8862. 10.1029/ja089ia10p08857

Yao Jin-Xing, 1985. A mechanism for pulsation in solar microwave bursts // Chin. Astron. Astrophys. Vol. 9. P. 241–245. https://doi.org/10.1016/0275-1062(85)90045-1

Yip W. K., 1970. Radiation of plasma waves by an electron stream in the solar corona // Aust. J. Phys. Vol. 23. P. 161–176. 10.1071/PH700161

Zheleznyakov V. V., Zlotnik E. Ya., 1975. Cyclotron wave instability in the corona and origin of solar radio emission with fine structure // Sol. Phys. Vol. 43. P. 431–451. DOI:10.1007/BF00153225

Zheleznyakov V. V., Zlotnik E. Ya., 1975. Cyclotron wave instability in the corona and origin of solar radio emission with fine structure III. Origin of zebra pattern // Sol. Phys. Vol. 44. P. 461–470. https://doi.org/10.1007/BF00153225

Chapter 3
SLOWLY DRIFTING RADIO FIBERS

Abstract. The fine structure in the continuum radiation of type IV solar radio bursts is very rich of various structures (zebra-structure, fibers, pulsations, spikes, etc.). But so far, there is no attention to occasionally appearing isolated fibers in the meter and decimeter ranges. Here we give and discuss the examples of dynamic spectra of such bursts obtained many years ago (in the meter waveband from 1969) and as well in recent years (in the decimeter and microwave wavebands from 2003 to 2013). Isolated fibers are observed mostly in the decimeter range (although there are examples in both the meter and microwave ranges), and they reveal a number of features of classical fibers bursts. As a mechanism generation of such fibers the process of interaction of whistlers with Langmuir plasmons was suggested. The analysis of conditions for realization of this process in solar magnetic arch structures and its efficiency was carried out. The estimates of intensity of low frequency turbulence (whistlers) and magnetic field strength in the solar corona were obtained by data of radio fibers.

3.1. Introduction

Observations with the radio spectrographs in meter and decimeter ranges began many years ago (Wild, Smerd, Weiss, 1963). Many characteristics of the solar radio bursts were obtained, including their fine structure, after the publications of Boischot, Haddock and Maxwell (1960) and Elgarøy (1959). With the development of spectral observations in the continuum emission of type IV radio bursts, broadband pulsations of different periods, the fastest spike-type bursts and the most mysterious periodic bands in emission and absorption – zebra structure and fiber-bursts or bursts with intermediate frequency drift were discovered. The development of solar radio astronomy is described in several large monographs, namely Kundu (1965), Zheleznyakov (1964, 1970) and Krüger (1979).

Theoretical models of the origin of the fine structure of type IV continuum radio bursts (zebra-structure, fibers, pulsations, spikes etc.) have been developing for more than 50 years (Chernov, 2006, 2011).

For the zebra structure, the model on the double plasma resonance is most often discussed (although a dozen alternative models have been proposed), and for fibers the model on whistlers. Although the latter immediately combined an explanation of both zebra stripes (with a variety of frequency drift) and fibers (usually with a constant negative frequency drift) on the grounds that observations sometimes showed a continuous transition on the spectrum of zebra stripes to fibers and back (Chernov et al., 1975; Chernov, 1976). At the same time, it was hardly noticed at the beginning that sometimes, instead of numerous zebra stripes or fibers, isolated stripes appeared. Since they were more often observed in the events where there were also numerous stripes, this suggested that the models used should allow the formation of unusual isolated fibers as well. All this was considered in the meter wavelength range. The first spectra of strange isolated slowly drifting fibers in the meter range were shown in (Boischot, Haddock, Maxwell, 1960) even before the first publication of Elgarøy about zebra structure. The authors called the unusual intertwined stripes in the event of November 4, 1957 as «spaghetti», although no one would doubt now that it was a zebra structure, noting after all a singularity: the stripes were not regular in frequency but intertwined with each other, and lasted about 4 minutes in the narrow frequency band 160–175 MHz.

And in about 50 minutes there were single bands, lasting more than a minute with a fluctuating frequency drift, but almost parallel to the time axis. Moreover already then the solar origin of the stripes was confirmed, as their spectra were identical in the two observatories, separated by 2,000 km. We are observing the fine structure of solar radio bursts already in the sixth cycle of solar activity (see https://www.izmiran.ru/stp/lars/). In the top ten works, the spectra obtained in the remote observatories managed to compare, and they always coincided in frequency and time, which confirms the solar nature of bursts (Chernov, 2011).

Slowly drifting fibers have already been recorded in the first observations with the IZMIRAN high-resolution spectrograph in the range 190–220 MHz in 1969 (see Fig. 3 in Markeev, Chernov, 1971 and Fig. 1 in Chernov, 1974) (see also[1] Gorgutsa et al., 2001). These first reports of such bursts were observed in groups

[1] https://www.izmiran.ru/stp/lars/

of fast spike-type bursts during noise storms. The frequency drift of the fiber was on average about 30 MHz/s through the entire range 190–220 MHz, although ordinary spikes usually show no frequency drift and occupy a narrow frequency band of 1–10 MHz. In this work, these bursts are referred to as slow drift spikes. In contrast to type III bursts particle beams must have a non-monotonic distribution of the particle velocity (with increasing velocity to the tail of the beam), which neutralizes the fast frequency drift. The first report of such bursts was in paper by Markeev and Chernov (1970). Furthermore, in several events we observed unusual long fibers (0.5–2 min) non-drifting (almost parallel to the time axis), which are close in parameters to the fibers in the paper by Boischot, Haddock and Maxwell (1960). Here, we show in Fig. 1 a remarkable example of such fibers from IZMIRAN's archive of spectra on the October 12, 1981. This phenomenon has been discussed in various aspects in the works of Aurass and Chernov (1983) and Chernov (1997).

A large radio burst in a wide band was associated with a large Hα flare of magnitude 3B with coordinates S15, E09. Fibers appeared at the very beginning of the phenomenon at 06:26 UT, with the maximum radio burst in the meter band (3000 s.f.u. at 204 MHz) occurring 7 min earlier than the maximum in the microwave band (about 2300 s.f.u. at 3000 MHz), i.e., the flare energy release began high in the corona. In the descending phase of the burst, the fibers were accompanied by a zebra structure (Fig. 3.1) for ~15 minutes in the meter range (Aurass, Chernov, 1983).

Subsequently, suggestions have been made to use just strange isolated fibers as important signs of other connections.

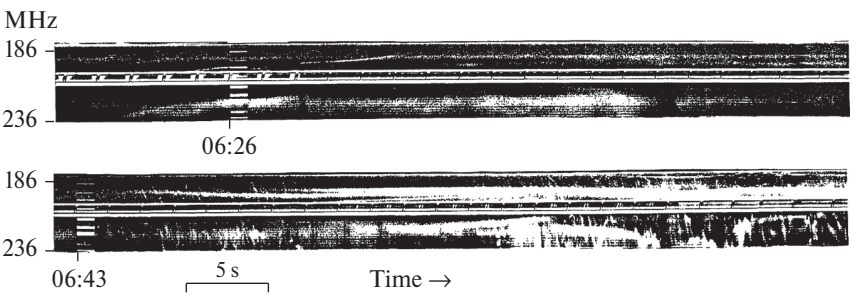

Fig. 3.1. Slowly drifting fibers in the flare continuum (after a type II burst at 06:26 UT) and the zebra structure background (at 06:43 UT, below) in a high resolution spectrum in the frequency range 186–236 MHz in the major radio burst of October 12, 1981 (IZMIRAN spectrograph, Gorgutsa et al., 2001)

For example, in the event of October 12, 1981 (Fig. 3 in Aurass, Chernov, 1983) and February 3, 1983 (Fig. 12 in Bakunin et al., 1991), the unusual long (0.5–2 min), almost non-drifting solitary fibers at the maximum phase of radio bursts in the meter range are recognized as signs of fast coronal mass ejections (CME) in large events. Analysis of the 3.02.1983 event in Bakunin et al. (1991) showed that the radio emission of fibers was associated with the capture of the whistler packet between the shock front and the tangential rupture, before the reverse shock wave.

With the development of radio spectral observations in the decimeter and microwave wavelengths, it became clear that slowly drifting fibers were observed there as well.

3.2. New observations

New observations do not necessarily correspond to the most recent by date. Basically, it means the registration of similar slow drifting fibers in the last 20 years, but hardly discussed in the publications. Most of these bursts have been observed in the decimeter band thanks to observations at station Huairou (NAOC, China; Fu et al., 2004).

One of the most evident examples of strange slow drifting fibers is the event on 30.11.2004 (Fig. 3.2), associated with a small C5 (GOES X ray) outburst.

The maximum radio emission was in the decimeter band (100 s.f.u. at 1415 MHz, 1 solar flux unit = 10^{-22} $Wm^{-2}Hz^{-1}$). The flare of C4.8 (GOES 1–8 Å) occurred in the active region (AR) of NOAA 10708 (N09 E33) between 06:32–07:22 UT [2].

The SXR (GOES) and 1415 MHz radio burst maxima coincided in time around 06:58 UT. A small intensity radio burst turned out to be rich in fine structure in the decimeter range 1–2 GHz. Almost from the beginning of the phenomenon, fiber bursts were observed, especially after 06:38 UT. Then a zebra structure, mainly in the cloud of spike bursts, and after 06:46 UT, groups of fibers, with different frequency drift and emission bandwidths, dominated. Occasionally, fibers consisting of spike-like bursts appeared, all the way up to our fiber at 06:59:52 UT. Such a complex set of almost simultaneous fine structures is difficult to analyze, so let us first consider our individual isolated fiber.

[2] https://solarmonitor.org/index.php?date=20041130&region=10708

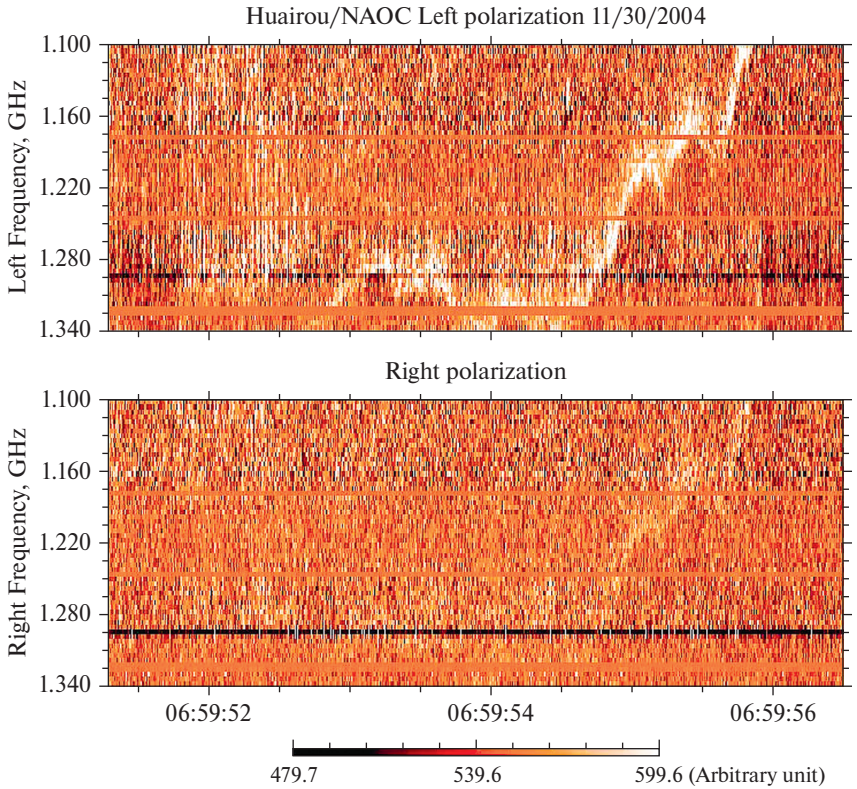

Fig. 3.2. Dynamic spectra of the Huairou station of the National Observatory of China in the left and right polarization channels of the November 30, 2004 event in the decimeter band 1.1–1.34 GHz (Fu et al., 2004)

This is an isolated fiber on a low continuum with saw-tooth changes of frequency drift in the range of 1.34–1.1 GHz for 2.5 s at some moments similar to a fiber burst (but without obvious absorption from the LF edge) and without zebra elements in the immediate surroundings. The origin of such a fiber remains unknown, although saw-tooth drift is often observed in zebra stripes. The radiation is strongly polarized, and one can only observe that the fiber appeared to be some sort of HF boundary of a weak continuum. All of the signs noted do not give clear preference to any model of zebra formation or fiber bursts. The latter also appear in groups and with a constant drift, most often to low frequencies.

Another unknown fiber in the same range was obtained on October 26, 2003 (Fig. 3.3), but in the course of a powerful X1.2

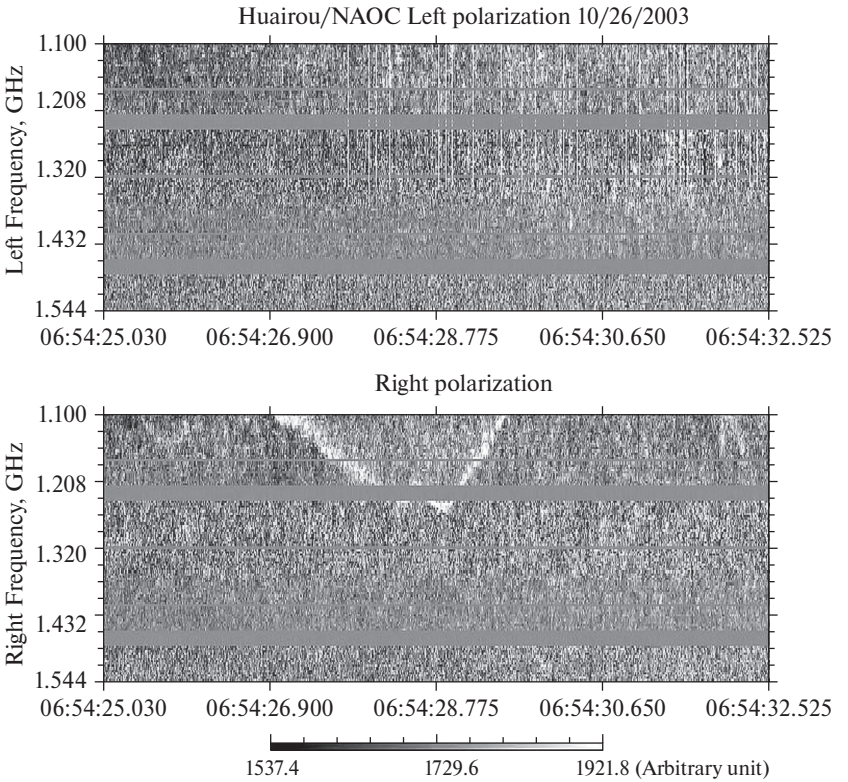

Fig. 3.3. Dynamic spectra of the Huairou station of the National Observatory of China in the left and right polarization channels of the October 26, 2003 event in the 1.1–1.54 GHz decimeter band (Fu et al., 2004)

(GOES) in AR 10486 (S15 E31) flare and a large type II+IV radio burst with a maximum in the decimeter range of 650 000 s.f.u. at 606 MHz[3].

About 20 short zebra structure series and fiber bursts against a background of fast decimeter pulsations were observed in the range of 1–2 GHz during more than 2 hours (06:13–08:40 UT). The parameters of the fine structure changed in a complex way. In the beginning, the emission was almost not polarized, which is unusual for the decimeter range. The main property of the zebra stripes was that they rapidly drift in the frequency and change signs when crossing the regions with pulsations. But after about 06:25 UT,

[3] https://solarmonitor.org/index.php?date=20031026&region=10486

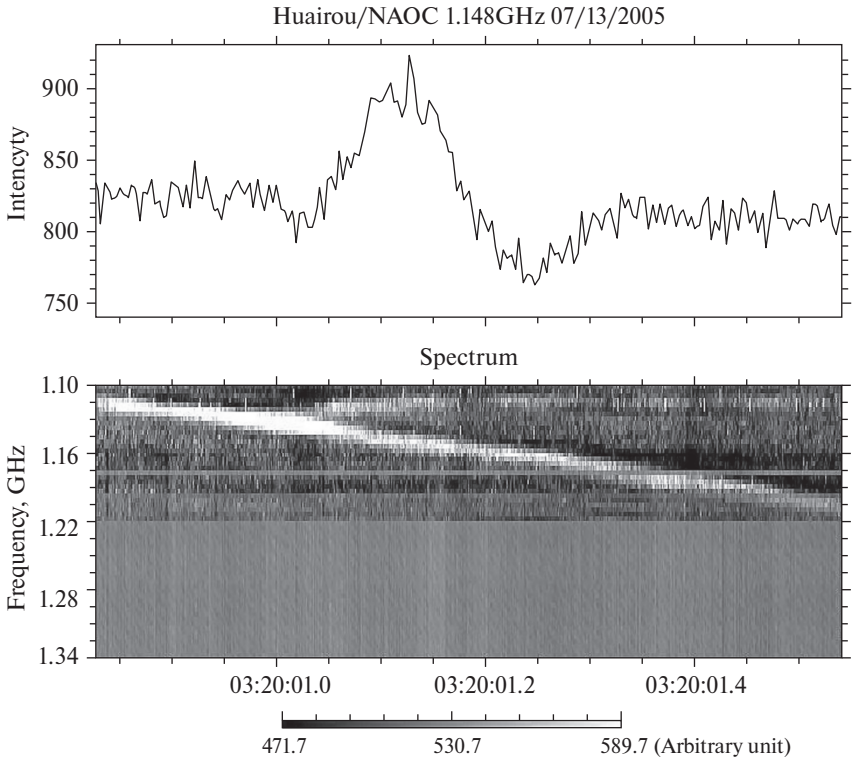

Fig. 3.4. Dynamic spectrum in the 1.1–1.34 GHz decimeter band. And the intensity profile at 1.148 GHz (in arbitrary units) from the Huairou station of the National Observatory of China in the July 13, 2005 event (Fu et al., 2004)

the polarization became strong right sign, indicating the dynamics of the radio sources.

An isolated fiber changes sharply the direction of frequency drift twice in 1.9 s in the range 1.1–1.214 MHz. There are no zebra stripes in the nearest spectrum bands and at the beginning and end of the fiber it is more like a fiber burst, only with the opposite frequency drift and no absorption from the LF edge of the fiber. This appeared at the time of the X-ray burst maximum and on a growing high type IV continuum, so it can be assumed that the source may have been magnetically trapped, but the absence of zebra and fiber bursts at this time complicates the choice of an unambiguous emission mechanism. The general appearance of fibers is more characteristic of fiber bursts, but with the source trapped between the leading edge fronts of the CME and the shock wave.

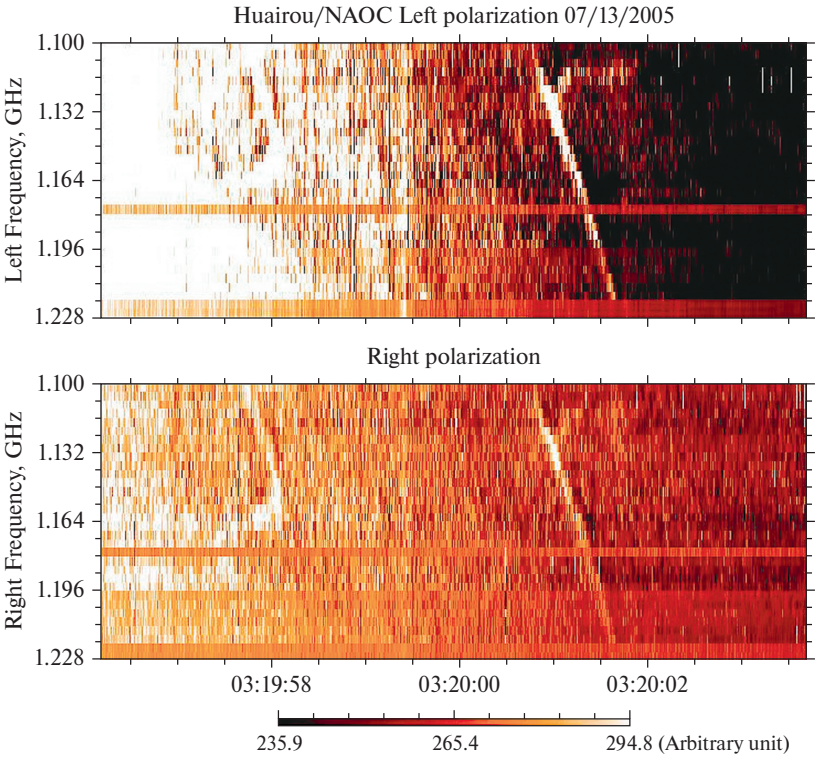

Fig. 3.5. Dynamic spectra of the Huairou station of the National Observatory of China in the left and right polarization channels of the July 13, 2005 phenomenon in the 1.1–1.228 GHz decimeter band (Fu et al., 2004)

Another example of an isolated fiber in the decimeter range is shown in Fig. 3.4.

This isolated fiber with a constant positive drift reveals absorption from the LF edge can almost definitely be considered as a fiber bursts type.

The event was rather complicated, after a moderate flare of M1.1 in the western region 10786, N11 W82, the continuum burst in the decimeter band lasted almost 2 hours. None of the observers recorded the II+IV burst, although there was a rich fine structure in the decimeter continuum: zebra, pulsations, fibers, spikes[4].

Moreover, our fiber appeared at the end of another continuum burst (Fig. 3.5).

[4] https://solarmonitor.org/data/2005/07/13/meta/noaa_events_raw_20050713.txt

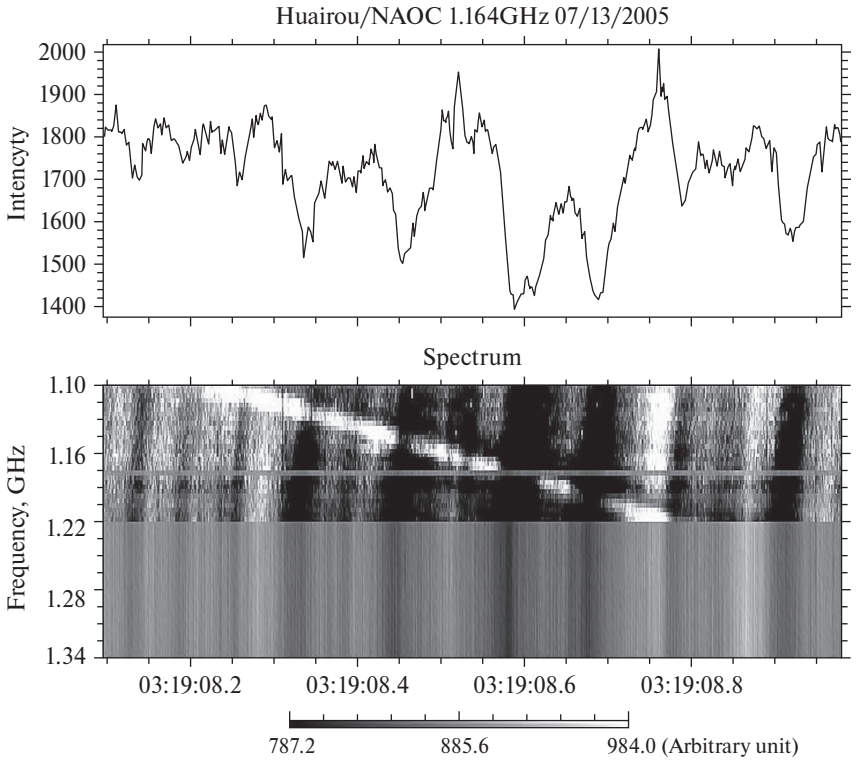

Fig. 3.6. Dynamic spectrum in the decimeter band 1.1–1.34 GHz, the Huairou station of the National Observatory of China and the intensity profile at 1.164 GHz (in arbitrary units) in the July 13, 2005 event (Fu et al., 2004)

And one minute before our burst, almost the same fiber was observed, but against a background of fast pulsations in emission and absorption, with the fiber reacting only to absorption (dips in the intensity profile shown above the spectrum in Fig. 3.6). Further, for almost 20 minutes, spikes appeared in the background of fast pulsations, zebra structure and fibers (fiber bursts).

In the microwave range, slow drifting fibers have also been observed, mostly during large radio bursts (Figs. 3.7 and 3.8). One may also note the isolated fiber in Fig. 3 in Fomichev, Chernov (2020) observed in a large radio burst on November 18, 2003 at 08:25:12–08:25:15 UT. It looks identical on the spectra of two observatories separated by nearly 7 thousand km, confirming the solar nature of the event. Although all three cases can be recognized as off spurs of a zebra structure with one or two stripes.

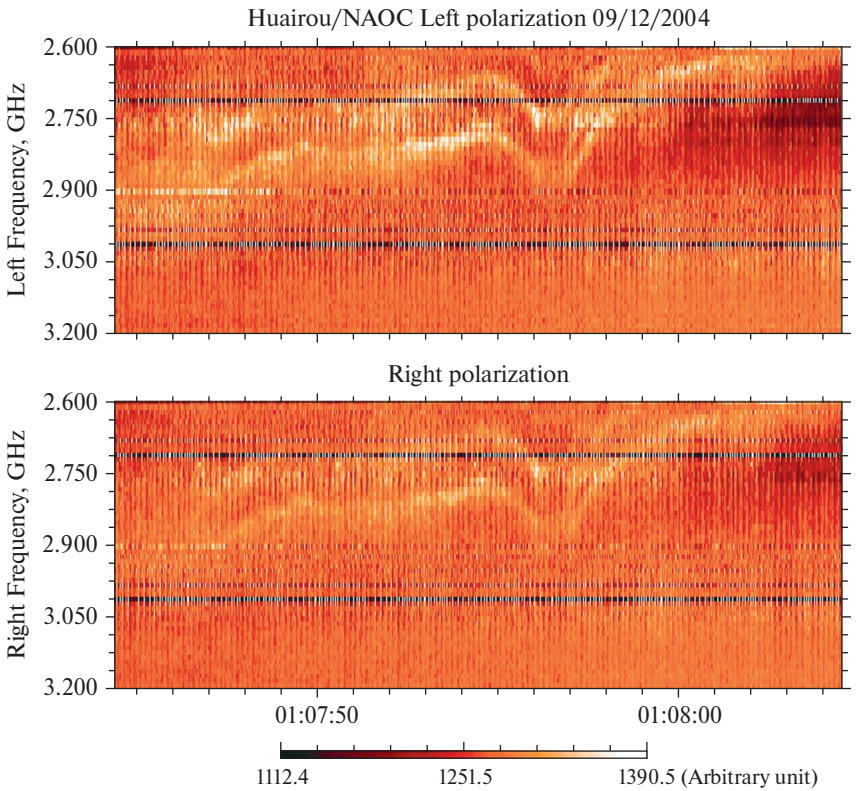

Fig. 3.7. Dynamic spectra of the Huairou station of the National Observatory of China in the left and right polarization channels of the September 12, 2004 event in the 2.6–3.2 GHz microwave band (Fu et al., 2004)

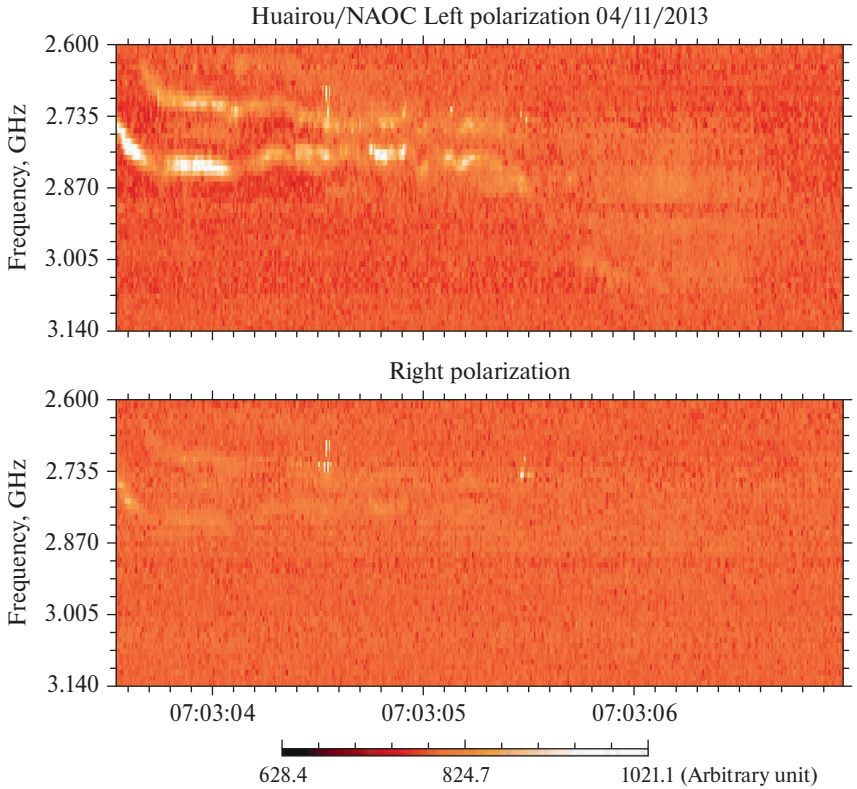

Fig. 3.8. Dynamic spectra of the Huairou station of the National Observatory of China in the left and right polarization channels of the November 4, 2013 event in the 2.6–3.14 GHz microwave band[5]

3.3. Discussion

1. Thus, isolated slow drifting fibers have been observed mainly in the decimeter range, although there are examples in both the meter and microwave ranges. They exhibit a number of features of classic fiber bursts. But why they are isolated, whereas fiber bursts tend to appear in large groups, which is naturally associated with the whistler model, whose excitation is characterized by periodicity, and related both to nonlinear instability processes (whistler scattering on fast particles, interaction with ion-sonic waves) and to the bounce period of the particle beam trapped in the magnetic trap (Chernov, 2006). The frequency drift differs sharply from the

[5] https://solarmonitor.org/index.php?date=20131104

fiber burst: sometimes it is almost absent (long fibers in the meter range, noted in the introduction). Or it has a saw-tooth character (Fig. 3.3).

All the slow drifting bursts (the examples of dynamic spectra of some bursts are shown above) have been observed at the background of wide band continua named as type IV radio burst. Sources of this continuum radio emission are coronal magnetic loops in the solar atmosphere (Stepanov, Zaitsev, 2018). In such magnetic arc structures loss cone distributions of fast electrons superimposed upon a thermal background are formed which are unstable for plasma waves (ω_l, k_l) and whistlers (ω_w, k_w). A coupling process of whistlers with plasma waves ($\omega + l \rightarrow t$) can lead to generation of electromagnetic (t) waves, in our case radio fibers. Such a mechanism was used to explain the generation of fibers with intermediate drift (Kuipers, 1975), later an analysis of the conditions for realization of this process and its efficiency in the solar corona was given in (Fomichev, Fainshtein, 1988). As is well known, the conditions of spatio-temporal synchronization (or the conservation laws for energy and moment) must be satisfied in such an interaction

$$\omega_l + \omega_w = \omega_t \quad \mathbf{k}_l + \mathbf{k}_w = \mathbf{k}_t . \tag{3.1}$$

The frequencies and wave numbers appearing in these relations must satisfy the dispersion relations for the corresponding branch of oscillations in a plasma:

$$\omega_l^2 = \omega_L^2 + k_l^2 V_{\mathrm{Te}}^2, \tag{3.2}$$

$$\omega_t^2 = \omega_L^2 + k_t^2 c^2, \tag{3.3}$$

$$\omega_w = k_w^2 c^2 \omega_H / \omega_L^2 . \tag{3.4}$$

Here $V_{\mathrm{Te}} = (k_B T/m_{\mathrm{e}})^{1/2}$ is the electron thermal velocity, k_B is the Boltzmann constant, $\omega_H = eH/\mathrm{m_e}c$ is the electron gyrofrequency, $\omega L = (4\pi e^2 N/m_{\mathrm{e}})^{1/2}$ is the electron Langmuir frequency, N is the electron density, and H is the constant magnetic field strength.

Equation (3.4) is written for the case of longitudinal propagation of a whistler and $\omega_w \ll \omega_H$. The basis for such an assumption is the fact that frequencies close to ω_{H} resonant cyclotron absorption becomes important. According to Ginzburg (1967), half-width of the resonance line $\Delta\omega/\omega = \sqrt{2}\, V_{\mathrm{Te}} n/\, c$ ($n = \omega L/(\omega\, \omega_H)^{1/2} \gg 1$ is the index of refraction for whistlers. For $\omega H\, /\omega L \sim 0.1$,

$V_{Te}/c \sim 1.5 \cdot 10^{-2}$ ($T \approx 10^6$ K) we obtain $\Delta\omega/\omega \sim 0.2$–$0.4$. Numerical calculations of the cyclotron absorption coefficient in the coronal plasma have also shown that whistlers are strongly damped at frequencies $\omega > \omega_H/2$.

For $\omega_l \approx \omega_L$, $\omega_t \geq \omega_L$ and $\omega_L \gg \omega_H$, the case of interest for us, and also using the relation $k_t^2 = k_l^2 + k_w^2 + 2k_l \cdot k_w \cdot \cos\theta$ (θ is the angle between the directions of propagation of the whistler and the plasmon) that follows from $\mathbf{k}_l + \mathbf{k}_w = \mathbf{k}_t$ we can obtain from Eqs. (3.1)–(3.4) the frequencies and the wave numbers of interacting waves. For the conditions in the sources of type IV bursts we obtain $k_l \approx k_w$ and $\mathbf{k}_l \approx -\mathbf{k}_w$, i.e., plasmons and whistlers with approximately equal and oppositely directed wave vectors take part in the interaction. Also, we can obtain the estimates for the frequencies and the wave numbers of interacting waves

$$\omega_l \approx \omega_L\,(1 + \beta_T^2\,\omega_w/2\omega_H),\ k_l \approx k_w \approx (\omega_L/c) \cdot (\omega_w/\omega_H)^{1/2}. \quad (3.5)$$

It should be noted that all the conclusions and estimates given above under assumption that HF electromagnetic waves are the ordinary mode. Analysis for the extraordinary showed that the synchronization conditions (3.1) are not satisfied for any values of k_l/k_w and ω_H/ω_L, and hence the generation of extraordinary waves through the interaction of plasma waves and whistlers is impossible. Therefore, the polarization of the radio emission in this case will correspond to the ordinary wave, which agrees with observations.

In the frames of this model the generation of whistlers occur in low part of the coronal magnetic loop, and propagating towards the higher levels of the solar atmosphere with decreasing magnetic fields whistlers will approach and reach the levels where strong resonance cyclotron absorption takes place because of increasing of parameter $\omega w/\omega H$. This effect can explain more rare registration of such fibers in meter waves range in comparison with decimeter wave range.

2. Let us use the relations obtained above to estimate the parameters of the sources of type IV radio bursts. First of all, let us estimate one important parameter, the turbulence level of whistlers in the source. To do so we use the data on the observed radio flux S and the brightness temperature T_{eff} of the emission in fibers. For frequency $f \approx 0.3$ GHz the observed values of S $\approx 10^2$–10^3 Wm^{-2} Hz^{-1} correspond to $T_{eff} \ll 10^{14}$ K. The brightness temperature T_{eff} of the emission is determined by formula

$$T_{eff} = 2\pi W_k / k_t^2 k_B, \quad (3.6)$$

where $W_k = W_t / \Delta k_t$ is spectral energy density. Substituting the expressions for $k_t = (\omega L/c) \cdot (2\omega_w/\omega_L)^{1/2}$ and $\Delta k_t = (\omega_L/c) \cdot (\omega_w/2 \cdot \omega_L)^{1/2}$ here and adopting the values $\omega_w/\omega_H = 0.25$, $\omega_H/\omega_L = 0{,}1$ we obtain $W_t \approx 10^{-9}$ erg $\cdot$ cm^{-3}. Then taking value of $W_l = 10^{-5} - 10^{-6}$ erg $\cdot$ см$^{-3}$ for the level of plasma turbulence in the source of type IV bursts (Stepanov, 1973) we obtain the estimation $W_w = 2 \cdot 10^{-10}$ erg $\cdot$ cm^{-3} for the level of low-frequency turbulence of the whistler type in a coronal arch.

Another important parameter that can be estimated from the characteristics of filamentary bursts is the magnetic field H. To find the magnetic field we use the value of frequency drift of bursts which within the frame-work of our model is determined by the group velocity of propagation of the whistlers, and we can write

$$(L_N/c) \cdot df/dt = (f_H \cdot f_w)^{1/2} (1 - f_w/f_H)^{3/2}, \quad (3.7)$$

where $L_N = N\ (dN/dr)^{-1}$ is the scale of electron density inhomogeneity in the solar corona. On the other hand, from Eqs. (3.1)–(3.4) it follows that $\Delta\omega_t = \Delta\omega_l + \Delta\omega_w$, $\Delta\omega_l = \frac{1}{2} \cdot \beta T^2 \cdot \omega_L/\omega_H \cdot \Delta\omega_w$ and $\Delta\omega_t \approx \Delta\omega_l$. On this basis we may adopt the emission and absorption bandwidths frequencies approximately equal, and write

$$\Delta f_b = f_w, \quad (3.8)$$

where Δf_b is the observed frequency bandwidth of brightening. Using the data on the frequency drift df/dt and Δfb (Elgaroy, 1982; Chernov, 2011) as well the model of the height distribution of electron density in the corona we can obtain estimates of the magnetic field in the emission source from Eqs. (3.7) and (3.8). Thus, using the doubled model of Newkirk for the density distribution, usual for the meter range, and values $df/dt = 7.4$ MHz/s, $\Delta f_b = 2.1$ MHz for source at frequency $f = 300$ MHz we obtain the estimate $H \approx 5$ Gs, and for the source at frequency $f = 150$ MHz with $df/dt = 3.1$ MHz/s, $\Delta f_b = 11$ MHz we obtain $H \approx 1.4$ Gs.

The Newkirk model predicts a variation of the electron density N_e, with the distance r, from the center of the Sun that has the form:

$$N_e = 4.2 \cdot 10^4\ 10^{4.32 R_\odot / r} = 4.2 \cdot 10^4\ e^{9.95 R_\odot / r}\ [\text{cm}^{-3}], \quad (3.9)$$

where $R_\odot$ is the solar radius (Newkirk, 1961).

Other peculiarities of the dynamic spectra of radio fibers (low frequency drift, irregular changes of frequency drift including changes of sign of drift, etc.) may be connected with features of non-linear processes of generation of whistlers and their interaction with fast electrons in arch-like magnetic structures in the solar atmosphere.

An isolated fiber means no bounce period and non-linear processes cause only a sawtooth-like nature of the frequency drift. In principle, both of these cases are perfectly acceptable. For example, in open magnetic field configurations. Interactions with fast particles are still possible, at least once. Multiple new injections of fast particles, leading to a change in the whistler instability from normal to anomalous resonance, are also possible (Chernov, 1990; Chernov, 1996). The latter process causes an abrupt change in the direction of the whistler group velocity, which determines the frequency drift, which explains the saw-tooth character of the fiber. However, the fiber in Fig. 3.6 in the background pulsation is surprising in the absence of a saw-tooth frequency drift, although new beams of fast particles clearly took place to be, according to the pulsation model in emission and absorption.

The absence of fiber frequency drift in the meter range can probably be explained by the advance of the whistler wave packet almost across the plasma frequency gradient (along the plasma levels). In addition, there is still the effect of some compensation of the whistler group velocity when its direction is changed. In this case a wave-like frequency drift should rather appear. When the whistler instability switches from a normal Doppler effect to an anomalous one, the whistler group velocity reverses (Chernov, 1996). If this process is slowed down (e.g., by additional particle injection), the fibers can remain almost parallel to the time axis on the spectrum.

3.4. Conclusion

The isolated radio fiber bursts observed mainly in the decimeter range and given in this paper, display a number of features of classical fiber bursts. The process of interaction of whistlers with Langmuir plasmons was suggested as a mechanism of such radio fibers generation. Analysis of the conditions for realization of this process in the coronal magnetic arch structures with forming of the distribution function of fast electrons of loss-cone type and its efficiency was carried out. Unusual peculiarities of dynamic spectra of such fibers (irregular frequency drift including a change of sign of frequency drift, etc.) can be connected with features of nonlinear

processes of generation of whistlers and their interaction with fast electrons in arch-like magnetic structures in the solar atmosphere. The estimates of intensity of low frequency turbulence of whistler type and magnetic field strength in the sources of radio emission were obtained by data on radio fibers.

Acknowledgments

The authors are grateful to Chinese colleagues for the kindly opportunity to work with the radio spectral data of the Huairou station of the National Astronomical Observatory of China (NAOC) in the frames of grants No. 2011T1J20. We are grateful to the RHESSI, GOES, and LASCO teams for open access to their data.

Data availability statement

The dynamic spectra given in Figs. 3.2–3.8 were produced by one of the authors (Chernov G. P.) during his visits to NAOC in the frames of grants No. 2011T1J20, and now they are part of his own archive. The data underlying this article are available on request to the corresponding author (Chernov G. P.).

References

Aurass H., Chernov G. P., 1983. Zebra pattern flux density observations during the type IV burst on October 12, 1981 // Sol. Phys. Vol. 84. P. 339–345.

Bakunin L. M., Ledenev V. G., Nefedyev V. P. et al., 1991. Spatial, spectral and polarization properties of radio emission of the 3 February, 1983 proton flare // Sol. Phys. Vol. 135. P. 107–129.

Boischot A., Haddock F. T., Maxwell A., 1960. Spectrum of 1957 November 4 solar outburst // Annalles d'Astrophysique, Vol. 23. P. 478–479.

Chernov G. P., 1974. Unusual solar meter radio bursts // Soviet Astr. Vol. 17. P. 788–792 (Astronomichesky Zhurnal. 50, 1254–1259, 1974).

Chernov G. P., 1976. Microstructure in the continuous radiation of type IV meter bursts. Observations and model of the source // Soviet Astronomy. Vol. 20. P. 449–459.

Chernov G. P., 1990. Whistlers in the solar corona and their relevance to the fine structures of type IV radio emission // Sol. Phys. Vol. 130. P. 75–82.

Chernov G. P., 1996. A manifestation of quasilinear diffusion in whistlers in the fine structure of type IV solar radio bursts // Astron. Rep. Vol. 40, No. 4. P. 561–568 (Astronomicheskii Zhurnal. 73. N 4. 614–622).

Chernov G. P., 1997. The relationship between fine structure of solar radio emission at meter wavelengths and coronal transients // Astronomy Letters. Vol. 23, No. 6. P. 827–837.

Chernov G. P., 2006. Solar radio bursts with drifting stripes in emission and absorption // Space Sci. Rev. Vol. 127. P. 195–326. DOI: 10.1007/s11214-006-9141-7

Chernov G. P., 2011. Fine structure of solar radio bursts, Heidelberg: Springer. 282 p.

Chernov G. P., Korolev O. S., Markeev A. K., 1975. Observations of a complex solar radio bursts with fine structure // Sol. Phys. Vol. 44. P. 435–446.

Elgarøy Ø., 1959. Observations of the Fine Structure of Enhanced Solar Radio Radiation with a Narrow-Band Spectrum Analyser // Nature. Vol. 184. P. 887–889.

Elgarøy Ø., 1982. Intermediate drift bursts. Report N 53. ITA, Univ. Oslo.

Ginzburg V. L., 1967. Propagation of Electromagnetic Waves in Plasma, Moscow: Nauka (2nd ed. Translated by J. B. Sykes and R. J. Taylor. Oxford; New York: Pergamon Press, 1970).

Fomichev V. V., Chernov G. P., 2020. Termination shock as a source of unusual solar radio bursts // Ap. J. Vol. 901, No. 65. 9 p. DOI: org/10.3847/1538-4357/abad9f

Fomichev V. V., Fainstein S. M., 1988. Theory of the fine structure of type IV radio bursts // Sov. Astron. Vol. 65(5). P. 552–556.

Fu Qi Jun, Ji H. R., Qin Z. H., Xu Z. C., Xia Z. G., Wu H. A. et al., 2004. A new solar broadband radio spectrometer (SBRS) in China // Sol. Phys. Vol. 222. P. 167–175.

Gorgutsa R. V., Gnezdilov A. A., Markeev A. K., Sobolev D. E., 2001. An upgrade of the IZMIRAN's solar digital radio spectrograph: first results // Astronomical and Astrophysical Transaction. Vol. 20. P. 547–549.

Kuijpers J., 1975. Generation of intermediate drift bursts in solar type IV continua through coupling of whistler and Langmuir waves // Solar Physics. Vol. 44. P. 173–193.

Kundu M. R., 1965. Solar radio astronomy. New York: Interscience. 660 p.

Krüger A., 1979. Introduction to Solar Radio Astronomy and Radio Physics. D. Reidel Publ. Comp. 332 p.

Markeev A. K., Chernov G. P., 1971. Observations of solar radio bursts with high spectral resolution // Soviet Astr. Vol. 14, No. 5. P. 835–839 (Astronomicheskii. Zhurnal. 47. N. 5.: 1044–1046, 1970).

Newkirk Gordon J., 1961. The solar corona in active regions and the thermal origin of the slowly varying component of solar radio radiation // Ap. J. Vol. 133. P. 983–1013. DOI: 10.1086/147104

Stepanov A. V., Zaitsev V. V., 2018. Magnetospheres of active regions on the Sun and stars. Mocow: M. Fizmatlit (Ed. in Russian). 387 p.

Stepanov A. V., 1973. On the mechanism of generation of solar radio bursts type IV // Astron. Zh. Vol. 50, No. 1243 (Sov. Astron., 17, 781, 1974).

Zheleznyakov V. V., 1964. Radio emission of the Sun and planets. Moscow: Nauka (Zheleznyakov V. V., 1970. Radio Emission of the Sun and Planets. New York, NY: Pergamon Press. 697 p.).

Chapter 4
FINE STRUCTURE OF TYPE IV SOLAR RADIO BURSTS, CONNECTED WITH STATIONARY AND MOVING SOURCES

Abstract. Different types of fine structure in the continuum emission of type IV radio bursts are considered with respect to different types of emission sources, stationary and moving. In the case of stationary sources, the origin of the fine structure is associated both with processes in individual magnetic loops (quasi-periodic acceleration, magneto hydrodynamic (MHD) waves) and with large-scale processes associated with the propagation of MHD disturbances, formation of loop arcades and simultaneous discrete particle accelerations, resulting in pulsating radio emission character. For the case of a moving source, the generation mechanism largely depends on the magnetic structure of the source (expanding magnetic arcade or isolated plasma cloud). In this case, the connection with coronal mass ejections and shock waves is also important. Second pulsations are explained by MHD oscillations of the source in the form of a magnetic loop or cloud. The absence of other fine structure in continuum of type IV moving bursts can be related to the critical loss-cone angle for whistler to be excited.

4.1. Introduction

All the types of solar radio bursts, type IV continuum radio bursts are characterized by the most diverse and complex fine structure of their dynamical spectra. Most such bursts are associated with powerful flares and coronal mass ejections (CMEs). The fine structure of the continuum radio emission has been studied since 1959, following observations by Elgarøy (1959). The variety of types of fine structure complicates its classification, and this makes its interpretation difficult. Nevertheless, it is possible to identify the main elements of the fine structure, as well as the most characteristic combinations of these elements. At the same time, according to observations on radio interferometers and radioheliographs, type IV radio burst sources can be both stationary and detecting movement. Accordingly, radio sources in

such cases are called «stationary sources» and «moving sources». Therefore, for a theoretical interpretation of fine structure of radio bursts it is necessary to take into account the type of source and physical conditions in which this or that mechanism of generation is realized. In this paper, based on the available experimental data, an attempt is made to classify the fine structure of type IV radio bursts taking into account the type of source.

4.2. Experimental data on type IV moving radio bursts

The dynamic spectra of moving sources are a uniform continuum drifting to low frequencies in the meter wave range (typically <200 MHz) for tens of minutes: simultaneous bursts of stationary sources last longer (hours) than moving bursts (tens of minutes). Large progress in type IV observations of moving bursts was made with the introduction of the Kulgoora radioheliograph, first at 80 MHz, then at 40, 160, and 320 MHz (Wild, 1967). Figure 4.1 shows an example of a moving type IV burst source («isolated plasma cloud»), when the radiation source at a fixed frequency of 80 MHz moved radially to very high heights.

Such source properties are consistent with the cyclotron nature of the emission of moderately relativistic electrons in the magnetic

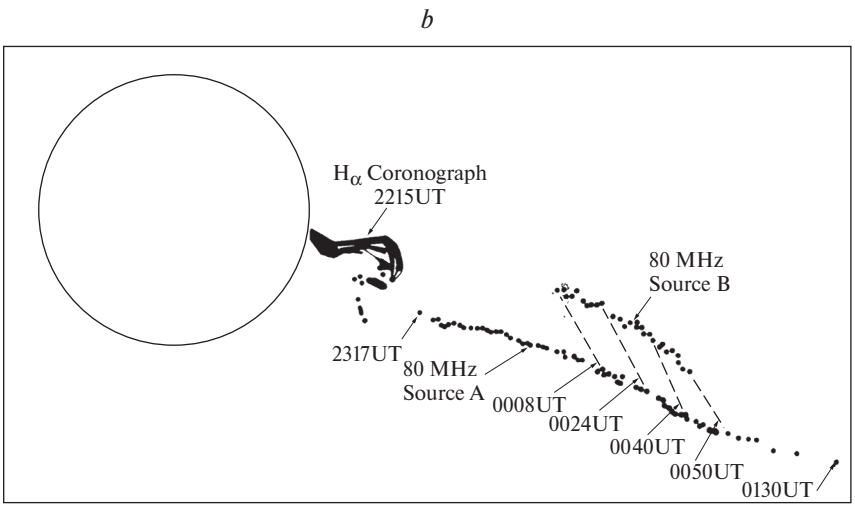

Fig. 4.1. The spatial relationship between the rising prominence observed in Hα (sketched from a photograph) and the 80 MHz radioheliogram sources (denoted by the positions of the centroids at various times) (fragment of Fig. 3 in Riddle, 1970)

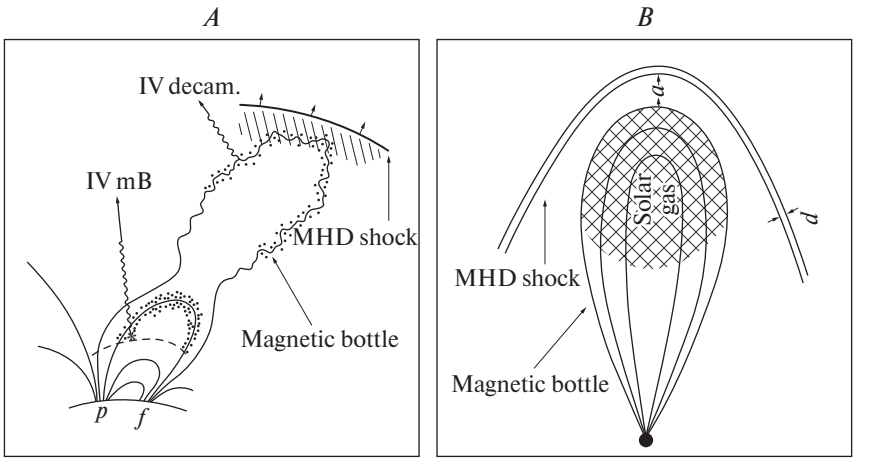

Fig. 4.2. Two types of possible sources of type IV moving radio bursts: (*A*) a moving front and (*B*) a magnetic cloud (Gopalswami, 2016)

field of the cloud. Gary et al. (1985) considered a moving type IV radio burst on June 29, 1980 at 02:33 UT on three frequencies of the Kulgoora radioheliograph, 40, 80, and 160 MHz, with simultaneous observations on the SMM coronagraph. The authors check the already known observations (Riddle, 1970) (see Fig. 4.1). But the authors showed that the radiation of the moving burst was at the second harmonic of plasma frequency. The 80 MHz source was moving along the dense part of the CME at the 40 MHz plasma level (plasma mechanism).

Another variety of type IV moving burst sources is the rising shock front (Fig. 4.2, A), where the appearance of radio emission is associated with synchrotron emission of electrons accelerated on the shock wave (Boischot, 1957; Gopalswami, 2016).

Obtaining images of type IV radio burst sources has led to much better understanding of the development of sources and processes of radiation generation (Pick, Vilmer, 2008). It was found that the most probable is the plasma mechanism of radiation at the fundamental plasma frequency or at its second harmonic. A similar conclusion was made in (Trottet et al., 1981) to explain the short-term modulations of the radiation of a moving type IV radio burst source. The moving radio bursts were associated with MeV electrons injected into expanding magnetic arcs behind the leading edge of the CME. Some narrow-band bursts were associated with explosive emissions (Pick et al., 2006).

With the development of optical observations on coronagraphs (SOHO/LASCO), type IV moving radio bursts began to be used to understand the nature of CMEs because of their close space-time relationship. The continuum usually contains no fine structure, except for pulsations with second or minute periods. Examples can be seen in the spectra of a new radio spectrograph in the 85–35 MHz range (Gauribidanur Low Frequency Solar Spectrograph near Bangalore, India) (Ramesh et al., 2013).

A variety of fine structure types of radio bursts are described in many articles (see, for example, Chernov, 2011, and literature cited there). The most characteristic elements are: a) fiber burst – look on the dynamic spectrum as a narrow-band drifting brightening of the continuum, accompanied on the low-frequency side by a similar band in the absorption; b) pulsations – quasi-regular sequence of broadband amplifications and attenuations of continuum, usually without noticeable frequency drift; c) zebra-structure – system of numerous frequency alternating bands in emission and absorption. We observe both regular zebra structures, when bands are characterized by almost constant or smoothly changing frequency drift, and irregular or non-stationary zebra structures with repeated and sharp changes in magnitude and direction of frequency drift almost synchronously in all bands; d) spikes – narrow-band and short-term bursts at the background of continuum radiation, etc. During powerful solar flares, different types of fine structure can be observed in various combinations.

4.2.1. The Bastille flare of July 14, 2000

A clear example of a moving source of an IV burst is the observations of the dynamical spectra during the famous Bastille flare of July 14, 2000 (X5.7/3B-class eruptive flare) (Reiner et al., 2001; Chertok et al., 2001). A detailed analysis of fine structure of the radio burst in the meter range is presented in (Chertok et al., 2001 and Caroubalos et al., 2001). The declining phase of the flare in the 270–180 MHz range of the IZMIRAN spectrum in Fig. 4.3 marks a drifting continuum without any clear signs of fine structure. According to data of the ARTEMIS-IV radio spectrograph, the absence of a fine structure in drifting continuum is also confirmed at higher frequencies, up to 600 MHz (Fig. 4.4).

It is important that this continuum accompanied a type II radio burst at lower frequencies. Only later appeared pulsations with

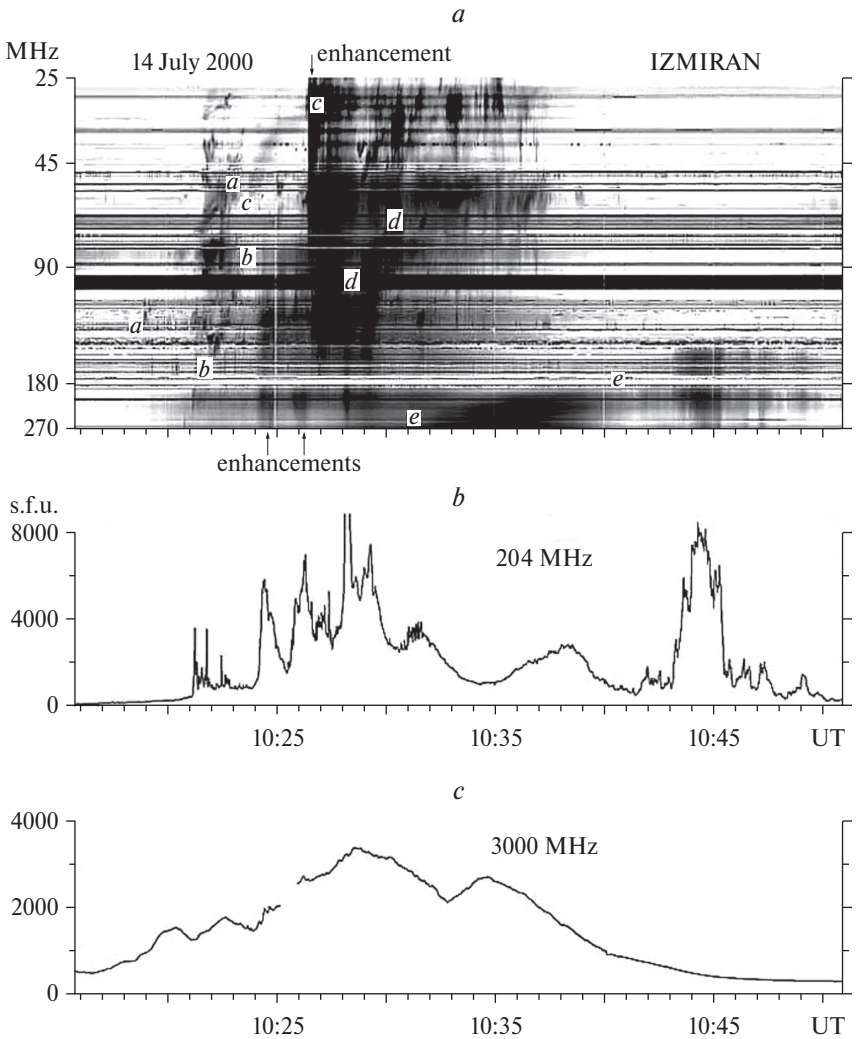

Fig. 4.3. The Bastille flare on July 14, 2000. According to IZMIRAN: (*a*) dynamic spectrum in the range 25–270 MHz; (*b*) and (*c*) time profiles at 204 and 3000 MHz. Along the vertical axes in parts (*b*) and (*c*) 1 s.f.u. = $= 10^{-22}$ W/m^{2}Hz. The spectrum (*a*) shows several type II bursts (aa, bb, cc) and a slowly drifting decimeter continuum (ee) (Fig. 3 in Chertok et al., 2001)

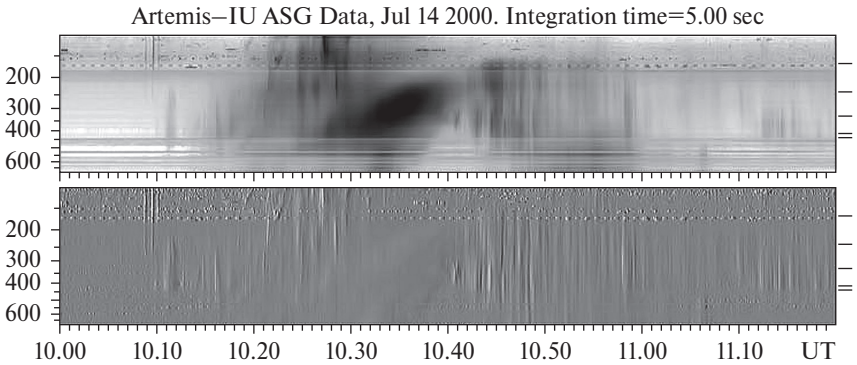

Fig. 4.4. According to the ARTEMIS-IV radio spectrograph data, the absence of a fine structure in the drifting continuum is also confirmed at higher frequencies, up to 600 MHz ARTEMIS-IV (fragment of Fig. 2 in Caroubalos et al., 2001)

periods of tens of seconds, but most likely related to the arising stationary type IV radio source (Fig. 5d in Chertok et al., 2001). A rich fine structure was observed in the stationary continuum from 10:38 UT to 10:50 UT in the 250 to 430 MHz range in the form of numerous fibers (fiber bursts) at the background of seconds pulsations. An illustrative example of such a fine structure is presented in (Caroubalos et al., 2001). A fragment of Fig. 6 from this work is shown in Fig. 4.5.

Adopting the possible radio source model shown in Fig. 4.2, we can say that the rich fine structure at the high frequencies of the meter range was excited in a closed loop (magnetic trap) type source, while the drifting continuum source was located higher in the magnetic cloud above the advancing front.

Analysis of simultaneous dynamic spectra of IZMIRAN and Chinese spectrographs in the 1–7.5 GHz range showed that the drifting continuum appeared still at frequencies around 1.5 GHz, as the non-drifting one did, after 10:45 UT. In (Wang et al., 2001) the spectrum obtained on the spectrograph of IZMIRAN was combined with the spectra of Chinese spectrographs in the 1–7.5 GHz range, and a fine structure in the form of drifting fibers in the 5.2–7.0 GHz frequency range was registered at the beginning of the phenomenon and in the 1.0–1.3 GHz frequency range at the very end of the phenomenon.

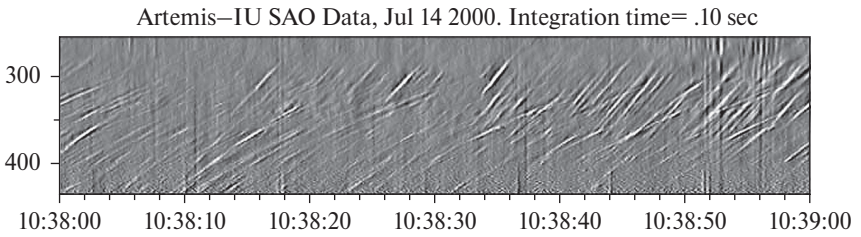

Fig. 4.5. Behavior of the derivative signal of the Bastille flare according to the ARTEMIS-IV radio spectrum during one minute in the 265–241 MHz range. Fine structure of the stationary source is impressive in its complexity: two families of fibers (fiber bursts) with different frequency drifts and overlapping each other were observed against the background of fast broadband pulsations of radiation. At the high-frequency edge of the spectrum, a developed zebra-structure is visible. (Fragment of Fig. 6 from Caroubalos et al., 2001)

A significant feature of the Bastille flare is revealed by a joint analysis of dynamic spectrographs from IZMIRAN spectrographs, SOHO/LASCO white light coronagraph data, and detailed TRACE EUV ultraviolet images (Chertok et al., 2001; Aschwanden, Alexander, 2001; Masuda et al., 2001). It turned out that the radio emission pulsations observed at different phases of the flare coincided with the formation of magnetic loop arcades, and the temporal characteristics of individual pulsations practically coincided with the time of the formation of individual loops and the time intervals between them.

4.2.2. The phenomenon of November 3, 2003

In a unique phenomenon on November 3, 2003 in the radiation of the moving continuum we observed unusual fibers in the meter range, passing into the decameter range on the spectrum WIND/WAVE (Fig. 4.6). The motion of the radio source in the meter range is shown in Fig. 6 in (Vršnak et al., 2006) by the source positions at several frequencies of the radioheliograph Nançay (France). The radio fiber source was located between two shock fronts after overtaking the fast front of the slow one (Chernov et al., 2007a). The frequency drift of the fibers was close to the drift of the type II burst band, and the emission of the fibers was probably caused by enhanced emission from inhomogeneities in the CME tail. Thus, unusual narrow-band fibers appear to be the predominant type of fine structure in the drift continuum.

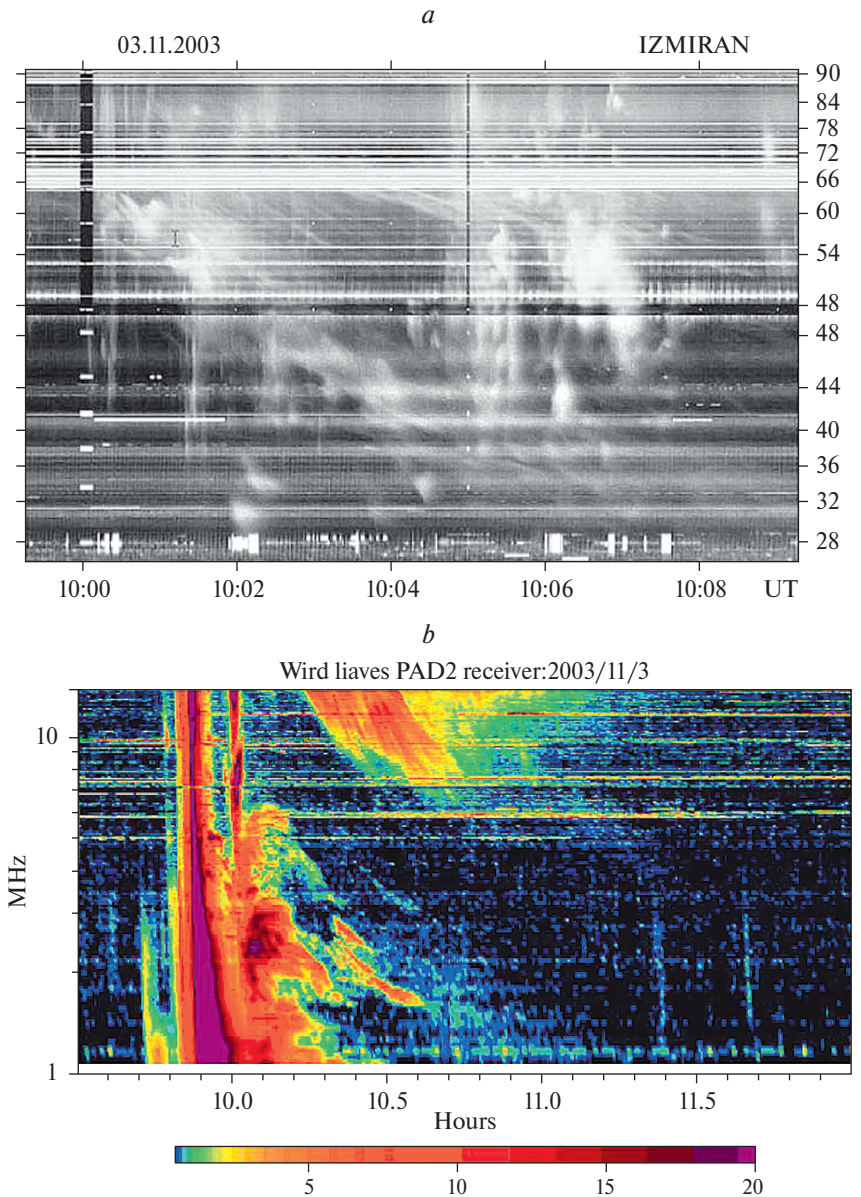

Fig. 4.6. The continuation of the filament structure in the continuum from the meter range to the decameter range and fragments of U-bursts and fibers in the type II burst in the low-frequency part of the spectrum: (*a*) spectrum of IZMIRAN spectrograph at 90–25 MHz, (*b*) spectrum RAD2, WIND/WAVE 14–1 MHz (Fig. 6 in Chernov et al., 2007a)

Similar fibers have been observed before thanks to simultaneous observations on spectrographs IZMIRAN and UTR-2 (Chernov et al., 2007b). In two phenomena, slow drifting fibers for nearly 4 min at 28–18 MHz on August 16, 2002, and two fiber fragments for 25 and 50 s at 19–21 MHz and 27.5–29.5 MHz on August 18, 2002, respectively, were observed against a diffuse continuum (Fig. 5 and 6 in Chernov et al., 2007b).

The radio sources of both phenomena were located between the leading edge of the CME and catching up it with fast shock fronts. The radiation came from elongated plasma inhomogeneities in the tail of the CME. It is interesting to note that in the first (and very weak) phenomenon, the fibers revealed a superfine structure in the form of periodic fibers (fiber bursts), with long fibers becoming similar to rope-like fibers (Chernov, 2008). It is assumed that the excitation of rope-like fibers is associated with the generation of whistlers in the magnetic trap between the leading edge of the CME and the shock front, where the velocity distribution function of energetic electrons with a loss-cone is formed. Therefore, even a single particle beam due to bouncing motions in such a trap will lead to periodic whistler excitation. Thus, the radio source of a type IV moving burst is not always uniquely explained by an advancing front with a magnetic cloud (Fig. 4.2); in each phenomenon the sources have their own features.

Pulsations of radiation with periods of tens of seconds are probably associated with MHD oscillations or MHD waves propagating from the bottom of the flare region.

In recent years, the development of observations with the CALLISTO and LOFAR radiospectrograph networks allows to analyze moving radio bursts in more detail (Morosan et al., 2021). It shows that half of all type IV bursts are associated with moving sources. A closer connection with CMEs was found, allowing us to analyze the mechanism of particle acceleration in the CME tail. In this work, authors admit the possibility of a cyclotron nature of the radio emission source at the initial temporal stage and with the predominance of the plasma mechanism at the subsequent stage, when the source rises to greater distances.

4.3. Source models and possible emission mechanisms

Based on the totality of experimental data, the following characteristics of type IV continuum burst sources can be noted.

1. Stationary sources – a wide range of frequencies (from microwave to meter wavelength range), a large variety of fine structure (zebra-structure, pulsations, fiber-bursts, spikes, points in emission and absorption, tadpoles, etc., as well as their combinations).

2. Moving sources – frequency range from decimeter to decameter range, fine structure – pulsations, fibers.

In most works theoretical interpretation of the fine structure of type IV radio bursts, associated with stationary sources, is based on the analysis of physical processes in a separate arc – a magnetic loop, in which the distributions of fast particles with loss-cone are naturally formed. Thus, within the framework of such a source model, the most common theory of zebra-structure generation – radiation at different levels of double plasma resonance (DPR), where the upper hybrid frequency (ω_{UH}) becomes equal to the integer number of electron cyclotron harmonics $s\omega_{Be}$: $\omega_{UH} = (\omega_{Pe}^2 + \omega_{Be}^2)^{1/2} = s\omega_{Be}$ (Zheleznyakov et al., 2016). As an alternative mechanism, the mechanism of non-linear interaction of Langmuir plasmons with whistlers $l + w \rightarrow t$ in a magnetic trap-type source is discussed. Within the framework of the same ideas, the generation of fibers in emission and absorption can be explained (Chernov, 2011). With the injecting accelerated electrons with a non-equilibrium momentum distribution into the trap, the development of cyclotron instability of Bernstein modes with their nonlinear conversion (fusion) into electromagnetic waves is possible. Such a model allows us to explain the generation of «tadpoles» and their various varieties (Zheleznyakov, Zlotnik, 1975).

A number of models are proposed to explain radio emission pulsations, caused by variations of medium parameters (density, magnetic field), associated with fast magnetosonic waves, excited in magnetic tubes. When interpreting the pulsations under the plasma mechanism of continuum generation, the periodic modulation of radio emission may also be a consequence of pulsating modes of beam and loss-cone instabilities (Zaitsev, Stepanov, 1975). Another approach explaining pulsations is based on the analysis of flares with a complex spatio-temporal structure. In such flares, the process of prolonged energy release occurs sequentially in different places in the active region (Ishkov et al., 1985). For example, in the well-known Bastille flare, a close correlation was established between the appearance of a sequence of separate short-period broadband radio bursts (which can be classified as pulsations) and

the formation of separate magnetic loops. Since such structures are observed in complex flares during the post-eruptive phase, the overall picture may include the propagation of a large-scale disturbance in the solar atmosphere that initiates successive processes of reconnecting magnetic field lines (e.g., in helmet-like magnetic field configurations) and simultaneous particle acceleration, formation of magnetic loops (together, forming a magnetic arcade), and generation of individual radio bursts upon injection of accelerated particles into individual loops (an example of this situation could be the Bastille flare (Reiner et al., 2001; Chertok et al., 2001)).

More complicated situation still exists with interpretation of fine structure in moving sources of type IV bursts. First, experimental data do not allow us to make a definitive conclusion about the nature of the generation mechanism of the continuum radio emission itself; in different cases there are arguments both in favor of the plasma generation mechanism, and in favor of the cyclotron (synchrotron) mechanism, or in their combination. Secondly, unlike stationary sources, the geometrical structure of the source is not clear – a magnetic cloud or an elongating region (possibly a magnetic tube) following a large-scale disturbance. In both cases, the connection of radio emission sources with CMEs and shock waves (type II bursts) is obvious.

A brief review of the fine structure in the known phenomena shows that in moving radio bursts only occasionally broadband pulsations with periods of a few seconds or tens of seconds appear. In several phenomena with specific source features (overtaking fronts), a series of fibers with frequency drift characteristic of type II bursts were observed. At the same time, these fibers sometimes reveal an ultra-fine structure in the form of rope-like fibers. The latter were associated with the source between the shock-wave fronts, in which periodic whistler packets can be excited.

The magnetic cloud, shown in Fig. 4.2 as a continuum source of type IV moving bursts, is a trap for flare electrons and protons. A magnetic loop with increased density is a resonator for fast magnetosonic waves excited by accelerated protons (Rosenberg, 1970). The oscillation period of a fast MHD mode in a loop with radius R much smaller than length L is approximately equal to value $T \approx R(C_A + C_s)^{-1/2}$, where C_A is the Alfven speed, C_s is the speed of sound. For real values in the corona of

$(C_A + C_s)^{1/2} \approx 10^8$ cm s^{-1} and $R \approx 10^8$–10^9 cm, the oscillation period can vary from 1 to 10 s. The fast MHD mode of oscillations changes the plug ratio in the loop with such a period. In the plasma mechanism, continuum emission is excited by energetic electrons with loss-cone instability, so MHD oscillations can lead both to periodic modulation of energetic electrons falling out from the trap and to changes in plasma parameters in the source, and, as a result, to pulsation of radio emission with the same period (Zaitsev et al., 1984). In sources that are magnetic traps for energetic electrons, whistler and Langmuir waves can also be excited simultaneously, whose fusion will lead to the generation of fibers as part of type IV bursts.

But we still need to understand why other types of fine structure (fiber-bursts, spikes, zebra-structure) are usually not observed and appear only in specific conditions, when the source is located, for example, between two shock fronts (Chernov et al., 2007a).

Such a cause may be related to the critical loss-cone angle for whistler excitation. According to estimates (Mann et al., 1989) for solar coronal conditions, this angle is $\sim 3.58°$ and it increases with increasing magnetic field strength. Attempts to relate the field increase to the passage of a fast MHD mode give too small an increase of $\sim 10^{-2}$, which is insufficient for an appreciable increase in the pitch-angle (Mann et al., 1989). However, if the perturbing agent is a shock front in which the field increases several times, the loss-cone instability increases dramatically.

4.4. Conclusion

A large variety of fine structure of dynamic spectra (temporal and spectral parameters) of solar continuum type IV radio bursts indicate, on the one hand, a great variety of physical parameters of radio emission sources (magnetic loops, loop arcades, magnetic clouds, regions behind CME and shock waves), on the other hand, possible connection with different mechanisms of radio emission generation (cyclotron or plasma). Close connection of type IV radio bursts with CME propagation in the solar atmosphere testifies also to close connection of radio emission characteristics with physical processes accompanying large-scale disturbances, in particular, with restructuring of magnetic structure of active regions, processes of magnetic reconnection, particle acceleration, and generation of turbulence of various types. Further observations and

studies of radio bursts with high temporal, spatial and spectral resolution are needed to elucidate the connection between all these processes and the fine structure of radio bursts. In particular, it is important to study the parameters of sources of individual pulses and their variations in the composition of long-term quasi-periodic structures of type IV continuum radio bursts. The absence of other fine structure in the continuum of moving type IV bursts may be due to the critical angle of the loss cone for whistler excitation.

Acknowledgments

The authors are grateful to the RHESSI, GOES, and LASCO CA teams for open access to their data.

References

Aschwanden M. J., Alexander D., 2001. Flare plasma cooling from 3 MK down to 1 MK modeled from Yohkoh, GOES, and TRACE observations during the Bastille Day Event (14 July 2000) // Sol. Phys. Vol. 204. P. 91–120.

Boischot A., 1957. Caracteres d'un type d'emission hertzienne associe a certaines Eruptions chromospheriques // Comptes Rendus. Acad. Sci. Paris. Vol. 244. P. 1326–1329.

Caroubalos C., Alissandrakis C. E., Hillaris A. et al., 2001. ARTEMIS IV radio observations of the 14 July 2000 large solar event // Sol. Phys. Vol. 204. P. 167–179.

Chernov G. P., 2011. Fine structure of solar radio bursts. Heidelberg: Springer. 282 p.

Chernov G. P., Kaiser M. L., Bougeret J.-L., Fomichev V. V., Gorgutsa R. V., 2007a Fine structure of solar radio bursts observed at decametric and hectometric waves // Sol. Phys. Vol. 242. P. 145–169. DOI: 10.1007/s11207-007-0258-y

Chernov G. P., Stanislavsky A. A., Konovalenko A. A. et al., 2007b. Fine structure of decametric type II radio bursts // Astronomy Letters. Vol. 33. P. 192–202. DOI: 10.1134/S1063773707030061

Chernov G. P., 2008. Unusual stripes in emission and absorption in solar radio bursts: Ropes of fibers in the meter wave band // Astronomy Letters. Vol. 34. P. 486–499. DOI: 10.1134/S1063773708070074

Chertok I. M., Fomichev V. V., Gnezdilov A. A. et al., 2001. Multi-scale temporal features of the 14 July 2000 meter wavelength dynamic radio spectrum compared with TRACE data // Sol. Phys. Vol. 204. P. 141–254.

Elgarøy Ø., 1959. Observations of the fine structure of Enhanced solar radio radiation with a narrow-band spectrum analyser // Nature. Vol. 184. P. 887–888. 10.1038/184887a0

Iskov V. N., Chertok I. M., Chernov G. P., Fomichev V. V. et al., 1985. Analysis of the flare of May 16, 1981 with a complex space-time structure using optical, X-ray and radio observations // Bull. Astr. Inst. Czechslovakia. Vol. 36. P. 81–97.

Gary D. E., Dulk G. A., House L. L. et al., 1985. The Type IV burst of 1980 June 29, 0233 UT: Harmonic plasma emission // Astron. Astrophys. Vol. 52. P. 42–50.

Gopalswami N., 2016. History and development of coronal mass ejections as a key player in solar terrestrial relationship // Geosci. Lett. Vol. 3, No. 8. P. 1–18. DOI: 10.1186/s40562-016-0039-2

Mann G., Baumgartel K., Chernov G. P., Karlicky M., 1989. Interpretation of a special fine structure in type IV solar radio bursts // Sol. Phys. Vol. 120. P. 383–391.

Masuda S., Kosugi T., Hudson H. S., 2001. A Hard X-ray Two-Ribbon Flare Observed with Yohkoh/HXT // Sol. Phys. Vol. 204. P. 55–67. 10.1023/A:1014230629731

Morosan D. E., Kilpua E. K.J., Carley E. P., Monstein C., 2019. Variable emission mechanism of a Type IV radio burst // Astron. Astrophys. Vol. 623, No. A63. P. 1–12. doi.org/10.1051/0004-6361/201834510

Morosan D. E., Kumari A., Kilpua E. K.J., Hamini A., 2021. Moving solar radio bursts and their association with coronal mass ejections // Astron. Astrophys. Vol. 647, No. L12. P. 1–5. https://doi.org/10.1051/0004–6361/202140392

Pick M., Forbes T. G., Mann G. et al., 2006. Multi-wavelength observations of CMEs and associated phenomena. Report of Working Group F // Space Sci. Rev. Vol. 123. P. 341–382. 10.1007/s11214-006-9021-1

Pick M., Vilmer N., 2008. Sixty-five years of solar radioastronomy: flares, coronal mass ejections and Sun–Earth connection // Astron. Astrophys. Rev. Vol. 16. P. 1–153. DOI: 10.1007/s00159-008-0013-x

Ramesh R., Kishore P., Mulay Sargam M. et al., 2013. Low-frequency observations of drifting, non-thermal continuum radio emission associated with the solar coronal mass ejections // The Astrophys. J. Vol. 778, No. 30. P. 1–8. DOI: 10.1088/0004-637X/778/1/30

Reiner M. J., Kaiser M. L., Karlicky M. et al., 2001. Bastille day event: a radio perspective // Sol. Phys. Vol. 204. P. 123–139.

Riddle A. C., 1970. 80 MHz observations of a moving type IV solar burst, March 1, 1969 // Sol. Phys. Vol. 13. P. 448–457.

Robinson R. D., 1986. The relation between flare-related metric continuum bursts and coronal mass ejections // Sol. Phys. Vol. 104. P. 33–39.

Rosenberg H., 1970. Evidence for mhd pulsations in the solar corona // Astron. Astrophys. Vol. 9. P. 159–162.

Trottet G., Kerdraon A., Benz A. O., Treumann R. A., 1981. Quasi-periodic short-term modulations during a moving type IV burst // Astron. Astrophys. Vol. 93. P. 129–135.

Vršnak B., Warmuth A., Temmer M. et al., 2006. Multi-wavelength study of coronal waves associated with the CME-flare event of 3 November 2003 // Astron. Astrophys. Vol. 448. P. 739–752. DOI: 10.1051/0004-6361:20053740

Wang S. J., Yan Y. H., Zhao R. Z., Fu Q. J. et al., 2001. Broadband radio bursts and the structures during the great solar event on 14 July // Sol. Phys. Vol. 204. P. 155–166.

Wild J. P., 1967. The radioherliograph and the radio astronomy programme of the Culgoora Observatory // Proc. Astron. Soc. Australia. Vol. 1. P. 28–30.

Zaitsev V. V., Stepanov A. V., 1975. On the nature of pulsations of type IV solar radio emission // Investigations on geomagnetism, aeronomy, and physics of the Sun. Vol. 37. P. 1–18.

Zaitsev V. V., Stepanov A. B., Chernov G. P., 1984. Pulsations of the type IV radio bursts as an indicator of protonability of solar flare // Sol. Phys. Vol. 93. P. 363–377.

Zheleznyakov V. V., Zlotnik E. Ya., 1975. Cyclotron wave instability in the corona and origin of solar radio emission with fine structure. III. Origin of zebra pattern // Sol. Phys. Vol. 44. P. 461– 470.

Zheleznyakov V. V., Zlotnik E. Y., Zaitsev V. V., Shaposhnikov V. E., 2016. The double plasma resonance effect and its role in radioastronomy // Phys.-Usp. Vol. 59, No. 10. P. 997–1120. DOI: https://doi.org/10.3367/UFNe.2016.05.037813

Chapter 5
ON THE ISSUE OF THE ORIGIN OF TYPE II SOLAR RADIO BURSTS

Abstract. Type II solar radio bursts are among the most powerful events in the solar radio emission in the meter wavelength range. It is generally accepted that the agents generating type II radio bursts are magnetohydrodynamic shock waves. But the relationship between the shock waves and the other manifestations of the large-scale disturbances in the solar atmosphere (coronal mass ejections, Morton waves, EUW waves) remains unclear. To clarify the problem it is important to determine the conditions of type II radio bursts generation. Here, the model of the radio source is based on the generation of radio emission within the front of the collisionless shock wave where the Buneman instability of plasma waves is developed. In the frame of this model, the Alfven magnetic Mach number must exceed the critical value, and there is a strict restriction on the perpendicularity of the front. The model allows to obtain the information about the parameters of shock waves and the parameters of the medium by the parameters of type II bursts. The estimates, obtained in this paper for several events with the band-splitting of the fundamental and harmonic emission bands of type II bursts, confirm the necessary conditions of the model. In this case registration of type II radio bursts is an indication on the propagation of shock waves in the solar atmosphere, and the absence of type II radio bursts is not an indication on the absence of shock wave. Such a situation should be taken into account when investigating the relationship between type II radio bursts and other manifestations of solar activity.

5.1. Introduction

Type II solar radio bursts are among the most powerful events in the solar radio emission in the meter wavelength range. On the dynamic spectrum, they appear as two harmonically related bands (in a ratio of 2/1) slowly drifting in frequency from high frequencies to low frequencies (Wild et al., 1954; Zheleznyakov, 1964; Kundu, 1965). In addition to the harmonic structure, bursts of this type have a various

fine structure of the dynamic spectra–splitting of each of the harmonic bands into two sub-bands, a herringbone structure characterized by the appearance of rapidly drifting bursts both towards low and towards high frequencies, patchy structure, etc.

At present, it is generally accepted that the agents generating type II radio bursts are magnetohydrodynamic shock (MHD) waves. Such MHD shock waves in the solar corona can be generated by solar flares, coronal matter ejections (CMEs), and fast plasma flows in the regions of reconnection of magnetic field lines (termination or quasi-stationary shock waves). In recent years, the spacecraft observations have shown (Cane, Erickson, 2005) that shock waves and type II radio bursts are also observed in the interplanetary plasma (they are called interplanetary shock waves, and decameter and kilometer type II radio bursts, respectively).

Numerous studies of the relationship between coronal shock waves and coronal (in the meter wavelength range) radio bursts of type II with interplanetary shock waves and decameter (Dm**)** and kilometer (km) radio bursts of type II, as well as the identification of the type of shock waves (explosive or piston, in front of the CME) still did not give a clear picture.

In studies of solar radio bursts of type II, a difficult situation has now emerged, when many papers appeared with a detailed investigation of the relationship between shock waves (sources of type II bursts) and coronal mass ejections (CMEs), but without taking into account the mechanisms of radio emission, without which it is impossible to understand the fragmented structure of the dynamic spectra, the connection between type II bursts in the meter range and type II interplanetary bursts (in Dm and km wavelengths), as well as the relationship of type II radio bursts with other manifestations of large-scale disturbances in the solar atmosphere (Moreton waves, extreme ultraviolet waves, EUV).

In a recent article by Cairns et al. (2020) it was shown that all the shock waves are piston waves at the leading edge of the CME, and only the bursts with very high initial frequencies (~800 MHz) could be connected with explosive shock waves. At the heights of decimeter-range sources, only waves in the extreme ultraviolet radiation (EUV) are usually observed, and CME formation occurs higher in the corona. Detailed analysis of the unique set of observational data on the event of November 4, 2015 (ground based and space observations in optic, X-ray and UV ranges, and in wide ra-

dio diapason from 1000 MHz to 40 kHz) during which three meter type II bursts were observed in the same active region, showed that only the last (and the weakest of the three) had continuation as an interplanetary burst up to frequencies of ~20 kHz. Type II bursts are interpreted in terms of shock-drift acceleration and magnetic-mirror reflection at shocks; development of a beam distribution of reflected electrons; growth of Langmuir waves via the beam instability, and non-linear wave-wave processes that convert Langmuir wave energy into radio emission near the electron plasma frequency f_{pe} and near $2f_{pe}$ (Knock et al., 2001).

In (Maguire et al., 2020) questions were raised not only about the relationship of type II bursts with CME (explosive or piston type of shock wave?), but also on the evolution of the Alfvén Mach number $M = V_{sh}/V_A$ (V_{sh} and V_A are the shock wave velocity and the Alfvén velocity) and on the initial and final frequencies of bursts. The Mach number was determined in three different ways: 1) from the geometry of the shock front propagation (in the CME images in extreme ultraviolet and LASCO), where the key parameter is the distance between the shock front and the CME nose; 2) by ratio of the CME velocity to the Alfvén velocity; and 3) by value of the band splitting in type II bursts according to the method proposed by Vršnak et al. (2002), where the origin of the splitting branches is interpreted in terms of the plasma emission from the upstream and downstream shock regions (behind and ahead of the shock front) in accordance with the model of Smerd et al. (1974). Analysis of the event of September 2, 2017 when the type II burst was observed at frequencies of 80–20 MHz (according to the Irish Low Frequency Array (I–LOFAR) data) showed that all three methods give consistent results and the same tendency of evolution of the Alfvén Mach number: the type II radio emission emerged from near the nose of the CME when M_A was in the range 1.2–1.4 at a heliocentric distance of ~1.6 Rs, and the emission ceased when the CME reached ~1.7 Rs, despite an increasing Alfvén Mach number up to 4. It was suggested that the radio emission cessation is due to the lack of quasi-perpendicular geometry at this altitude, which inhibits efficient electron acceleration and subsequent radio emission.

The work of Zucca et al. (2014) showed a detailed correspondence between CME and the shock front as a piston one in the phenomenon of November 6, 2013. The interpretation of splitting of the second harmonic at frequencies of 550–150 MHz as radia-

tion ahead of the front and behind the front is confirmed by observations of radio sources with the radioheliograph in Nançay. However, the authors do not continue their analysis of the continuation of the burst at lower frequencies of 80–40 MHz (shown there in Figs. 2 and 11). It was suggested that at these distances the shock front of blast type was formed as a result of interaction the CME with the coronal hole, propagated independently of CME, and had no continuation at km waves.

In paper of Corona-Romero et al. (2015) it is affirmed that all the interplanetary shock waves associated with km type II bursts were explosive, at least beyond ~21 R_S (i.e., at frequencies ≤1 MHz). A blast regression technique is used to determine the speed and position of the front. It was found that the velocity of shocks near the Earth's orbit in all the considered 8 phenomena (CME/shock front) was higher than the speed of the corresponding CMEs, and the calculated time and velocity agree with their values measured in the Earth's orbit.

The first concepts, that type II radio bursts are observed only at meter wavelengths, have changed in recent years with the expansion of qualitative observations. In particular, the bursts have been observed with the initial frequencies far in the decimeter range, ~800 MHz (Cairns et al., 2020) or even ~1200 MHz (Pohjolainen et al., 2008), that is, at the altitudes where type II bursts can only be caused by explosive shock waves.

An intermediate case is the work of Zimovets et al. (2012), which presented the results of unique observations of the type II burst on November 3, 2010: simultaneous observations of radio spectrum in the range of 550–150 MHz, the positions of radio sources at ten frequencies between 445 and 151 MHz with the Nançay radioheliograph, plasma ejections in the extreme ultraviolet lines (AIA/SDO) and hard X-ray source (RHESSI). It has been shown that the onset of the type II burst was associated with a shock wave at the leading edge of the plasma ejection, i.e., unambiguously with a piston shock wave. But after about 20 s, the velocity of the shock front doubled, it moved away from the ejection and then propagated like an explosive front. The authors estimated the Mach number from the parameters of splitting of the second harmonic bands and obtained very small values, M 1.06–1.16. The authors conclude that in this case, the particles were somehow accelerated since the type II burst was observed.

The results of a statistic study of the relationship between shock waves and their velocities with CME for 1997–2005 were given in the work of Rahman et al. (2012). It was found that out of 101 CMEs, 52 phenomena did not contain both meter and km type II bursts. In 38 events, both meter and km bursts were observed. But the continuation of the meter burst in the km range was observed only in 23 phenomena. 12 interplanetary CMEs (ICMEs) had high velocities, $\geq$2000 km/s. It is noteworthy that velocities of the interplanetary shock waves in all the phenomena exceeded velocities of the corresponding interplanetary (MP) CMEs. In all 101 events shock wave arrived the Earth's orbit before (MP) CME, and the distance between shock wave and (MP) CME was minimum ($\sim$17 R_S) in the events with high velocity, but the distance was maximum ($\sim$35 R_S) in the events in which CME was accompanied only by a km type II burst (without the meter one).

The issue of the relationship between meter type II bursts with interplanetary bursts was considered in the work of Cane and Erickson (2005). Over three years of observations on WIND/WAVES, 31 km type II bursts were detected as a direct continuation of meter bursts. The most important result is a different nature of the bursts, since all km bursts were characterized by the absence of a clear harmonic structure and clumpy parameters. All the interplanetary bursts were associated with piston shock waves in the front of fast CMEs, and meter bursts with other shock waves (possibly explosive). Thus, they were not their direct continuation in the interplanetary space.

Dependence of different manifestation of type II radio bursts in decametric, metric and kilometric ranges on power of the solar flares was discussed in review of Pick et al. (2006). It was remarked that the blast-wave shocks, connected with the metric type II burst, did not propagate in the interplanetary space. In most cases the type II radio bursts in decametric and kilometric range were connected with the piston shocks. The unclear connection of type II radio bursts in decametric and metric ranges with different eruptive events observed in white light, radio, optical lines, UV, and X-rays was also noted.

Although the idea, that a driver for type II radio bursts is a shock wave, is generally accepted, all the estimations of their parameters (velocity, Alfven number M) and plasma parameters (magnetic field, density) were done in many works only from kinematic con-

siderations in terms of plasma parameters and the shock front velocity without considering a specific mechanism of radio emission. For example, Bacchini et al. (2015) consider the acceleration of particles to speeds above the ion-acoustic speed sufficient for type II radiation. Their calculations show that a perpendicular wave can exist at the beginning, and it becomes parallel with distance in the corona. Obviously, such estimates cannot unambiguously explain the beginning and end of the emission from a type II burst.

Similar estimates were made by Mann et al. (1995). The critical values of the Mach number M_{cr} for quasi-parallel fronts are between 1.2 and 2.3, and for quasi-perpendicular fronts are between 1.5 and 2.8. It was concluded that a longitudinal wave is considered preferable, but the possibility of a perpendicular wave is not excluded.

It is necessary to note also that type II radio emission exhibits often burst-like and irregular (fragmented) dynamic spectra. It means, that the conditions for the radio emission to be generated are fulfilled irregularly and in distinct regions along large-scaled shock front.

Below, for clarification of these issues, we discuss the possibility of obtaining information on the parameters of solar plasma and shock waves necessary for generation of type II radio bursts.

5.2. Discussion of the mechanism of radio emission

Experimental data on type II bursts (high effective radiation temperature $T_{\text{eff}} - T_c$, sharp non-stationarity and a narrow frequency band, the complexity of the dynamic spectrum, short duration) indicate a coherent generation mechanism, since it is coherent radiation that is closely related to wave amplification that is realized only in limited frequency intervals and with special types of plasma particle velocity distribution that exist for a limited time. At present, it is generally accepted that the agent generating type II radio bursts is magnetohydrodynamic shock (MHD) waves. Such MHD shock waves in the solar corona can be generated, for example, by solar flares and coronal matter ejections (CMEs). This connection is supported by the numerous studies of the connection between type II radio bursts and these eruptive phenomena (CME, ultraviolet waves, Moreton waves) (e.g., Smith, Harvey, 1971; Harvey et al., 1974; Thompson et al., 2000; Klassen et al., 2000; Tripathi, Raouafi, 2007; Warmuth, 2010; Zhukov, 2011), as

well as a proximity of the estimated velocities of agents exciting type II radio bursts and the Alfvén velocities in the solar corona. In constructing the theory of type II radio bursts, the most difficult problem was the generation of plasma waves, in particular, the implementation of non-equilibrium electron distribution functions in the shock front. A number of theories have been put forward to address this problem.

In papers of Cairns et al. (2020) and Knock et al. (2001) the generation of type II bursts is associated with the drift acceleration of electrons at the perpendicular shock front, the formation of fluxes of accelerated electrons, the excitation of Langmuir waves in the region ahead of the shock front and their transformation through non-linear wave-wave processes into radio emission at frequencies close to the electron plasma frequency f_{pe} and its second harmonic $2f_{pe}$. Such model was used in many papers (Knock et al., 2001; Vršnak et al., 2001; Vršnak et al., 2002; Zucca et al., 2014; Maguire et al., 2020; Cairns et al., 2020) in the analyses of type II radio bursts. However, within the framework of such a model, a number of the problems remain in the interpretation of such characteristics of bursts as a narrow bandwidth of the emission bands in frequency and a fine structure of the bands of splitting type. This model explains the acceleration and the formation of fluxes of accelerated electrons and the excitation of Langmuir waves in the upstream region of the shock front, but the issue of formation of fluxes of accelerated electrons in the downstream region remained uncleared. Therefore, the origin of split-structure in the frame of this model remains also unknown.

Another approach for explanation of the complex structure of type II radio bursts is based on the possibility for radio emission to be generated in different parts of the shock front (McLean, 1967). Particularly, Holman and Pesess (1983) suggested that the electrons responsible for the type II bursts might get accelerated from the shock flanks. In recent paper (Majumdar et al., 2021) it was shown that in the event of January 26, 2014 (with CME and type II burst) the source of radio emission was indeed located in the flank of the shock front. Nevertheless, the geometrical interpretation presuming a several source-emission sources cannot account for behavior of the splitting structure (synchronized intensity and frequency drift variation) because of the space separation of such sources and their moving in different coronal regions.

The most consistent theory of the generation of type II radio bursts was put forward by Pikel'ner and Guntsburg (1963) and later developed in (Zheleznyakov, 1965; Zaitsev, 1965; Zaitsev, Kaplan, 1966; Zaitsev, 1968; Zaitsev, 1977). It is based on the laminar theory of weak collisionless shock waves (M < 2) propagating perpendicular to the magnetic field.

If the number of collisions in plasma is sufficiently small (as occurs in the solar atmosphere– chromosphere and corona), the shock front is an oscillatory structure consisting of a sequence of solitons of compression or rarefaction (Sagdeev, 1964). The type and scale of this structure depend on the Alfvenic Mach number $M = V_{sw}/V_A$ (here, V_{sw} is the shock wave speed and $V_A = H_0/(4\pi N_0 m_i)^{1/2}$ is the Alfven velocity), the angle θ between the front plane and the direction of undisturbed magnetic field H_0, and the parameter $\alpha = H_0^2/4\pi N_0 m_e c^2 = \omega_{H_0}^2/\omega_{L_0}^2$, where $\omega_{H_0} = eH_0/m_e c$, $\omega_{L0} = (4\pi e^2 N_0/m_e)^{1/2}$, N_0 and H_0 – electron density and strength of the upstream magnetic field, correspondently, and c is the speed of light. Here value $\theta = 0$ corresponds to transverse propagation of the shock wave relatively the upstream magnetic field, and $\theta = \pi/2$ corresponds to longitudinal propagation. As shown by Zaitsev (1970), shock waves differ qualitatively at $\theta < \theta_{cr}$ and $\theta > \theta_{cr}$ ($\sin\theta_{cr} = V_{sw}/c$). The shock transition occurs through a sequence of solitary compression waves at $\theta < \theta_{cr}$ and through a sequence of rarefaction waves at $\theta > \theta_{cr}$. The characteristic scale of a solitary wave, e.g., for compression waves at $\theta \approx 0$ (quasi-transverse propagation) is $\delta \approx c/\omega_{L0}\,(1 + \alpha + \alpha^2 m_e/m_i)/(1 + \alpha m_e/m_i)^{3/2}$. The inhomogeneity of the magnetic field in solitons makes the electrons drift in the plane of the shock front. The relative drift velocity of electrons and ions $V_* = 4 \cdot 2^{1/2} \cdot 3^{-3/2}\, c\, \omega_{H_0}\, (\omega_{L_0}^2 + \omega_{H_0}^2)^{-1/2}\, (M - 1)^{3/2}$ exceeds the thermal electron velocity $V_{Te} = (kT/m_e)^{1/2}$ if

$$M > M_{cr} = 1 + [8\pi N_0\, kT(1 + \alpha)\, H_0^{-2}]^{1/3} \qquad (5.1)$$

($k = 1.38 \cdot 10^{-16}$ erg/K is the Boltzmann constant) (Zaitsev, 1969). This leads to the generation of plasma oscillations (the Buneman instability) and, as a result of the induced scattering of plasma waves on fast electrons, to the generation of electromagnetic radiation. This mechanism made it possible to develop a comprehensive model of the source of classical type II bursts (Zaitsev, 1977) and to explain all the parameters of radio bursts including the fine structure.

Within the frame of this theory, the observed characteristics of type II radio bursts are related both to the parameters of the solar corona and to the parameters of shock waves: 1. The observed frequency of the fundamental tone of type II radio bursts f is close to the plasma frequency of plasma waves excited in the shock front which is determined by the value concentration of electrons N in that section of the front, where the supercriticality (the ratio of the relative drift velocity of electrons and ions) is maximum, it is essential that value $N > N_0$ (concentration of electrons in upstream region of the shock. 2. The same statement is valid for the observed relative frequency drift velocity $f^{-1}df/dt$. 3. The splitting of the dynamic spectra δf of type II bursts is due to the fact that the maximum supercriticality on the forward slope of the leading soliton is realized at lower values of the plasma concentration than on the trailing slope due to the heating of electrons by the Buneman instability. Thus, it is possible to formulate a system of equations connecting the quantities f, $f^{-1}df/dt$, and δf determined from the dynamic spectrum with unknown values of the concentration N_0, magnetic field H_0, and Mach number M (Zaitsev, 1968; Fomichev, 1972).

This system of equations includes not only the effects associated with the inhomogeneity of the concentration and magnetic field in the solar corona, but also effects caused by changes in the intensity of shock waves. This means that from the observed characteristics of type II bursts, one can obtain important information on the nature of the propagation of shock waves in the inhomogeneous plasma of the solar corona, as well as the parameters of the latter (magnetic field, density). The first such estimates were given in (Zaitsev, 1968; Fomichev, 1972). The obtained calculations for M, H_0 and front velocity V_R for nine bursts were very diverse. Despite the fact that each phenomenon is purely individual, it was concluded that the onset of the burst is associated with the achievement of the Mach number of the critical value, and the end of the burst with a possible overturning of the front, when the Mach number continues to grow ($M > 2$). The absence at that time of information about the trajectory of the shock front relative to the magnetic field lines did not allow to associate the interruption or termination of radio emission generation with the type of shock wave (perpendicular or longitudinal).

The laminar structure of shock waves moving along the magnetic field in plasma with $\beta = 8\pi N_0 kT/H_0^2 \ll 1$ exists in the range

$1 < M < 1.5$. The front of the shock wave also involves a drift current directed across the disturbed magnetic field. However, the relative velocity of electrons and ions V_d in this case is much lower than the electron thermal velocity V_{Te}; therefore, the ordinary Buneman instability occurring in transverse shock waves does not develop. Instead, a modified Buneman instability with a very low excitation threshold $V_d > V_{Ti}$ develops in longitudinal shock wave at $Te \approx Ti$. The excitation condition begins to be satisfied in front sections at Alfvenic Mach number $M > 1 + (V_{Ti}/2V_A)^{1/2}$ (Zaitsev, Ledenev, 1976). As a result, longitudinal waves are excited at the lower hybrid frequency $\omega \approx (\omega_{H_e} \omega_{H_i})^{1/2}$ with an energy density of about $W \approx N_0 m_e V_d^2$ in the saturation mode (Galeev, Sagdeev, 1973). The energy of these waves is transferred to particles; electrons are heated to the temperature $Te \approx Ti \approx H_0^2/8\pi N_0$, i.e., acquire an average thermal velocity $V_t \approx \frac{1}{2} (m_i/m_e)^{1/2} V_A$. In the solar corona, $V_A \approx 5 \cdot 10^7 - 10^8$ cm/s; therefore, $V_t \approx (1-2) \cdot 10^9$ cm/s significantly exceeds the thermal velocity of electrons in the undisturbed corona ($V_{Te} \approx 5 \cdot 10^8$ cm/s), and the concentration of fast electrons escaping beyond the front can reach $Ns \sim \frac{1}{2} (m_e/m_i)^{1/2} N_0 \approx 10^{-2} N_0$ according to the conclusions made by Zaitsev and Ledenev (1976). In other words, the front of a longitudinal shock wave at $\beta \ll 1$ and at sufficiently large Mach numbers is an emitter of fast electrons, which, falling into a cold plasma behind the front, can excite coherent plasma waves and be a source of radio emission. But in this case, it remains difficult to explain the narrow frequency range of radio emission and the appearance of split components of each of the harmonics of type II bursts. The lower efficiency of longitudinal shock waves for generating type II bursts fully explains the statistics in the work of Rahman et al. (2012): only in 23 events out of 101 the meter burst continued at km waves, since the appearance of longitudinal shock waves in the interplanetary medium is more likely than the perpendicular ones.

Thus, in the frame of the discussed model of the source of type II radio bursts, the following conditions must be fulfilled: 1) the shock wave must be relatively intense, since the excitation of turbulence in shock waves requires that the Mach number exceed a certain critical value M_{cr}, and 2) the shock wave must be perpendicular, a slight deviation Θ from $\Theta = 0$ makes the conditions for the excitation of plasma waves in the shock front more stringent, and at $\Theta \geq V_{sw}/s \approx 0.033 \approx 2°$, the generation of plasma waves stops

almost completely. It means that the source of radio emission can be formed at any part of the shock front (bow or flanks) simultaneously or in different times, depending on where and when the specified conditions are fulfilled (sufficient intensity and perpendicularity of the shock front, that is $M > M_{cr}$ and $\Theta = 0$), and the dynamic spectrum of type II radio bursts can represent either continuously drifting stripes or have an interruptive and a blob structure.

Important role of variation of this angle is confirmed by the two-dimensional MHD-modeling of the filament explosion accompanied by coronal EIT waves, diming and CME formation, carried out by Pomoell et al. (2008). Figure 6 in their paper shows the geometry of the magnetic field and the shock front, where it can be seen that the leading edge of the front propagates strictly perpendicularly to the force lines, and on the side parts the front crosses the force lines four times, therefore, on these parts of the front, radiation can be interrupted. Another interesting type II burst is considered by Christaphi et al. (2020). The burst observed on July 15, 2017 at LOFAR's LBA station in the 3–50 MHz range, at the initial stage (the first 30 seconds) was without frequency drift and then continuously transformed into a type II-like burst with the negative frequency drift. The authors attribute this phenomenon to the formation of a shock front during the interaction of CME with a coronal ray. Here, the radiation was not interrupted, the front remained perpendicular only on the flanks of the front. But at the first stage, it spread the coronal beam, and the radiation source moved almost along the levels of equal density. Subsequently, the front shifted almost across the levels, which is responsible for the appearance of the frequency drift.

Thus, although the question of shock waves as drivers of type II solar radio bursts is considered as generally accepted, however many questions, such as the relationship of shock waves with flares and coronal mass ejections, the type of shock waves (perpendicular or longitudinal), the relationship of meter type II radio bursts with kilometric type II bursts, and coronal shock waves with interplanetary shock waves are awaiting their decision. In this connection, it is of interest to analyze the origin of the fragmented structure of type II burst. Such a structure may be connected with propagation of shock wave in the inhomogeneous (density, magnetic field) solar atmosphere. In this case the characteristics of type II bursts reflect the characteristics of the medium where shock was propagating,

and a possibility appears to know what parameters of the medium and their variations can lead to forming these dynamic spectrum (with interruptions and reactivations of radio emission).

To make clear this issue it is important to determine an adequate mechanism for the generation of type II radio bursts. Below we will try to get the additional answers to these questions using the data from observations of several type II bursts in the frame of the generation mechanism within front of a collisionless shock wave (based on the development of Buneman instability of plasma waves), which makes it possible to obtain estimates of the corona and shock waves parameters. We will be interested, in particular, in estimations of the Alfven Mach number M, the critical value M_{cr} and their variation during type II radio bursts (or their fragments), that is, the parameters which can determine a duration of the radio emission.

5.3. Observations and results

Dynamic spectra of the type II radio bursts are very diverse, associated primarily with the diffuseness of the spectrum and the clumpy structure of the spectrum, when it is difficult to trace both harmonic bands and their clear splitting into two sub-bands. Therefore, it is necessary to choose suitable type II bursts and, basing on their parameters, to answer the questions why intensive bursts in the meter range after powerful flares sometimes do not extend in the decametric and kilometric ranges, and, vice versa, less expressive bursts after moderate flares are observed in the interplanetary space. The complexity of unambiguous judgments on these issues is discussed in the review by Pick et al. (2006). There it was noticed that the blast wave associated with a meter type II burst rarely passes into the interplanetary space. And most of the type II radio bursts in the Dm and km ranges are associated with piston shock waves. It is also noted that the picture sometimes becomes more complicated when the radiation is clearly emanating from the flanks of the shock front. However, the generation mechanism in this paper is only mentioned, that this is a plasma mechanism in the presence of fast particles, and it is not verified what is the reason for the beginning and end of type II radiation (without estimates of the critical Mach number).

For further analysis we use the database of radio spectral observations at IZMIRAN (https://www.izmiran.ru/stp/lars/Mo-

reSp.html) and the dynamic spectra of type II bursts, which were given and discussed in the published papers. Additional data are obtained from the CME catalog (SOHO/LASCO) and radio spectra (WIND/WAVE and STEREO AB spacecraft). Data on flares in the optical, ultraviolet and X-ray ranges from the SDO spacecraft are available at https://solarmonitor.org/index.php?date To answer the questions why large bursts in the meter range after powerful flares sometimes do not go into the Dm and km ranges, and, vice versa, less expressive bursts after moderate flares continue in the interplanetary space, we estimate the parameters of shock waves generating type II radio bursts. Here we estimate the Alfvén Mach number at the moments of the beginning and end of the type II radio bursts (or their separate fragments) and compare them with the critical value of the Alfvén Mach number. As indicated in the previous section, in the frame of the model with excitation of plasma turbulence within the front of a collisionless shock wave, the observed characteristics of type II radio bursts (frequency of the fundamental tone f, relative frequency drift velocity $f^{-1}df/dt$, splitting of dynamic spectra δf) are related both to the parameters of the solar corona, and with the parameters of shock waves (Zaitsev, 1968; Fomichev, 1972).

1. The observed frequency of the fundamental tone of type II radio bursts, more exactly the low frequency line f_L in bursts with splitting, is close to the plasma frequency of plasma waves excited in the shock front which is determined by the value concentration of electrons N in that section of the front, where the supercriticality (the ratio of the relative drift velocity of electrons and ions) is maximum, it is essential that the value $N > N_0$ (concentration of electrons in upstream region of the shock,

$$f = 1/2\pi\ (N_0 Z\, 4\,\pi e^2/m_e)^{1/2}, \tag{5.2}$$

where

$$Z = 0.94\ (1 + 0.28\ \mathrm{M}^2)^{1/2} - 0.06. \tag{5.3}$$

2. Time differentiation of (5.2) (neglecting the changing of Mach number in comparison with the changing of electron density) gives expression for relative frequency drift velocity

$$f^{-1}\ df/dt = 1/2\ V_{sh} \cdot L^{-1}\ (N_0) \cdot (\cos\alpha)^{-1}, \tag{5.4}$$

where α is angle between the density gradient and the direction of the shock motion, and $L = N_0\ (dN_0/dR)^{-1}$ is a scale of inhomogeneity of density in the undisturbed solar atmosphere.

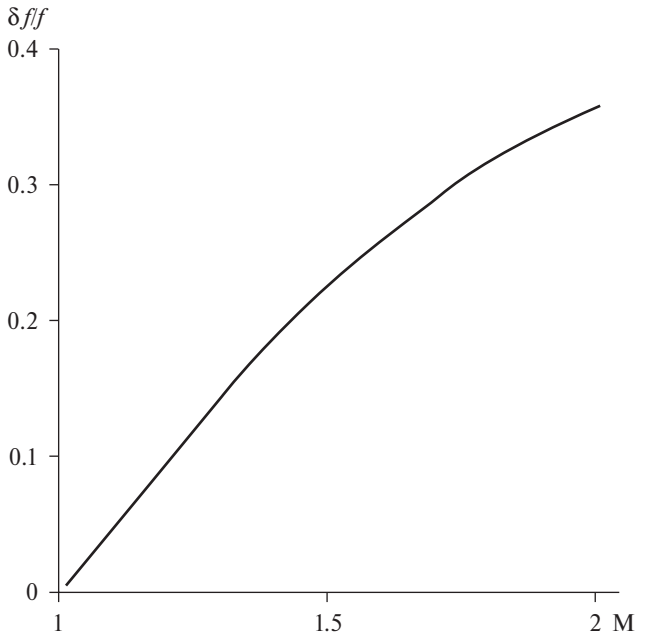

Fig. 5.1. Dependence of Mach number on relative value of frequency splitting $\delta f/f$ of fundamental band of solar type II bursts (Fomichev, 1972)

3. The splitting of the dynamic spectra δf of fundamental and harmonic bands of type II bursts in two sub-bands (low frequency f_L and upper frequency f_U) is due to the fact that the maximum supercriticality on the forward slope of the leading soliton is realized at lower values of the plasma concentration than on the trailing slope due to the heating of electrons by the Buneman instability. The expression of the dependence of relative value of splitting $\delta f/f$ on Mach number M is rather cumbersome (Zaitsev, 1968; Fomichev, 1972; Zaitsev, 1977). Such a dependence is shown in Fig. 5.1.

It is important to note that the observed frequency of the fundamental tone of type II radio bursts (or the frequency of the low frequency line in bursts with splitting f_L) is close to the plasma frequency of plasma waves excited within the shock front which is determined by the value of concentration of electrons N in that section of the front, where the ratio of the relative drift velocity of electrons and ions is maximum, but not by the value concentration of electrons N_0 in the upstream region of shock.

Derived a self-consistent system of equations connects the quantities f, $f^{-1}df/dt$, and $\delta f/f$ determined from the dynamic spectrum with unknown values of the concentration N_0, magnetic field H_0, and Mach number M, the solution of which gives the sought parameters.

The procedures of estimation of the shocks and of the plasma parameters are as follows. Firstly, for each frequency f, Mach number M is evaluated by the observable relative value of splitting $\delta f/f$ from the known dependence of $\delta f/f$ on M (or from Fig. 5.1) and Z. Then, from equations (5.2) and (5.4) N_0 can be obtained:

$$N_0 = 1.2 \cdot 10^4 \cdot f^2 \cdot \mathrm{Z}^{-1}, \tag{5.5}$$

and by known L (N_0) the velocity of shock wave can be obtained

$$V_{\mathrm{sh}} = 2L\,(N_0) \cdot f^{-1} \cdot df/dt \cdot (\cos\alpha)^{-1}\,, \tag{5.6}$$

and magnetic field

$$H_0 = 4.9 \cdot 10^{-10} \cdot V_{\mathrm{sh}} \cdot f \cdot M^{-1} \cdot \mathrm{Z}^{-1/2}. \tag{5.7}$$

In these expressions f is in MHz, and V_{sh} is in cm/s.

Because of the plasma nature of the mechanism of generation of radio emission, all the estimations of parameters of the environment and shocks depend on the coronal density model $N(R)$. Here we will use the often used 2 Newkirk density model (Newkirk, 1961). Frequency drift of type II radio bursts depends on both shock velocity, angle α between the density gradient and direction of the shock motion, as well as on shock wave intensity (because $N = N_0 \cdot Z$). In each separate event the value of angle α is unknown, therefore further we possess the averaged value (in the angle interval $(0 - \pi/2)$) $\cos\alpha = 0.636$, it corresponds if to use the 3 Newkirk density model. In the cases when the harmonic emission band in type II bursts is stronger and better defined than the fundamental band then all the measurements were performed at the harmonic emission band and divided into two for the fundamental band.

5.3.1. Event of November 3, 2003

This event is the example of a large burst with a continuation of radio emission in the decameter wavelength range (at 09:50–10:10 UT in Fig. 5.1). This was a GOES X3.9 class flare, and it was already the third flare of this class in the active region NOAA 10488 (N08W77) during the day. The phenomenon was very

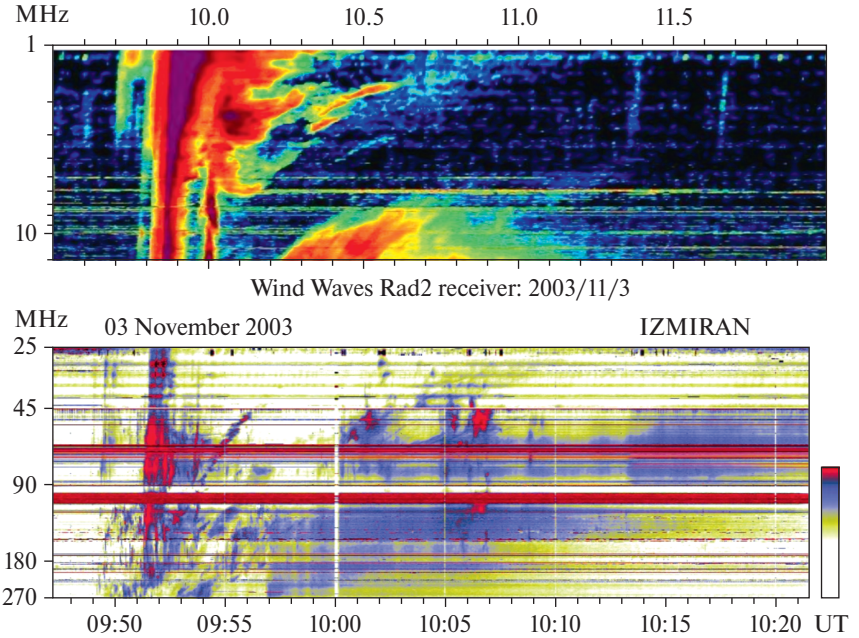

Fig. 5.2. Dynamic spectra of type II radio bursts in the phenomenon of November 3, 2003 in the meter range (IZMIRAN, below) and in the decameter range (above, the wind waves Rad2 spectrum)

complex and was described in details in the works of Chertok et al. (2005), Vršnak et al. (2006), and Chernov et al. (2007). The detailed analysis of the observations (the H_α wave signature, soft X-ray wave signature, the EUV wave signature, the radio date of the Nancay Multifrequency Radioheliograph, the dynamic spectra from a number ground-based observatories covering the range 20–800 MHz and 0.8–4.5 GHz, the radio emission spectrum in the range 1.075–13.825 MHz from the wind spacecraft) did not allow to get a clear answer on the question whether the shock waves (generating the type II bursts) are the CME-driven shocks or are of the flare initiated shocks (Vršnak et al., 2006).

Here we will be interested in the parameters of shock waves generating the type II bursts. By the IZMIRAN's data the type II burst started at 09:49 UT at 270 MHz (Fig. 5.2). The dynamic spectrum shows a complex pattern with several type II emission bands and multilane structure. For analysis we chose the fragment

of the dynamic spectrum in the time interval 10:00–10:08 UT in the frequency range 90–28 MHz where it is possible to measure the parameters of the splitting lanes (oblique dark lines in Fig. 5.3). Consider the segment of the burst at the fundamental band in the time interval 10:00:30–10:01:30 UT in the frequency range 66–48 MHz. This segment started about 10:00:30 UT in the frequency range 62–54 MHz, and at this moment (beginning of the segment) the frequency drift (df/dt) of the band at the fundamental frequency between 10:00:30 and 10:01 UT turns out to be about 0.11 MHz/s, the relative drift rate amounts to $(df/dt) \cdot f^{-1} \sim 0.002 \text{s}^{-1}$, the frequency of the low frequency sub-band $f_L \sim 54$ MHz, the frequency of the upper frequency sub-band $f_U \sim 62$ MHz, the splitting of the dynamic spectra δf is about 8 MHz. Following the procedure of estimation of the shocks and of the plasma parameters (Zaitsev, 1968; Fomichev, 1972), using these data we obtain the Alfven magnetic number $M \sim 1.33$, and $Z \sim 1.1$. It means that the electron density in the upstream of the shock $N_0 \sim 3 \cdot 10^7$ cm^{-3} corresponds to the plasma frequency ~50 MHz. For the standard 2 Newkirk coronal density model we obtain then the estimates of the full shock velocity $V_{sh} \sim 2200$ km/s and the magnetic field $H_0 \sim 3.3$ G. At last, we have an estimates of the critical value of the Alfven magnetic numbers $M_{cr} \sim 1.15$ and 1.2 for the coronal temperatures $T \sim 10^6$ K and $2 \cdot 10^6$ K, correspondingly.

At the moment of the end of this segment (10:01:30 UT) the parameters of the radio burst were as follows: the frequency drift $df/dt \sim 0.08$ MHz/s, the relative drift rate $(df/dt) \cdot f^{-1} \sim 0.0016$ s^{-1}, the frequency of the low frequency sub-band $f_L \sim 48$ MHz, the frequency of the upper frequency sub-band $f_U \sim 54$ MHz, the splitting of the dynamic spectra δf is about 6 MHz. Then, we obtain the estimates $M \sim 1.27$, $Z \sim 1.07$, $N_0 \sim 2.5 \cdot 10^7$ c^{-3}, $V_{sh} \sim 2000$ km/s, $H_0 \sim 2.5$ G, and the critical value of the Alfven magnetic numbers $M_{cr} \sim 1.14$ and 1.18 for the coronal temperatures $T \sim 10^6$ K and $2 \cdot 10^6$ K, correspondingly. The estimates presented above show that the parameters of the shock remain practically constant, and the condition $M > M_{cr}$ is fulfilled during all the duration of the segment. Therefore, the most probable reason of the end of the segment is that the shock wave enters a region where the magnetic field orientation was very different, and the shock wave became a parallel (that is a condition of the perpendicularity was violated).

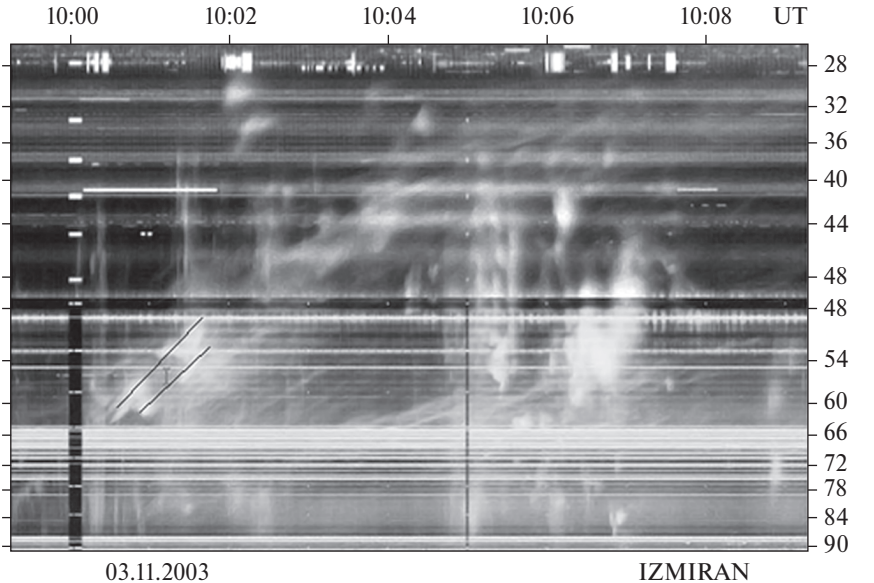

Fig. 5.3. An enlarged fragment of the spectrum of the IZMIRAN radio burst on November 3, 2003. Thin oblique dark lines show the split bands at the first harmonic used to determine the Mach number. Two marks of 48 MHz on the Y-axis is a result of stacking of partly overlapping frequency bands (90–45 MHz and 50–25 MHz) of two spectrographs

It should be noted that in accordance with the observations on SOHO/LASCO C2 (Solar and Heliospheric Observatory), https://cdaw.gsfc.nasa.gov/movie/make_javamovie.php?-date=20031103&img1=lasc2rdf&img2=wwaves. velocity of the CME was about ~1500 km/s in the beginning of the event with a low slowing-down up to distances 30 *RS*. According to Vršnak et al. (2006) the shock front overtook the CME. The estimates of the velocity of shock wave obtained above (~ 2000 km/s) are in a good accordance with these data.

5.3.2. Event of February 21, 1999

This event was included in the list of 18 coronal type II bursts recorded in the decimetric-metric wavelength range and was discussed in Vršnak et al. (2002). The dynamic spectrum of the type II burst (their Fig. 1) showed the fundamental and harmonic emission bands, both frequency bands split in two sub-bands at frequencies below 100 MHz. The measurements were performed at the harmonic emission band because of stronger intensity, and only

a part of the fundamental band could be seen in this event. The upper frequency (f_U) and low frequency (f_L) bands of the band-split emission are marked there by the lines that follow the two emission ridges. In this dynamic spectrum it can be seen three consecutive fragments with interruption of the radio emission between the fragments. Following the method in the previous section we determine the parameters of shock wave and the solar corona during all the fragments. For the estimates we used the two-fold Newkirk density model (2N model) and all the parameters of radio emission will be given for the fundamental band.

Fragment 1 ($\sim$ 10:00:30–10:02:00 UT):

The beginning: $f_L \sim 36.5$ MHz, the relative frequency splitting $\delta f \cdot f^{-1} \sim 0.13$, the Alfven magnetic number $M \sim 1.27$, and $Z \sim 1.07$. It means that the electron density and the plasma frequency in the upstream region of the shock $N_0 \sim 1.28 \cdot 10^7$ cm^{-3} and $f_0 \sim 32.5$ MHz. For the relative drift rate $(df/dt) \cdot f^{-1} \sim 0.0013$ s^{-1} we obtain the estimates of the shock velocity $V_{sh} \sim 1000$ km/s and the magnetic field $H_0 \sim 1.25$ G. At last, we have the estimates of the critical value of the Alfven magnetic numbers $M_{cr} \sim 1.15$ and 1.2 for the coronal temperatures $T \sim 10^6$ K and $2 \cdot 10^6$ K, correspondingly.

The end: $f_L \sim 32$ MHz, the relative frequency splitting $\delta f \cdot f^{-1} \sim$ ~ 0.14, the Alfven magnetic number $M \sim 1.32$, and $Z \sim 1.086$, the electron density and the plasma frequency in the upstream region of the shock $N_0 \sim 1.08 \cdot 10^7$ cm^{-3} and $f_0 \sim 29.5$ MHz. For the relative drift rate $(df/dt) \cdot f^{-1} \sim 0.0012$ s^{-1} we obtain the estimates of the shock velocity $V_{sh} \sim 1050$ km/s and the magnetic field $H_0 \sim 1.1$ G. At last, the estimates of the critical value of the Alfven magnetic numbers give $M_{cr} \sim 1.15$ and 1.19 for the coronal temperatures $T \sim 10^6$ K and $2 \cdot 10^6$ K, correspondingly.

Fragment 2 ($\sim$ 10:03:30–10:04:45 UT):

The beginning: $f_L \sim 28.5$ MHz, the relative frequency splitting $\delta f \cdot f^{-1} \sim 0.13$, the Alfven magnetic number $M \sim 1.28$, and $Z \sim 1.07$, the electron density and the plasma frequency in the upstream region of the shock $N_0 \sim 9.4 \cdot 10^6$ cm^{-3} and $f_0 \sim 27.5$ MHz. For the relative drift rate $(df/dt) \cdot f^{-1} \sim 0.0012$ s^{-1} we obtain the estimates of the shock velocity $V_{sh} \sim 1100$ km/s and the magnetic field $H_0 \sim 1.0$ G, the estimates of the critical value of the Alfven magnetic numbers give $M_{cr} \sim 1.15$ and 1.19 for the coronal temperatures $T \sim 10^6$ K and $2 \cdot 10^6$ K, correspondingly.

The end: $f_L \sim 27.0$ MHz, the relative frequency splitting $\delta f \cdot f^{-1} \sim 0.14$, the Alfven magnetic number $M \sim 1.34$, and $Z \sim 1.09$, the electron density and the plasma frequency in the upstream region of the shock $N_0 \sim 8.2 \cdot 10^6$ cm^{-3} and $f_0 \sim 25.8$ MHz. For the relative drift rate $(df/dt) \cdot f^{-1} \sim 0.0012$ s^{-1} we obtain the estimates of the shock velocity $V_{sh} \sim 1150$ km/s and the magnetic field $H_0 \sim 1$ G, the estimates of the critical value of the Alfven magnetic numbers give $M_{cr} \sim 1.14$ and 1.17 for the coronal temperatures $T \sim 10^6$ K and $2 \cdot 10^6$ K, correspondingly.

Fragment 3 ($\sim$ 10:05:30–10:07:00 UT):

The beginning: $f_L \sim 26$ MHz, the relative frequency splitting $\delta f \cdot f^{-1} \sim 0.14$, the Alfven magnetic number $M \sim 1.3$, and $Z \sim 1.08$, the electron density and the plasma frequency in the upstream region of the shock $N_0 \sim 7.7 \cdot 10^6$ cm^{-3} and $f_0 \sim 25$ MHz. For the relative drift rate $(df/dt) \cdot f^{-1} \sim 0.0012$ s^{-1} we obtain the estimates of the shock velocity $V_{sh} \sim 1000$ km/s and the magnetic field $H_0 \sim 0.94$ G, the estimates of the critical value of the Alfven magnetic numbers give $M_{cr} \sim 1.13$ and 1.16 for the coronal temperatures $T \sim 10^6$ K and $2 \cdot 10^6$ K, correspondingly.

The end: $f_L \sim 24.0$ MHz, the relative frequency splitting $\delta f \cdot f^{-1} \sim$ ~ 0.14, the Alfven magnetic number $M \sim 1.3$, and $Z \sim 1.08$, the electron density and the plasma frequency in the upstream region of the shock $N_0 \sim 6.6 \cdot 10^6$ cm^{-3} and $f_0 \sim 23$ MHz. For the relative drift rate $(df/dt) \cdot f^{-1} \sim 0.001$ s^{-1} we obtain the estimates of the shock velocity $V_{sh} \sim 1090$ km/s and the magnetic field $H_0 \sim 0.9$ G, the estimates of the critical value of the Alfven magnetic numbers give $M_{cr} \sim 1.12$ and 1.15 for the coronal temperatures $T \sim 10^6$ K and $2 \cdot 10^6$ K, correspondingly.

The obtained estimates of the parameters of shock waves (Alfven magnetic number M) and of the solar corona (density, magnetic field and the critical value of the Alfven magnetic numbers M_{cr}) show that the condition $M > M_{cr}$ is fulfilled during the duration of all three segments. Moreover, the relatively small variability of these parameters during all the burst allows to assert that the most possible reason of the origin of such fragmented structure in type II radio burst (with the attenuation or cessation of emission between the fragments) is that the shock wave enter a region where the magnetic field orientation was very different, and the shock wave became longitudinal (that is a condition of the perpendicularity was violated).

By the data of SOHO/LASCO C2, C3 (https://cdaw.gsfc.nasa.gov/CME_list/) the velocity of the corresponding CME was $\sim$ 480 km/s in the beginning of the event with a low slowing-down, and the velocity became $\sim$ 345 km/s at 20 *RS*.

5.3.3. Event of October 9, 1997

The dynamic spectrum of band-split type II burst in this event is given in Vršnak et al. (2001) (their Fig. 3a). It is an example of metric (i.e., coronal) type II burst in the 80–50 MHz range with well defined band-splitting. The obtained values of the relative split ($\delta f \cdot f^{-1}$) and the relative frequency drift((df/dt) $\cdot f^{-1}$) are also shown there as a function of time t (at six time moments). It can be noted that the relative split was approximately constant, and the relative frequency drift showed a slight decrease. Below, following our model, we give the estimates of the parameters of shock waves and the medium at the same time moments as given in the paper.

Moment 1: the Alfven magnetic number $M \sim 1.4$, and $Z \sim 1.16$, the electron density and the plasma frequency in the upstream region of the shock $N_0 \sim 6.3 \cdot 10^7$ cm^{-3} and $f_0 \sim 69.5$ MHz, the shock velocity $V_{sh} \sim 680$ km/s and the magnetic field $H_0 \sim 1.65$ G, the estimates of the critical value of the Alfven magnetic numbers give $M_{cr} \sim 1.24$ and 1.3 for the coronal temperatures $T \sim 10^6$ K and $2 \cdot 10^6$ K, correspondingly.

Moment 2: the Alfven magnetic number $M \sim 1.35$, and $Z \sim 1.1$, the electron density and the plasma frequency in the upstream region of the shock $N_0 \sim 5.7 \cdot 10^7$ cm^{-3} and $f_0 \sim 67$ MHz, the shock velocity $V_{sh} \sim 600$ km/s and the magnetic field $H_0 \sim 1.45$ G, the estimates of the critical value of the Alfven magnetic numbers give $M_{cr} \sim 1.24$ and 1.3 for the coronal temperatures $T \sim 10^6$ K and $2 \cdot 10^6$ K, correspondingly.

Moment 3: the Alfven magnetic number $M \sim 1.37$, and $Z \sim 1.15$, the electron density and the plasma frequency in the upstream region of the shock $N_0 \sim 4.7 \cdot 10^7$ cm^{-3} and $f_0 \sim 62$ MHz, the shock velocity $V_{sh} \sim 670$ km/s and the magnetic field $H_0 \sim 1.4$ G, the estimates of the critical value of the Alfven magnetic numbers give $M_{cr} \sim 1.24$ and 1.3 for the coronal temperatures $T \sim 10^6$ K and $2 \cdot 10^6$ K, correspondingly.

Moment 4: the Alfven magnetic number $M \sim 1.34$, and $Z \sim 1.09$, the electron density and the plasma frequency in the upstream region of the shock $N_0 \sim 4 \cdot 10^7$ cm^{-3} and $f_0 \sim 57$ MHz, the shock

velocity $V_{sh} \sim 690$ km/s and the magnetic field $H_0 \sim 1.37$ G, the estimates of the critical value of the Alfven magnetic numbers give $M_{cr} \sim 1.23$ and 1.29 for the coronal temperatures $T \sim 10^6$ K and $2 \cdot 10^6$ K, correspondingly.

Moment 5: the Alfven magnetic number $M \sim 1.35$, and $Z \sim 1.1$, the electron density and the plasma frequency in the upstream region of the shock $N_0 \sim 3.1 \cdot 10^7$ cm^{-3} and $f_0 \sim 53$ MHz, the shock velocity $V_{sh} \sim 675$ km/s and the magnetic field $H_0 \sim 1.3$ G, the estimates of the critical value of the Alfven magnetic numbers give $M_{cr} \sim 1.23$ and 1.29 for the coronal temperatures $T \sim 10^6$ K and $2 \cdot 10^6$ K, correspondingly.

Moment 6: the Alfven magnetic number $M \sim 1.25$, and $Z \sim 1.07$, the electron density and the plasma frequency in the upstream region of the shock $N_0 \sim 3 \cdot 10^7$ cm^{-3} and $f_0 \sim 49.2$ MHz, the shock velocity $V_{sh} \sim 700$ km/s and the magnetic field $H_0 \sim 1.65$ G, the estimates of the critical value of the Alfven magnetic numbers give $M_{cr} \sim 1.23$ and 1.28 for the coronal temperatures $T \sim 10^6$ K and $2 \cdot 10^6$ K, correspondingly.

These estimates show an approximate constancy of the intensity (the Alfven magnetic number) and shock velocity practically during all the duration of this type II burst. However, the estimates at the sixth moment (end of the last segment of the band) give the Alfven magnetic number $M \leq M_{cr,}$ therefore the cease of radio emission can also be interpreted as a consequence of the relative weakening of shock wave.

By the data of SOHO/LASCO C2, C3 (https://cdaw.gsfc.nasa.gov/CME_list/) the velocity of the corresponding CME was ~247 km/s in the beginning of the event with a small acceleration, and the velocity became ~456 km/s at 20 *RS*.

5.3.4. Event of November 4, 1997

This event was also discussed in Vršnak et al. (2001), and it is an example of the type II burst in the dekameter to kilometer wavelength range associated with the shock detected by *in situ* measurements at 1 AU. The dynamic spectrum of this burst in the frequency range 250–120 kHz is given in their Fig. 2, and it shows a fragmented, patchy emission pattern. For our analysis we used the fragment at 19:30:00–20:15:00 UT. To estimate the parameters of shock wave and the parameters of the interplanetary plasma the density model and normalization procedure of Leblanc et al.

(1998) was adopted, and the radial motion of the radio source was assumed as presumably corresponding to the shock velocity in the range of radial distances from the Sun $R > 10$ *RS*.

The beginning: $f_L \sim 137$ kHz, the relative frequency splitting $\delta f \cdot f^{-1} \sim 0{,}33$, the Alfven magnetic number $M \sim 1.85$, and $Z \sim 1.25$, the electron density and the plasma frequency in the upstream region of the shock $N_0 \sim 1.84 \cdot 10^2$ cm^{-3} and $f_0 \sim 122$ kHz. For the relative drift rate $(df/dt) \cdot f^{-1} \sim 3.9 \cdot 10^{-5}$ s^{-1} we obtain the estimates of the shock velocity $V_{sh} \sim 1000$ km/s and the magnetic field $H_0 \sim 3 \cdot 10^{-3}$ G, the estimates of the critical value of the Alfven magnetic numbers give $M_{cr} \sim 1.1$ for the temperatures $T \sim 10^5$ K.

The end: $f_L \sim 122$ kHz, the relative frequency splitting $\delta f \cdot f^{-1} \sim 0{,}3$, the Alfven magnetic number $M \sim 1.85$, and $Z \sim 1.25$, the electron density and the plasma frequency in the upstream region of the shock $N_0 \sim 1.46 \cdot 10^2$ cm^{-3} and $f_0 \sim 110$ kHz. For the relative drift rate $(df/dt) \cdot f^{-1} \sim 3.9 \cdot 10^{-5}$ s^{-1} we obtain the estimates of the shock velocity $V_{sh} \sim 900$ km/s and the magnetic field $H_0 \sim 3 \cdot 10^{-3}$ G, the estimates of the critical value of the Alfven magnetic numbers give $M_{cr} \sim 1.08$ temperatures $T \sim 10^5$ K.

In this event the constancy of the parameters of the shock wave is in accordance with the connection of the shock wave with the coronal mass ejection. Under such conditions the fragmented structure of radio emission can be observed when specified conditions (sufficient intensity and perpendicularity of the shock front, that is $M > M_{cr}$ and $\theta < \theta_{cr}$) are not satisfied during the propagation of shock in some regions of the solar atmosphere.

Note also, by the data of SOHO/LASCO C2, C3 (https://cdaw.gsfc.nasa.gov/CME_list/) the velocity of the corresponding CME was ~700 km/s at 20 *RS*, that is the shock front overtook the CME.

It can be noted that the estimated values of the strength of the upstream magnetic field in general are in good agreement with the results of Vrsnak et al. (2002), namely, the magnetic field strength is about 5–1 G at $R \sim (0.6–1)$ *RS*. The estimates of parameters of the shock wave and, especially, of the magnetic field strength in the interplanetary space (at distances >10–20 *RS*) by the parameters of the kilometer type II bursts were obtained in the first time.

5.4. Conclusion

The presented analysis shows that the physical relationship between CME/flare and the coronal waves (Moreton waves, EUV

waves, shock waves) is quite complex. Comparison of observations with theoretical analysis provides an evidence that the coronal shock and the associated type II burst emission can be due to the energy release in the flare as well as to the CME expansion. Investigations of the parameters of type II radio burst can give a valuable information about the MHD shock evolution in the non-homogeneous coronal and interplanetary plasma, as well as on the parameters of the medium where shock wave is propagating. But when analyzing such radio bursts it is important to take into account the generating mechanism of radio emission. In many papers the generation of type II bursts is associated with the drift acceleration of electrons at the perpendicular shock front, the formation of fluxes of accelerated electrons, the excitation of Langmuir waves in the region ahead of the shock front and their transformation through non-linear wave-wave processes into radio emission at frequencies close to the electron plasma frequency f_{pe} and its second harmonic $2f_{pe}$. However, within the framework of such a model, a number of the problems remain in the interpretation of such characteristics of bursts as the narrow bandwidth of the emission bands in frequency and such a fine peculiarity of the structure of bands as the band splitting. This model explains the acceleration and the formation of fluxes of accelerated electrons and the excitation of Langmuir waves in the upstream region of the shock front, but the issue of formation of fluxes of accelerated electrons in the downstream region remained not resolved. Therefore, the origin of split-structure in the frame of the model, where the lower frequency and the higher frequency bands are emitted from the upstream and downstream region of the shock, remains unknown.

Here we used the model of the classical type II bursts based on the generation of plasma oscillations (the Buneman instability) within the front of collisionless shock wave and the induced scattering of plasma waves on fast electrons. This mechanism allows to explain all main parameters of radio bursts including the fine structure. In the frame of this model of the source of type II radio bursts, two conditions must be fulfilled: 1) the shock wave must be relatively intense (the Mach number exceed a certain critical value M_{cr}), and 2) the shock wave must be perpendicular, a slight deviation from perpendicularity Θ ($\sim 2^{o}$) results in cessation of the generation of plasma waves. It means that shock wave is not a source of radio emission if any of these conditions is not satisfied. It means

also that the source of radio emission can be formed at any part of the shock front (bow or flanks) simultaneously or in different times, depending on where and when the specified conditions are fulfilled, and the dynamic spectrum of type II radio bursts can either represent continuously drifting stripes or have an interruptive and a blob structure. In particular, the analysis of the fragmented dynamic spectra in a number of the event showed that the condition $M > M_{cr}$ was fulfilled throughout all the fragments, and the most possible reason of the end of radio emission in the fragments was the transiting a shock wave from a perpendicular shock to a longitudinal shock (that is a condition of the perpendicularity was violated).

Investigation of band-splitting presented in this paper shows that it can be consistently interpreted in terms of the emission from the regions within the forward slope and the trailing slope of the leading soliton of collisionless shock wave. In the frame of such a model it is possible to estimate the parameters of the shock and their evolution during the propagation in the inhomogeneous magnetoplasma, and the parameters of the medium (density and magnetic field) where the shock is propagating. The results obtained here show that the reason for fragmented structure of type II bursts can be both the variation of intensity of the shock wave during propagation in a strongly inhomogeneous and turbulent plasma and the transiting of the shock from perpendicular to longitudinal and vice versa.

It should be remarked that the dynamic spectra of type II bursts have very diverse fine structure. Besides the fundamental and harmonic bands, their split in two sub-bands, the herringbones, fragmentation of the radio emission, there are many nother types of fine structure of the dynamic spectra. A number of types of the fine structure in the meter range were observed with the IZMIRAN's radio spectrographs and in papers (e.g., Korolev et al., 1973; Urbarz et al., 1977; Fomichev, Chertok, 1977; Markeev et al., 1981; Ishkov et al., 1985). Many of these types of fine structure were confirmed by the high-resolution LOFAR observations of a strongly fragmented type II burst on August 25, 2014 (Magdalenic et al., 2020). In addition, in this paper it was reported on the first observation of a peculiar splitting of the already split harmonic band. Now it is not clear whether such a peculiarity is intrinsic (common) for type II radio bursts or not. In the frame of the model used here the reason of such double spitting can be a collisionless shock wave which has

the second source of emission connected with the second well-formed soliton. Such situation needs a special theoretical analysis. But it is also very likely that such structure can appear if several sources of the radio emission are formed along the large scale shock front where the condition for generation of radio emission are fulfilled. Taking into account the various location and spacing of these sources (with various parameters) the simultaneous presence of these sources can result in forming of the different type of fine structure (double splitting, many lines, blobs and others).

Our analysis allows to conclude that meter bursts starting at frequencies <200 MHz usually turn into interplanetary bursts as long as the perpendicularity of the shock front remains. Bursts starting in the decimetric wavelength range (>500 MHz) do not go into the long wave range; they are usually associated with explosive shock fronts that slow down even in the meter range. Thus, registration of type II burst is the evidence of the propagation of perpendicular shock wave, but the absence of type II burst is not the evidence of the absence of shock wave. Such a situation can be one of the reasons of the ambiguous relationship of type II radio bursts with the other manifestations of the solar activity (H_α wave, Moreton wave, EUV wave).

Acknowledgment

The authors are grateful to the referees for constructive remarks and comments, and to the SOHO / LASCO, the WIND / WAVE teams for the open data policy.

References

Bacchini F., Susino R., Bemporad A., Lapenta G., 2015. Plasma physical parameters along CME-driven Shocks. II. Observation-simulation comparison // Ap. J. Vol. 809. P. 58–70. DOI:10.1088/0004-637X/809/1/58

Cane H. V., Erickson W. C., 2005. Solar Type II Radio Bursts and IP Type II Events // Ap. J. Vol. 62. P. 1180–1194.

Cairns I. H., Kamen A. Kozarev, Nariaki V. Nitta, Neus Agueda et al., 2020. Comprehensive Characterization of Solar Eruptions with Remote and *In-Situ* Observations, and Modeling: The Major Solar Events on 4 November 2015 // Sol. Phys. Vol. 295. P. 32–48. https://doi.org/10.1007/s11207-020-1591-7

Corona-Romero P., Gonzalez-Esparza J. A., Aguilar-Rodriguez E., De-la-Luz1 V., Mejia-Ambriz J. C., 2015. Kinematics of ICMEs/Shocks:

Blast Wave Reconstruction Using Type-II Emissions // Sol. Phys. Vol. 290. P. 2439–2454. DOI:10.1007/s11207-015-0683-2

Chernov G. P., Kaiser M. L., Bougeret J.-L., Fomichev V. V., Gorgutsa R. V., 2007. Fine Structure of Solar Radio Bursts Observed at Decametric and Hectometric Waves // Sol. Phys. Vol. 241. P. 145–169. DOI:10.1007/s11207-007-0258-y

Christaphi, Nicolina, Hamish A. S. Reid, Eduard P. Kontar, 2020. First Observation of a Type II Solar Radio Burst Transitioning between a Stationary and Drifting State // Ap. J. Vol. 893, No. 115. 11 p. https://doi.org/10.3847/1538-4357/ab80c1

Fomichev V. V., 1972. Propagation through the solar corona of the shock waves responsible or type II radio bursts // Sov. Astron Zh. Vol. 16. P. 284–28.

Fomichev V. V., Chertok I. M., 1977. The fine structure of solar radio bursts at meter wavelengths. A Survey // Radiophysics and Quantum Electronics. Vol. 20, No. 9. P. 869–898.

Harvey K. L., Martin S. F., Riddle A. C., 1974. Correlation of a flare-wave and type II burst // Sol. Phys. Vol. 36. P. 151–155.

Holman G. D., Pesess M. E., 1983. Solar Type II Radio Emission and the Shock Drift Acceleration of Electrons // Ap. J. Vol. 267. P. 837–843.

Ishkov V. N., Fomichev V. V., Chertok I. M., 1985. Some dynamical phenomena in flares with compound space-time structure. Physics of solar flares. Moscow: Nauka. P. 35–43.

Klassen A., Aurass H., Mann G., Thompson B. J., 2000. Catalogue of the 1997 SOHO–EIT coronal transient waves and associated type II radio burst spectra // Astron. Astrophys. Suppl. Vol. 141. P. 357–369.

Kundu M. R., 1965. Solar Radio Astronomy. New York: Interscience. 660 p.

Knock S. A. et al., 2001. Theory of type II radio emission from the foreshock of an interplanetary shock // JGR. Vol. 106. P. 20541–25051. https://doi.org/10.1029/2001JA000053

Korolev O. S., Markeev A. K., Fomichev V. V., Chertok I. M., 1974 // Sov. Astron. Zh. Vol. 17, No. 6. P. 777–780.

Leblanc Y., Dulk G., Bougeret J.-L., 1998. Tracing the Electron Dencity from the Corona to 1 AU // Sol. Phys. Vol. 183. P. 165–180.

Maguire C. A., Eoin P. Carley, Joseph McCauley, Peter T. Gallagher, 2020. Evolution of the Alfvén Mach number associated with a coronal mass ejection shock // A&A. Vol. 633, A56. https://doi.org/10.1051/0004–6361/201936449

Magdalenic Jasmina, Christophe Marqué, Richard A. Fallows et al., 2020. Fine Structure of a Solar Type II Radio Burst Observed by LOFAR // Ap. J. L. Vol. 897, L15. 9 p. https://doi.org/10.3847/2041–8213/ab9abc

Majumdar, Satabdwa, Srikar Paavan Tadepalli, Samriddhi Sankar Maity et al., 2021. Imaging and Spectral Observations of a Type-II Radio Burst Revealing the Section of the CME-Driven Shock That

Accelerates Electrons // Sol. Phys. Vol. 296, No. 62. 16 p. https://doi.org/10.1007/s11207–021–01810–8
Mann G. T. Classen, Aurass H., 1995. Characteristics of coronal shock waves and solar type 11 radio bursts // A&A. Vol. 295. P. 775–881.
Markeev A. K., Fomichev V. V., Chertok I. M., 1981. Solar Maximum Year // Proceedings of international workshop, Simferopol, March. Vol. 2. P. 105–110.
Newkirk G.Jr., 1961. The Solar Corona in Active Regions and the Thermal Origin of the Slowly Varying Component of Solar Radio Radiation // Ap. J. Vol. 133. P. 983–1013.
Pikelner S. B., Gintsburg M. A., 1963. The Mechanism of Type II Bursts of Solar Radio Emission // Sov. Astron. Zh. Vol. 7. P. 639–642.
Pick M., Forbes T. G., Mann G. et al., 2006. Multi-wavelength Observation of CMES and Associated Phenomena // Space Sci. Rev. Vol. 123. P. 341–382. DOI:10.1007/s11214-006-9021-1
Pohjolainen S., Pomoell J., Vainio R., 2008. CME liftoff with high-frequency fragmented type II burst emission // A&A. Vol. 490. P. 357–363. https://doi.org/10.1051/0004–6361:200810049
Pomoell J., Vainio R., Kissmann R., 2008. MHD Modeling of Coronal Large-Amplitude Waves Related to CME Lift-off // Sol. Phys. Vol. 253. P. 249–261.
https://doi.org/10.1007/s11207–008–9186–8
Rahman A. M., Umapathy S., Shanmugaraju A., Moon Y.-J., 2012. Solar and interplanetary parameters of CMEs with and without type II radio bursts // Adv. Space Res. Vol. 50. P. 516–525. https://doi.org/10.1016/j.asr.2012.05.003
Smerd S. F., Sheridan K. V., Stewart R. T., 1974. On Split-Band Structure in Type II Radio Bursts from the Sun // IAU Symp., 57. Ed. G. A. Newkirk. Dordrecht; Boston: Reidel. P. 389–393.
Smith S. F., Harvey K. L., 1971. The nature of coronal wave fronts // Physics of the Solar Corona / Ed. C. J. Macris. Dordrecht: Reidel. 156 p.
Tripathi D., Raouafi N., 2007. On the relationship between coronal waves associated with a CME on 5 March 2000 // Astron., Astrophys. Vol. 473. P. 951–957. 10.1051/0004–6361:20077255
Vršnak B., Aurass H., Magdalenić J., Gopalswamy N., 2001. Band-splitting of coronal and interplanetary type II bursts // A&A. Vol. 377. P. 321–329.
Vršnak B., Magdalenić J., Aurass H., Mann G., 2002. Band-splitting of coronal and interplanetary type II bursts II. Coronal magnetic field and Alfvén velocity // A&A. Vol. 396. P. 673–682.
Vršnak B., Warmuth A., Temmer M., Veronig A., Magdalenić J. et al., 2006. Multi-wavelength study of coronal waves associated with the CME-flare event of 3 November 2003 // A&A. Vol. 448. P. 739–752.
Warmuth A., 2010. Large-scale waves in the solar corona: The continuing debate // Adv. Space Res. Vol. 45. P. 527–536.

Wild J. P., Roberts J. A., Murray J. D., 1954. Radio Evidence of the Ejection of Very Fast Particles from the Sun // Nature. Vol. 173. P. 532–534.
Zaitsev V. V., 1965. A Theory for Type II Bursts of Solar Radio Emission // Sov. Astron. J. Vol. 9, No. 4. P. 572–578.
Zaitsev V. V., Kaplan S. A., 1966. Nonthermal radio emission generated by coherent plasma waves // Astrophysics. Vol. 2. P. 87–98.
10.1007/BF01006079
Zaitsev V. V., 1968. Parameters for Shock Waves Generating Type II Solar Bursts, and for Coronal Magnetic Fields // Sov. Astron. Zh. Vol. 12, No. 4. P. 610–614.
Zaitsev V. V., 1969. Structure of solitary waves in rarefied plasma // Radiophys. Quantum Electron. Vol. 12. P. 622–631. https://doi.org/10.1007/BF01033147
Zaitsev V. V., 1970. The Structure of Relativistic Solitons in a Magnetoactive Plasma // Soviet Zh. Exp. Teor. Fiz. Vol. 31. P. 729–732.
Zaitsev V. V., Ledenev V. G., 1976. Generation of fast electrons in shock waves propagated along a magnetic field // Sov. Astron. Lett. Vol. 2. P. 172–174.
Zaitsev V. V., 1977. Theory of solar type II and III radio bursts // Radiophys. Quantum Electron. Vol. 20. P. 951–965.
Zimovets I., Vilmer N., Chian A. C.-L., Sharykin I., Struminsky, 2012. Spatially resolved observations of a split-band coronal type II radio burst // A&A. Vol. 547, No. A6. 14 p.
Zheleznyakov V. V., 1964. Radio emission of the Sun and planets. Moscow: Nauka (Zheleznyakov V. V., 1970. Radio Emission of the Sun and Planets. New York, NY: Pergamon Press. 697 p.)
Zheleznyakov V. V., 1965. On the Origin of Solar Radio Bursts in the Meter-Wavelength Range // Sov. Astron. Zh. Vol. 9. P. 191–197.
Zhukov A. N., 2011. EIT wave observations and modeling in the STEREO era // J. Atmosph. Solar-Terr. Phys. Vol. 73. P. 1096–1116. 10.1016/j.jastp.2010.11.030
Zucca et al., 2014. Understanding Coronal Mass Ejections and Associated Shocks in the Solar Corona by Merging Multiwavelength Observations // Ap. J. Vol. 795, No. 68. 15 p. DOI:10.1088/0004-637X/795/1/68

Chapter 6
ON IMPROVING THE ZEBRA MODEL ON DPR ON THE BACKGROUND OF COMPLEX SPECTRA

Abstract. Understanding the nature of the fine structure of radio emission is one of the most important criteria for testing the mechanisms of radio emission. The discussion on the origin of the zebra structure (ZS) has been going on for more than 50 years (Chernov, 2011). In these works it is usually postulated that the Double Plasma Resonance (DPR) mechanism always works if there are fast particles in the magnetic trap. However, it encounters difficulties in explaining the dynamics of the bands (sharp change in the frequency drift of the bands, a large number of harmonics, frequency splitting of the bands, their ultra-thin structure in the form of millisecond spikes, the transition of radio fibers into zebra stripes and back). So, works on its improvement began to appear (mostly in a dozen papers by Karlitsky and Yasnov). The whole game goes on the variability of the ratio of magnetic field and density height scales and the toleration of some plasma turbulence in the source. This already indicates the unsuitability of the DPR model. Several phenomena are known in which the ratio of height scales does not change in the ZS loop-source. It was noted earlier that realization of the DPR at many harmonics of the cyclotron frequency is not realized for any known models of the density and magnetic field in the corona (Chernov, 2019, p. 215–220). It was shown that all the main details of the sporadic zebra-structure in the August 1, 2010 phenomenon (and in many other phenomena) can be explained within the framework of a unified model of zebra-structure and radio fibers in the interaction of plasma waves with whistlers. The main changes in the zebra-structure bands are caused by the scattering of fast particles on whistlers, leading to a switch of the whistler instability from the normal Doppler effect to the anomalous one.

6.1. Introduction

Understanding the nature of fine structure of the radio emission of solar radio bursts is one of the most important criteria for testing

radio emission mechanisms. The zebra structure belongs to the most remarkable type of fine structure. It appears on dynamical spectra as regular bands in emission and absorption. It has been described in numerous papers and monographs since the first publication by Elgaroy (1959): Kuijpers, 1975; Slottje, 1981; Chernov, 1976, 2006, 2011. The discussion about the origin of zebra structure has been going on for more than 50 years (Chernov, 2011). The most frequently discussed mechanism is based on double plasma resonance (Zheleznyakov, Zlotnik, 1975a):

$$\omega_{UH} = (\omega_{Pe}^2 + \omega_{Be}^2)^{1/2} = s\omega_{Be}, \qquad (6.1)$$

where ω_{Pe} is the electron plasma frequency, ω_{Be} is the electron gyro frequency under conditions where $\omega_{Be} \ll \omega_{Pe}$ (Kuijpers, 1975; Zheleznyakov, Zlotnik, 1975a, b; Kuijpers, 1980; Mollwo, 1983, 1988; Winglee, Dulk, 1986). These works usually postulate that the mechanism always works if there are fast particles in the magnetic trap. However, it faces a number of difficulties in explaining the dynamics of the ZS bands (sharp changes in the frequency drift of the bands, a large number of harmonics, frequency splitting of the bands, and their ultrafine structure in the form of millisecond spikes). Therefore, works on both its improvement (Karlický et al., 2001; LaBelle et al., 2003; Kuznetsov, Tsap, 2007) and creation of new models began to appear.

In a dozen of works by Karlitsky and Yasnov, the method of estimating the number of harmonics of electron gyro-frequency was improved within the framework of the DPR, mainly in the direction of its increase, bringing it to 170–200. At the same time, no comparisons with other models were made as a rule. Here, we will note some of their important results with attraction of their discussion in the framework of the alternative zebra model on whistlers.

6.2. Complex spectra of zebra pattern

Fig. 6.1 and 6.2 show the spectra of zebra structure with different band parameters both with time and at different frequencies. Here it is difficult to justify the application of the mechanism on the DPR even for some parts of the spectrum, ignoring the others.

Almost simultaneously with the DPR model, an alternative mechanism for the interaction of plasma waves (l) with whistlers (w) was proposed, $l + w \rightarrow t$ (Chernov, 1976, 1990). In this mo-

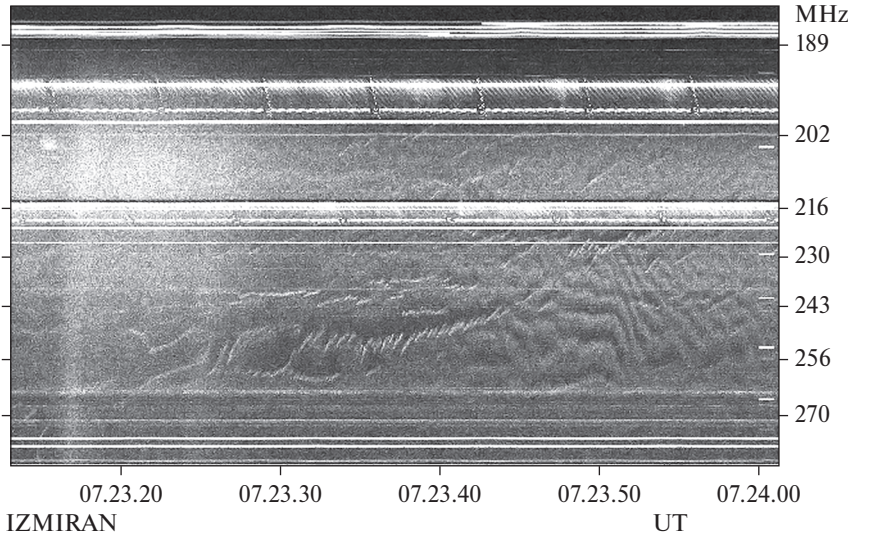

Fig. 6.1. Complex zebra structure in the range of 180–270 MHz in the event of 18.07.2000

del, the above-mentioned subtle effects of the zebra-structure (ZS) bands are explained by quasi-linear effects of the interaction of fast particles with whistlers. The mechanism with whistlers became its natural development after its application by Kuijpers (Kuijpers, 1975) for fibers (fiber bursts), when in some phenomena a continuous transition of ZS bands into fiber-bursts and back was observed. The most important details of this mechanism are presented in the Discussion section.

In the primary work on the DPR mechanism of Zheleznyakov and Zlotnik (1975a) it was shown that the relative width of the increment band in the hybrid band turns out to be incredibly narrow $\delta\omega/\omega_{Be} \sim 2.5 \cdot 10^{-4}$. Such a value is obtained only under the condition that the dispersion of the particle beam velocities is generally discarded as an infinitesimal quantity in the estimates. In Benáček, Karlický, Yasnov, 2017, it is shown that taking into account the hot particle velocity dispersion and the cold plasma temperature severely limits the efficiency of the DPR mechanism. Karlický and Yasnov then made major contributions to improve the mechanism on DPR in a dozen of their papers. In a recent paper Yasnov and Karlický (2020) made an important update in this activity.

In the paper of Yasnov and Chernov (2020) it was pointed out the importance in analyzing any event of taking into account the variation of the ratio of the magnetic field and density height scales in the source of the zebra structure. For example, in (Yasnov, Chernov, 2020) this ratio was considered constant and the advantage of the whistler mechanism was shown for the 21.06.2011 event.

In the introduction of (Yasnov, Karlický, 2020) the authors mentioned all the main papers on zebra-structure observations and theoretical mechanisms to explain it (more than 20 papers), which saves us from repeating them here. They proposed an improved method to determine the gyro-harmonics of zebra bands, which is essential to determine the electron density and magnetic field strength in the zebra source. Compared to previous methods, a new assumption is made that the ratio $R = L_{bh}/L_{nh}$ (where L_{bh} and L_{nh} are the magnetic field height and density scales) varies in the source in a more generalized form. Almost free manipulation of the variability of R allows to obtain for the 21.06.2011 phenomenon new values of gyro-harmonics numbers around 115 (instead of 50–60 in (Yasnov, Chernov, 2020)), and in other phenomena up to 170. These estimates are not in agreement with the previous results of Benacek et al. (2017), where it is shown that in real parameters the amplitude of the loss-cone instability increment drops significantly by the 30th harmonic.

This fact alone demonstrates the unsuitability of the proposed model improvement on the DPR, in particular for determining the harmonic number of zebra-structure bands by manipulating the variability of the ratio of the height scales of the magnetic field and the density in both one phenomenon and different ones.

In previous papers (Karlický, 2014) it was assumed that all frequency variations of zebra stripes are caused by some kind of turbulence. Recent papers attribute everything to the propagation of a fast magnetosonic wave (Karlický, 2022), since a strict period of fluctuations coinciding with the classical *cosine* function has been determined. Interestingly, the 17.08.1998 phenomenon is analyzed once again, after first being considered in Zlonik et al. (2009). These are fast pulsations of zebra-structure packets (similar to type III bursts) against a background of pulsations in absorption. Zlonik et al. (2009) believed that two non-equilibrium distribution functions were present in the source: one with a loss-cone velocity distribution, responsible for the continuum emission, and the other

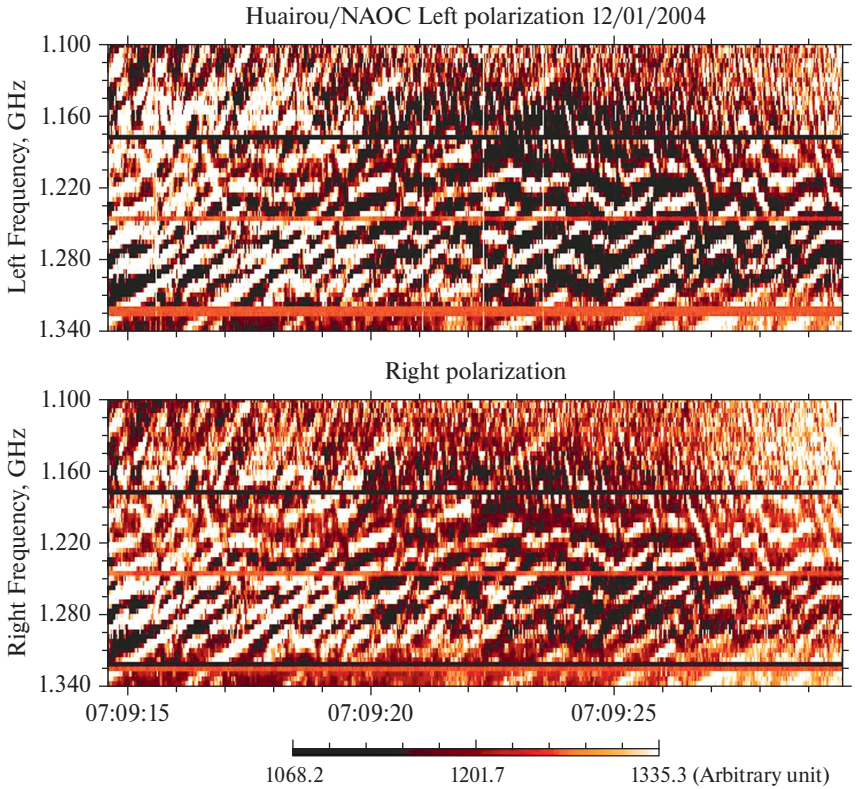

Fig. 6.2. Complex event of 1.12.2004 with smooth transition of fibers (fiber bursts) into zebra-structure bands with saw-tooth frequency drift in the range 1.1–1.34 GHz (Huairou station, PRC)

of DGH type, capable of inducing the DPR effect by inducing the zebra structure. Karlický (2022) does not mention this. The DPR mechanism is assumed to work and the harmonic number at the lower frequency is determined by a new method developed (mentioned above).

So large unlikely harmonics stimulate one to recall an alternative interpretation of this phenomenon. The review by Chernov (2019, pp. 72 and 73) notes some properties on the spectrum with ZP packets that have not been considered anywhere since the work of Zlotnik et al. (2009). Not all ZP packets have negative frequency drift (like type III bursts). A number of moments with positive drift can be seen. It is also visible between ZP packets, and one can see continuous zebra stripes throughout the five packets with notice-

able saw-tooth frequency drift. Between the ZP packets pulsations in absorption have a varied frequency drift.

Similar spectra with almost vertical zebra packets have been observed in many phenomena, starting with the excellent example in Fig. 6 in (Slottje, 1972). In the phenomenon of 03.07.1974, similar zebra packets appeared for several hours (Slottje, 1971; Chernov, 1976). Previously, we have already shown the advantage of the whistler model for interpretation of the 21.06.2011 phenomenon (Yasnov, Chernov, 2020). Even earlier, a mechanism with whistlers based on the scattering of fast particles on whistlers was used to explain the saw-tooth frequency drift of zebra stripes in the known phenomenon of 25.10.1994 (Chernov, 2005). Whistlers are always generated simultaneously with plasma waves at the upper hybrid frequency by fast particles with a cone velocity distribution. The scattering process on whistlers was used in (Chernov, 1990) and in more detail in (Chernov, 1996, 2005). There, an important property of the process is considered: change in the direction of the frequency drift of zebra bands must correlate with change in the direction of the spatial drift of their radio sources (see Fig. 2 in Chernov, 2019, p. 13). When fast particles scatter on whistlers, the distribution function changes, the generation of whistlers can switch repeatedly from normal Doppler effect to anomalous one. In these cases, the group velocity of whistlers changes sign to opposite (smoothly or sharply depending on the parameters of fast particles). And as a result, the frequency drift of the bands synchronously changes to reverse. Karlicky and Yasnov usually analyze phenomena with regular zebra bands, but more often the spectra are very complex with superposition not only of fast pulsations, but with fiber bursts with different frequency drift, which are sometimes difficult to distinguish from ZSs.

We are now reviewing a large archive of major phenomena in order to find out what model explains better than most of them. In the DPR model the whole game is based on the variability of the ratio of the magnetic field height and density scales. This already shows unsuitability of the DPR model. Several phenomena have already been selected in which it is clear that the ratio of height scales does not change in a loop. And, Karlicky and Yasnov usually analyze phenomena with a large number of bands without touching many other effects on the same spectrum. For example, ignoring explanations for the saw-tooth

frequency spectrum of the bands, connection with fast pulsations, abrupt transitions, jumps in band parameters at the same frequencies, and other points.

6.3. Discussion

Application of the DPR mechanism is simply postulated. After a large review by Zheleznyakov et al. (2016), there is now no need to repeat its description in detail. It remains the most cited in the analysis of the zebra structure. It is based on the generation of plasma waves at the upper hybrid frequency ω_{UH} by fast electrons with velocity distribution function with a loss cone. Their subsequent transformation into electromagnetic waves produces continuum radiation that can be sharply amplified at DPR levels, where ω_{UH} is approximately equal to an integer number s of electron cyclotron harmonics ($\approx s\omega_{ce}$). This simple algebraic relation is the basis of the beautiful zebra-structure theory (which has become almost classical) presented by Zheleznyakov and Zlotnik (1975b) and supported later by Winglee and Dulk (1986).

The basic condition for existence of many DPR levels implies that the scale of magnetic field heights should be much smaller than the scale of density heights. However, this condition is shown in the listed works in the form of a hypothetical scheme without numerical scales on the axes, including Fig. 2 in the review by Zheleznyakov et al. (2016).

If we try to use for this purpose the known analytical expressions for density and magnetic field dependence in the corona, no known models confirm the possibility of the formation of many DPR levels in reasonable sizes of zebra-structure sources. For illustrative purposes, see Figs. 6 and 7 in (Chernov, 2019, p. 217), raising doubts in general about the use of a model on DPR to explain the numerous zebra stripes, even disregarding many effects of the complex dynamics of stripes.

Fig. 6.4 shows the calculation of DPR levels using the usual (conventional) parameters of the coronal plasma using the barometric formula: electron temperature $T_e = 1.2 \cdot 10^6$ K, initial plasma frequency $f_{P0} = 3800$ MHz at altitude $h_{B0} = 20\,000$ km. If we use the dipole dependence of the magnetic field for cyclotron harmonics, harmonics with $s \geq 50$ go to much higher altitudes ≥100 000 km. Thus, excitation of waves simultaneously at 34 DPR levels in the corona is not feasible in any real density and magnetic field models.

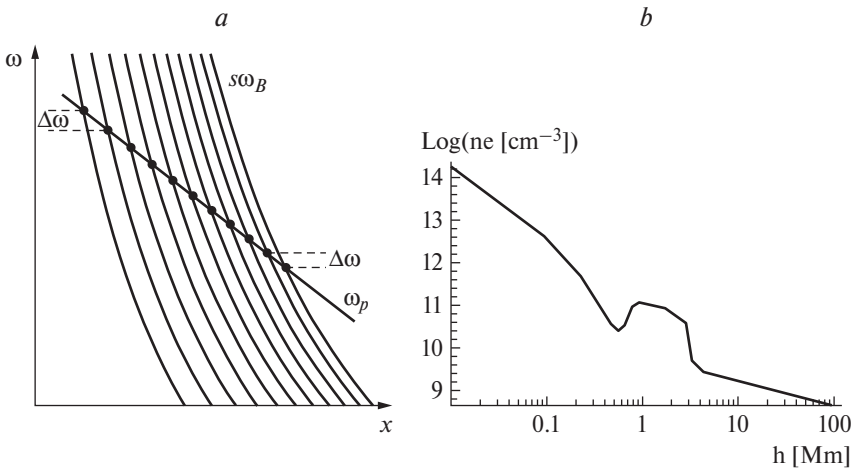

Fig. 6.3. Cyclotron frequency harmonics $s\omega_{Be}$ and the plasma frequency ω_{Pe} as functions of the coordinate x: (*a*) for the same signs of LB and LN and for $|LB| < |LN|$ (Zheleznyakov et al., 2016); (*b*) the electron density profile as a function of height in the solar atmosphere according to Selhorst et al. (2008), used by Yasnov and Karlicky (2015)

In recent works, Karlický and Yasnov proposed an exotic model (Fig. 3b) with a hump on a smooth density decay (Selhorst et al., 2008), on the steep slopes of which DPR conditions must be fulfilled to generate a large number of harmonics (Yasnov, Karlický, Stupishin, 2016).

Fig. 6.1 shows a spectrum with the duration of about 45 s with a complex zebra structure, but in the absence of regular bands, it is difficult to find a moment where one could at least apply the DPR mechanism. A broad band in the absorption is wedged between the zebra structure, against which a chain of narrow-band (rope-like) fibers develops (Chernov, 1997, 2008).

In Fig. 6.2, the structure of bands changes dramatically in 15 s, the fibers (similar to fiber bursts, smoothly transforming into zebra stripes with a wave-like frequency drift). Obviously, the ratio of the field height and density scales cannot change appreciably in a few seconds.

Zebra spectra with saw-tooth frequency drift of the bands were considered in (Karlicky, 2014) on the example of the spectra of the Ondřejov observatory in the decimeter band in the 01.08.2010 phenomenon. Without going into details, we note that the aim of the

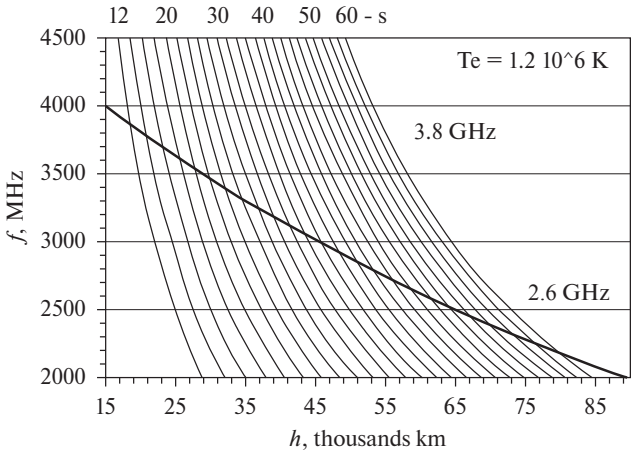

Fig. 6.4. Altitude dependence of the plasma frequency in accordance with the barometric law (heavy line) and altitude profiles of the electron cyclotron harmonics *s* (light lines) in the solar corona. For the electron temperature $T_e = 1.2 \cdot 10^6$ K and initial frequency $f_{P0} = 3800$ MHz at the altitude of $h_{B0} = 20\,000$ km, 34 DPR levels form between 2600 to flame 3800 MHz in the plasma layers (from Laptuhov, Chernov, 2009)

paper was to show that within the model on the DPR, the source of the zebra structure is in a turbulent state based on the Fourier analysis of the time profiles of the intensity of bands with frequency (and from the relations $\omega_{UH} \approx \omega_{pe}$ and $n_e \sim \omega_{pe}^2$ with the plasma density). The Fourier profile of the density fluctuations is taken as the calculated zebra band profile (apparently assuming that this does not require proof). The power spectrum of fluctuations has a stepped form (degree slope) with index – 5/3, coinciding with the Kolmogorov spectrum for turbulence.

Independently of this work, it was shown in (Chernov et al., 2018) that all the main details of the sporadic zebra-structure in the August 1, 2010 phenomenon can be explained within the framework of a unified model of zebra-structure and radio fibers in the interaction of plasma waves with whistlers (without strong plasma turbulence in the source). The main changes in zebra-structure bands are caused by the scattering of fast particles on whistlers, leading to a switch of the whistler instability from the normal Doppler effect to the anomalous one (Chernov, 1996, A Manifestation of Quasilinear Diffusion in Whistlers in the Fine Structure of Type IV Solar Radio Bursts). There the main refer-

ences on fan instability one can find in papers: Gendrin, 1981; Shapiro, Shevchenko, 1987; Parail, Pogutse, 1981.

6.4. Simulation

In connection with the remark above about impossibility of obtaining many levels of DPR in any known density and magnetic field models (see Fig. 6.4), we can mention the work of M. Karlický (2022) (Modeling of the solar radio zebra). In fact, it is not a simulation, but a fitting of the plasma parameters in the source to obtain model points on the zebra band on the spectrum coinciding with the observed ones, without calculating the radiation generation in the framework of the mechanism on the DPR, but simply plotting a graph like Fig. 6.4. And the main conclusion at the end confirms our conclusion (without reference), since the chosen field values do not coincide with any known models. There is also a businesslike conclusion at the end: it is necessary to continue calculations of the increments of the upper hybrid waves for large harmonic numbers (in the paper $s = 120–124$).

On the spectrum of Fig. 6.2 at its beginning one can see a smooth transition of fibers (fiber bursts) into zebra stripes with saw-tooth frequency drift. The same transition or reverse transition was observed in the phenomenon 01.08.2010. Karlicky (2014) does not discuss this effect, which is probably due to the fact that earlier in (Karlicky, 2013) the whistler model of fiber excitation (Kuijpres, 1975) was rejected and a new, or tweaked model was proposed by Treumann et al. (1983) based on Alfvén solitons.

6.5. Explosive instability
(Fomichev, Fainstein, Chernov, 2009)

The proposed mechanism, based on stabilization of explosive instability in the cascade of ion-sound harmonics, turns out to be much more effective than the mechanism of generation of ion-sound harmonics under the interaction of whistlers. It provides a large number of sound harmonics with frequency separation independent of the ratio of plasma and cyclotron frequencies in the source and growing with frequency (in accordance with observations). No additional rigid conditions are imposed. The former condition of acceleration of mono-speed beams of weakly relativistic particles, which is usually realized in any large flare, remains.

6.6. Related experiments and observations

6.6.1. Laboratory experiments
(Viktorov, Mansfeld, Golubev, 2015)

To confirm the effectiveness of the DPR mechanism, reference is sometimes made to perhaps the only work on the generation of radiation at the DPR in a laboratory plasma experiment (Viktorov et al., 2015 (EPL, 109 (2015) 65002)). Although now references to it are gradually quieting down (Chernov, 2019) (Latest data...), since ambiguous results are demonstrated there: the radiation recorded only complex bands at the second harmonic of the cyclotron frequency, while the experiment demonstrated the third harmonic as well (in Fig. 2). And if it were so easy to model, one would expect the experiment to be repeated many times, which would really be a proof of the mechanism's work. However, there were only assurances of the authors (after the report at the conference in response to questions) that they are trying to obtain radiation at the third harmonic. It is noteworthy that Viktorov et al. (2015) show in their experiment the simultaneous generation of whistlers at frequency near

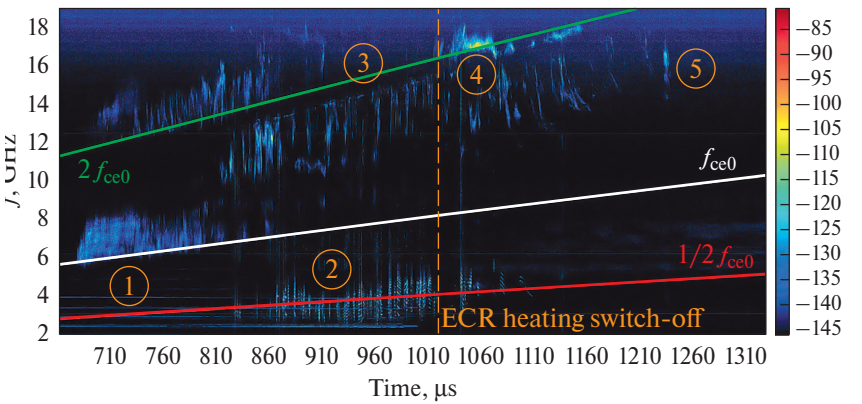

Fig. 6.5. Dynamic spectrum of the plasma radiation. The types of kinetic instabilities considered in the paper are highlighted: 1 – the initial stage of ECR discharge (rarefied plasma); 2 and 3 – stages of the developed discharge (dense plasma); 4 – the beginning phase of plasma decay (dense plasma); 5 – decaying plasma (rarefied plasma). Three lines on the spectrogram show time variation of the corresponding frequencies $2f_{ce0}$ (green), f_{ce0} (white) and $1/2f_{ce0}$ (red), where $f_{ce0} \equiv f_{ce}$ (z center) is the electron cyclotron frequency in the center of the magnetic trap on its axis (fragment Fig. 2 from Viktorov et al., (2015)). Note the strict periodicity of whistler generation

0.5 f_{ce} in Fig. 3b and a complex-shaped band near frequency of 2 f_{ce} in Figs. c and d), but the authors did not include these facts in the topic of their paper.

The world network of CALLISTO radio telescopes does not yet allow us to use its spectra; almost 90% of them are subject to local interferences and the low frequency resolution of the pure spectra does not allow us to record the ZS bands.

6.6.2. Zebra pattern in decametric radio emission of Jupiter (Panchenko et al., 2018)

Observations of the ZPs similar to the zebra patterns (ZPs) in the solar radiation (Litvinenko et al., 2016) were performed by the large ground-based radio telescope URAN-2 (Poltava, Ukraine). ZPs are strongly polarized radio emission with a duration from 20 s to 290 s and flux densities $\sim 10^5$–10^6 Jy (normalized to 1 AU), that is, 1–2 orders lower than for its moon Io decametric radio emission (DAM) (Fig. 6.6). The frequency splitting between stripes slightly increases with the emission frequency (in 43 events), usually between 0.5 and 1.5 MHz. In all examples, the strips exhibit rapid wave-like frequency drift, remaining quasi-equidistant to one another. All these facts are similar to solar ZP.

Unlike the solar corona, Jupiter's plasma is strongly anisotropic, that is, $f_{pe} \ll f_{ce}$, in most of regions of the magnetosphere. Therefore, the mechanism of DPR with electrons cannot explain our observations since it requires extremely high plasma density which is very unlikely in Jovian magnetosphere. Zlotnik et al. (2016) proposed an alternative mechanism of zebra structure formation in Jovian kilometer radiation. The model is based on the DPR at the ion cyclotron harmonics. The mechanism involves excitation of the ion cyclotron waves at low hybrid frequency and then a non-linear transformation of this low-frequency emission to the high-frequency wave due to coalescence process with a high frequency mode.

The DPR with the ions can be operated in the regions where $f_{pe} \ll f_{ce}$, which is fulfilled in most of regions of the Jovian magnetosphere. Therefore, the DPR effect at the ion cyclotron harmonics can be realized for much less plasma density than the DPR effect at the electron cyclotron harmonics. In this case, $f_{LH} \approx f_{pi}$ (f_{pi} is the ion plasma frequency) and the resonance condition is $f_{LH} = sf_{ci}$. The low-frequency plasma waves cannot escape the source and

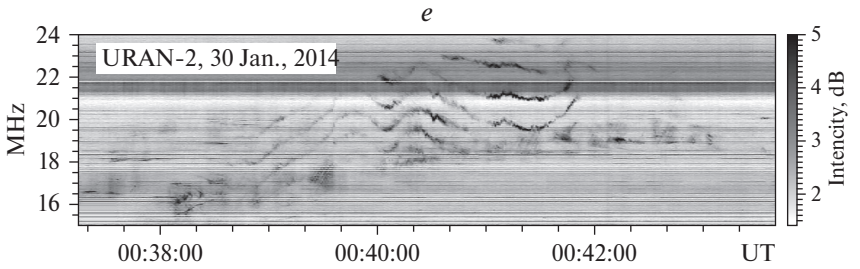

Fig. 6.6. Examples of ZPs observed by URAN-2 radio telescope (fragment of Fig.1 from Panchenko et al. A&A 610, A69 (2018))

should be first transformed to the high frequency electromagnetic waves (f_{em}) in a non-linear coalescence process with a high-frequency mode (e.g., with plasma waves at upper hybrid frequency). Coalescence of these waves ($f_{em} = sf_{ci} + f_{ce}$) results in generation of electromagnetic waves with a spectrum in the form of ZP. Nevertheless, additional theoretical studies are needed to clarify the non-linear modes conversion from the low-frequency ion cyclotron waves to the high-frequency electromagnetic waves.

6.7. Preliminary conclusions

A brief review of possible alternative mechanisms of excitation of zebra-structure in connection with the noted difficulties of the DPR mechanism shows that the whistler mechanism and explosive instability (scattering of non-linear ion-sound waves on particles) can serve as possible models for simultaneous excitation of many zebra bands. They do not require any additional conditions (or constraints) on the plasma parameters.

There are more developed theories, but there is no final decision on them. For example, propagation through a medium with inhomogeneities assumes their presence with certain small scales (Laptuhov, Chernov, 2009).

We have considered several of the most recent events with new peculiar elements of zebra patterns. Important new results are obtained by simultaneous studies of the positions of radio sources, using Nançay Radio Heliograph at 164 and 236 MHz. In particular, correlation between the direction (sign) of the frequency drift of stripes on the spectrum and the direction of drift of source in space is discovered. In most events the polarization corresponds to

the O-radio mode. All new properties are considered in the light of both what was known earlier and new theoretical models. All the main properties of the emission and absorption stripes can be explained in a model involving interactions between electrostatic plasma waves and whistlers, taking into account the quasi-linear diffusion of fast particles with the loss-cone distribution on whistlers. Within the framework of this mechanism alone not simply the stripes in the emission and absorption are explained, but also the entire dynamics of stripes on the spectrum and of their radio sources (splitting of stripes, movements of the sources, superfine spiky structure).

In two events (July 24, 2004 and November 3, 2004) the large-scale ZP consisted of small-scale fiber bursts. The appearance of such uncommon fine structure is connected with the following special features of the plasma wave excitation in the radio source: both whistler and plasma wave instabilities are too weak at the very beginning of the events (the continuum was absent), and the fine structure is almost invisible. Then, whistlers generated directly at DPR levels «highlight» the radio emission only from these levels due to their interaction with plasma waves.

A unique fine structure was observed in the event December 13, 2006: spikes in absorption formed dark ZP stripes against the absorptive type III-like bursts. The spikes in absorption can appear in accordance with the well-known mechanism of absorptive bursts. The additional injection of fast particles filled the loss-cone (breaking the loss-cone distribution), and the generation of the continuum was quenched at these moments, which was evidenced by the formation of bursts in absorption. The maximum absorptive effect occurred at the DPR levels. The parameters of millisecond spikes are determined by small dimensions of the particle beams and local scale heights in the radio source.

Thus, in each new event new special features of the fine structure are revealed. However, they are usually related with the varied conditions in the source. In such a case, one ought not to find a special emission mechanism for each event, which was repeatedly done before. The DPR model helped to understand several aspects of unusual elements of ZPs. In this connection, the calculations of growth rates of upper hybrid waves with a different distribution function of fast electrons inside of the loss-cone is very important (Kuznetsov, Tsap, 2007). However, discussions concerning the va-

lidity of taking into account of one or several harmonics in a hybrid band continue. At the same time, Laptuhov and Chernov (2009) showed that simultaneous existence of several tens of the DPR levels in the corona is impossible for any realistic profile of the plasma density and magnetic field (if we do not assume the order of magnitude of the local density and magnetic field scale heights to be smaller).

Since all known models still have deficiencies, the attempts to create new theories continue. We examined three new theories. The formation of transparency and opacity bands during the propagation of radio waves through regular coronal inhomogeneities is the most natural and promising mechanism. It explains all main parameters of regular ZP. The dynamics of ZP stripes (variations in frequency drift, stripe breaks, etc.) can be associated with the propagation of inhomogeneities, their evolution, and disappearance. Inhomogeneities are always present in the solar corona, however direct evidences of the existence of inhomogeneities with scales of several meters in the corona are absent, although ion-sound waves could serve this purpose.

The mechanism of scattering of fast protons on ion-sound harmonics in explosive instability looks as very uncommon, and it requires a number of strict conditions. Although fast protons always exist in large flares, and the presence of non-isothermic plasma is completely feasible in the shock wave fronts.

The last two models could be useful in describing large radio bursts. All three models are related to a compact radio source. The number of discrete harmonics does not depend on the ratio of the plasma frequency to the gyrofrequency in the development of all three models. The latter circumstance can eliminate all difficulties that arise in the DPR model.

The short event May, 29 2003 provided a wealth of data for studying the superfine structure with millisecond resolution. All the emission in the spectrum in 5.2–7.6 GHz frequency range consisted of spikes of 5–10 ms duration in the instantaneous frequency band of 70 to 100 MHz. These spikes make up a superfine structure of different drift bursts, fiber bursts and zebra pattern stripes. The coalescence of plasma waves with whistlers in pulse regime of the interaction between whistlers and ion-sound waves ensures best explanation for generating spikes (as initial emission).

We have shown that polarization of the ZP corresponds to the ordinary wave mode and it changes in accordance with the dynamics of flare processes. Simultaneous or consecutive appearance of ZP in different frequency bands is obviously connected with the dynamics of flare processes.

A future analysis is needed to clarify whether a radio source showing ZP is really related to a closed magnetic loop, and if it is located at lower altitudes than the source of the pulsations, as is shown by the radio spectrum of ZP at the high frequency boundary of pulsations. New solar radio spectral imaging observations should help to compare the source sizes of different fine structures, and reveal their possible motion.

In Chapter 5 the model of the radio source of type II bursts is based on the generation of radio emission within the front of the collisionless shock wave where the Buneman instability of plasma waves is developed. In the frame of this model, the Alfven magnetic Mach number must exceed the critical value, and there is a strict restriction on the perpendicularity of the front.

In the whistler model radio sources of fiber bursts and ZP are moving, and the spatial drift of ZP stripes should change synchronously with the changes of frequency drift in the dynamical spectrum. In the DPR model, the ZP source must be rather stationary.

In almost all papers the interpretation of ZP begins with the most accepted DPR model. Above, we highlighted several additional problems with this model in the explanation of complicated events. We showed that the event on December 14, 2006 examined in highly cited papers in terms of the DPR model, could be likewise explained in terms of the whistler model, taking into account the propagation of whistlers along a magnetic trap.

The «fingerprint» form of the ZP in the decameter band is also discussed in the DPR model, whereas it can be simply related with the whistler propagation in magnetic islands. Zlotnik et al. explain the fast frequency drift and lifetime of the ZP in terms of the FMA waves which modulate the DPR mechanism, while Karlický (2013) used the density perturbations in the FMA waves (modulating the continuum emission) as a source of ZP without any attraction of the DPR.

The DPR mechanism was even used to interpret zebra-like stripes in microwave radiation of the Crab Nebula pulsar, despite numerous problems with the plasma parameters. Those problems

motivated Karlický to develop a ZP model, based on the FMA waves, for pulsars.

Simultaneous appearances of fibers and ZP, and the smooth transition of zebra-stripes into the fibers and back indicate the united mechanism for the formation of different drifting stripes in emission and absorption within the framework of the interaction of plasma waves with whistlers, taking into account quasi-linear interaction of whistlers with fast particles and with ion-acoustic waves.

In contrast with the DPR model, the whistler model explains many specific features of ZP:

– weak zebra stripes with different scales in a broadband frequency range;

– simultaneous appearance of fiber bursts, fast pulsations and spike-bursts;

– the oscillatory frequency drift and the frequency splitting of stripes;

– change in the spatial drift of radio source synchronously with the frequency drift of stripes in the spectrum;

– the millisecond superfine structure of stripes;

– the rope-like fibers.

Presence of ion-acoustic waves can be considered justified in the source in the vicinity of magnetic reconnection with the outgoing shock fronts. The propagating ion-acoustic waves can serve as natural heterogeneities, passing through which electromagnetic waves shape the additional stripes of transparency and opacity in the spectrum. Laptukhov and Chernov (2019) showed that alternating transparency and opacity stripes in the spectrum of radio waves passing through such plasma structure (the ZP effect) can be observed at any angle of incidence.

It should be noted that the relative significance of these several recently proposed mechanisms remains uncertain. Simultaneous or consecutive appearance of ZP in different frequency bands is obviously connected with the dynamics of flare processes.

For a comprehensive discussion of comparative analysis of observations of ZP and fiber bursts and different theoretical models we refer the reader to the review of Chernov (2011).

Due to the joint observations using Chinese spectrographs at the YNAO and Huairou observatories and at the Institute of Terrestrial Magnetism, Ionosphere, and Radio wave Propagation, Russian Academy of Sciences, we demonstrated a wide variety of

sporadic ZPs in the decimeter and microwave ranges during the event on August 1, 2010. The ZPs were observed in a pulsing regime with a sharp (saw-toothed shape) variation in the direction of the drift of stripes. Various combinations of zebra stripes with fiber bursts and their continuous transition from one form to another were observed. The zebra stripes reveal a superfine structure of millisecond duration.

General properties of the fine structure of radio emission are usually related to the dynamics of the burst process: sign and degree of the circular polarization, various combinations of the ZPs and fiber bursts, and pulsing character on the dynamical spectrum.

The main details of the sporadic ZP in the event on August 1, 2010, were explained within the model of the ZPs and fiber bursts during the interaction of the plasma waves with whistlers. Main variations in the ZPs stripes are caused by the scattering of fast particles on whistlers, which leads to the switching of whistler instability from the normal Doppler effect to the anomalous one.

We demonstrated several events with radio fine structures in which the positional observations could be a determining factor for selection of the radio emission mechanism. It is very important to compare the source sizes of continuum and different fine structures, and to know whether the radio source is moving (shock wave) or not.

Radio sources of fiber bursts and ZP in the whistler model must have moving sources, and the spatial drift of ZP stripes should change synchronously with changes of frequency drift in the dynamical spectrum. In the DPR model the ZP source must be rather stationary.

References

Benáček, Karlický, Yasnov, 2017. Temperature dependent growth-rates of the upper-hybrid waves and solar radio zebra patterns // Astron. Astrophys. Vol. 598, A108. DOI.org/10.1051/0004-6361/201629395

Chernov G. P., 1976. Microstructure in the continuous radiation of type IV meter bursts. Modulation of continuous emission by wave packets of whistlers // Soviet Astronomy. Vol. 20. P. 582–589.

Chernov G. P., 1990. Whistlers in the solar corona and their relevance to fine structures of type IV radio emission // Solar Physics. Vol. 130. P. 5–82.

Chernov G. P., 1996. A Manifestation of Quasilinear Diffusion in Whistlers in the Fine Structure of Type IV Solar Radio Bursts // Astronomy Reports. Vol. 40, No. 4. P. 561–568.

Chernov G. P., Stanislavsky A. A., Konovalenko A. A. et al. Fine structure of decametric Type II radio bursts // Astron. Lett. 2007b. Vol. 33. P. 192–202.

Chernov G. P., 2005. Manifestation of Quasilinear Diffusion on Whistlers in the Fine-Structure Radio Sources of Solar Radio Bursts // Plasma Physics Reports. Vol. 31. P. 314–324.

Chernov G. P., 2008. Unusual stripes in emission and absorption in solar radio bursts: Ropes of fibers in the meter wave band // Astron. Lett. Vol. 34. P. 486–499. https://doi.org/10.1134/S1063773708070074

Chernov G. P., 2011. Fine Structure of Solar Radio Bursts. Heidelberg: Springer. 282 p.

Chernov G. P., 2019. Latest data on the fine structure in solar radio emission. Lambert Academic Publisher. 284 p. Riga, Latvia, www.omniscriptum.com

Chernov G. P., Fomichev V. V., Cych R. A., 2018. A Model of Zebra Patterns in Solar Radio Emission // Geomagnetism and Aeronomy. Vol. 58, No. 3. P. 394–406.

Elgaroy Ø., 1959. Observations of the fine structure of enhanced solar radio radiation with a narrow-band spectrum analyser // Nature. Vol. 184. P. 887–888. https://doi.org/10.1038/184887a0

Fomichev V. V., Fainstein S. M., Chernov G. P., 2009. A Possible Interpretation of the Zebra Pattern in Solar Radiation // Plasma Physics Reports. Vol. 35, No. 12. P. 1032–1035.

Karlický M., Bárta M., Jiřička K., Mészárosová H., Sawant H. S., Fernandes F. C.R., Cecatto J. R., 2001. Radio bursts with rapid frequency variations – lace bursts // Astron. Astrophys. Vol. 375. P. 638–642. DOI:10.1051/0004-6361:20010888

Karlicky M., 2013. Radio continua modulated by waves: Zebra patterns in solar and pulsar radio spectra // A&A. Vol. 552, A90. 9 p. DOI:10.1051/0004-6361/201321356

Karlický M., 2014. Frequency variations of solar radio zebras and their power-law spectra // Astron. Astrophys. Vol. 561, A34. 4 p. https://doi.org/10.1051/00046361/201322547

Karlický M., 2022. Simulations of the solar radio zebra // A&A. Vol. 661, A56. 8 p. https://doi.org/10.1051/0004–6361/202142497

Kuijpers J., 1975. Collective wave-particle interactions in solar type IV radio sources: Ph. D. Thesis. Utrecht University. Netherlands. P. 49–70.

Kuijpers J., 1980 / Eds. M. R. Kundu, T. E. Gergely. Theory of type IV dm Bursts // Radio Physics of the Sun. P. 341.

Kuznetsov A. A., Tsap Yu. T., 2007. Loss-cone instability and formation of zebra patterns in type IV solar radio bursts // Sol. Phys. Vol. 241. P. 127–148. DOI:10.1007/S11207-006-0351-7

LaBelle J., Treumann R. A., Yoon P. H., Karlický M., 2003. A Model of Zebra Emission in Solar Type IV Radio Bursts // Ap. J. Vol. 593. P. 1195–1207. 10.1086/376732

Laptuhov A. I., Chernov G. P., 2006. New mechanism for the formation of discrete stripes in the solar radio spectrum // Plasma Phys. Rep. Vol. 32. P. 866–871. https://doi.org/10.1134/S1063780X06100060

Laptuhov A. I., Chernov G. P., 2009. Concerning Mechanisms for the Zebra Pattern Formation in the Solar Radio Emission // Plasma Physics Rep. Vol. 35. P. 160–168. DOI:10.1134/S1063780X09020081

Litvinenko G. V., Shaposhnikov V. E., Konovalenko A. A. et al., 2016. Quasi-similar decameter emission features appearing in the solar and jovian dynamic spectra // Icarus. Vol. 272. P. 80–87. https://doi.org/10.1016/j.icarus.2016.02.039

Mollwo L., 1983. Interpretation of patterns of drifting ZEBRA stripes // Sol. Phys. Vol. 83. P. 305–320. https://doi.org/10.1007/BF00148282

Mollwo L., 1988. The magneto-hydrostatic field in the region of zebra patterns in solar type IV dm-bursts // Sol. Phys. Vol. 116. P. 323–348. https://doi.org/10.1007/BF00157482

Panchenko M., Rošker S., Rucker H. O., Brazhenko A., Zarka P., Litvinenko G., Shaposhnikov V. E., Konovalenko A. A., Melnik V., Franzuzenko A. V., Schiemel J., 2018. Zebra pattern in decametric radio emission of Jupiter // A&A. Vol, 610, A69. 9 p, DOI:10.1051/0004-6361/201731369

Selhorst C. L., Silva-Válio A., Costa J. E.R., 2008. Solar atmospheric model over a highly polarized 17 GHz active region // Astron. Astrophys. Vol. 488. P. 1079. DOI: https://doi.org/10.1051/0004-6361:2007917

Slottje C., 1971. Proceedings of second meeting of Centr. European Solar Radio Astronomers. Utrecht. P. 88.

Slottje C., 1972. Peculiar absorption and emission microstructures in the type IV solar radio outburst of March 2, 1970 // Solar Phys. Vol. 25. P. 210–231. https://doi.org/10.1007/BF00155758

Slottje C., 1981. Atlas of fine structures of dynamics spectra of solar type IV-dm and some type II radio bursts. The Netherlands: Dwingeloo Observatory.

Treumann R. A., Gudel M., Benz A. O., 1990. Alfven wave solitons and solar intermediate drift bursts // Astron. Astrohys. Vol. 236. P. 242–249.

Viktorov M., Mansfeld D., Golubev S., 2015. Laboratory study of kinetic instabilities in a nonequilibrium mirror-confined plasma // EPL (Europhysics Letters). Vol. 109. 65002. 6 p. DOI:10.1209/0295-5075/109/65002

Winglee R. M., Dulk G. A., 1986. The electron-cyclotron maser instability as a source of plasma radiation // Astrophys. J. Vol. 307. P. 808–819. DOI:10.1086/165742

Yasnov L. V., Karlický M., Stupishin A. G., 2016. Physical Conditions in the Source Region of a Zebra Structure // Solar Phys. Vol. 291. P. 2037–20470. DOI:10.1007/s11207-016-0952-8

Yasnov L. V., Chernov G. P., 2020. Alternative Models of Zebra Patterns in the Event on June 21, 2011 // Solar Phys. Vol. 295, No. 13. 14 p. doi.org/10.1007/s11207-020-1585-5

Yasnov L. V., Karlický M., 2020. Magnetic Field, Electron Density and Their Spatial Scales in Zebra Pattern Radio Sources // Sol. Phys. Vol. 295, No. 96. 12 p. doi.org/10.1007/s11207-020-01652-w

Zheleznyakov V. V., Zlotnik E. Ya., 1975a. Cyclotron wave instability in the corona and origin of solar radio emission with fine structure // Sol. Phys. Vol. 43. P. 431–451.

Zheleznyakov V. V., Zlotnik E. Ya., 1975b. Cyclotron wave instability in the corona and origin of solar radio emission with fine structure. III. Origin of zebra pattern // Sol. Phys. Vol. 44. P. 461–470.

Zheleznyakov V. V., Zlotnik E. Ya., Zaitsev V. V., Shaposhnikov V. E., 2016. Double plasma resonance and its manifestations in radio astronomy // Phys.-Usp. Vol. 59, No. 10. P. 997–1120. https://doi.org/10.3367/UFNe.2016.05.037813

Zlonik E. Ya., Zaitsev V. V., Aurass H., Mann G. A., 2009. Special radio spectral fine structure used for plasma diagnostics in coronal magnetic traps // Solar Phys. Vol. 255. P. 273–288. https://doi.org/10.1007/s11207-009-9327-8

Zlotnik E. Y., Shaposhnikov V. E., Zaitsev V. V., 2016. Interpretation of the Zebra Pattern in the Jovian Kilometric Radiation // J. Geophys. Res.: Space Phys. Vol. 121, 5307.

Acknowledgments

Most of the figures used in Chapters 2–5 were taken from the author's open access articles. The author is grateful to Open Research Support <orsupport@springernature.com> for granting permission to use publicly available materials.

Each chapter contains several figures (without links) taken from the author's personal long-term archive in IZMIRAN.